University of Milano – Bicocca

Faculty of Mathematical, Physical and Natural Sciences
Department of Earth and Environmental Sciences (DISAT)

XXVIII Cycle
Ph.D. School in Environmental Sciences

Development and climate interpretation of mass balance and future assessment about Alpine glaciers, by theoretical models, included in Project of Interest NextData

PhD candidate:
Dr. Massimiliano Moretti
Mat. 071925

Supervisor: **Prof. Valter Maggi**
Co-tutor: **Prof. Antonello Provenzale**
External Advisor: **Prof. Carlo Baroni**
Coordinator: **Prof. Marco Vighi**

I amar prestar aen, han mathon ne nen, han mathon ne chae a han noston ned 'wilith.

The world is changed;

I can feel it in the water,

I can feel it in the earth,

I can smell it in the air.

Galadriel (The Lord of the Rings – The Fellowship of the Ring)

For too long I've been parched of thirst and unable to quench it.

Too long I've been starving to death and haven't died. I feel nothing.

Not the wind on my face nor the spray of the sea. Nor the warmth of a woman's flesh.

You best start believing in ghost stories Miss Turner. You're in one.

Barbossa (Pirates of the Caribbean – The Curse of the Black Pearl)

Dying is the day worth living for

Barbossa (Pirates of the Carribean – At World's End)

… the biggest will become medium or small glaciers and the actual medium and small glaciers will disappear following their climate fate!

Glossary of acronyms

Acronym	Explanation
AIC	Akaike's information criterion
BCSD	Bias-Correction Spatial Disaggregation
CMIP5	Coupled Model Intercomparison Project Phase 5
CO_2	Carbon Dioxide
CRU	Climate Research Unit
CSV	Comma-Separated Values
CSIRO	Commonwealth Scientific and Industrial Research Organisation
DEM / DTM	Digital Elevation / Terrain Model
DISAT	Dipartimento di Scienze dell'Ambiente e del Territorio
ECA&D	European Climate Assessment & Dataset
ECMWF	European Centre for Medium-Range Weather Forecasts
ELA	Equilibrium Line Altitude
E-OBS	European Observations
GAR	Greater Alpine Region
GCM	Global Climate Model
GDAL	Geospatial Data Abstraction Library
GHG	Greenhouse Gas
GIS	Geographical Information System
GPS	Global Positioning Systems
GRASS	Geographic Resources Analysis Support System
GTS	Global Telecommunication System
HISTALP	Historical Instrumental Climatological Surface Time Series Of The Greater Alpine Region

IPCC	Intergovernmental Panel on Climate Change
IPCC-AR	IPCC-Assessment Report
LIDAR	Laser Imaging Detection and Ranging
MGM	Minimal Glacier Model
NASA	National Aeronautics and Space Administration
NEX-GDDP	NASA Earth Exchange Global Daily Downscaled Projections
OGR	OpenGIS Simple Features Reference Implementation
PDF	Probability Distribution Function
QCCCE	Queensland Climate Change Centre of Excellence
QGIS	Quantum GIS
RADAR	Radio Detection and Ranging
RCP	Representative Concentration Pathway
R-K	Runge - Kutta
SAGA	System for Automated Geoscientific Analyses
UAV	Unmanned Aerial Vehicle
UN A/Res	United Nations general Assembly Resolution
WGI	World Glacier Inventory
WGMS	World Glacier Monitoring Service
WMS	Web Map Service

Glossary of units of measure

Physical dimension	Unit of measure
α_m	$m^{1/2}$
Altitude h	m a.s.l.
Basal share stress	Pa
CO_2	GigaTonn of CO_2 equivalent/year
Δh	m
Density	g/cm^3 or kg/m^3
dL/dt	M
Gravity acc.	m/s
H_m	M
Latitude	° N
Length	m or km
Longitude	° E
Mass Balance	m w.e. or mm w.e.
Precipitation	mm
Spatial Resolution	° x ° or km x km
Slope	° or %
Surface	km^2
Temperature	°C

Contents

Abstract

Mountain glaciers are rapidly retreating in most of the world, especially evident on the southern side of the European Alps, where large amounts of ice mass have been lost in the last fifty years, following climate change and warming in high-altitude regions.
The objective of this thesis was to provide simple methods for reproducing and assessing glacier behavior, using reachable parameters and datasets in order to reproduce this methodology on a larger amount of glaciers.
In this work, it is adopted a Minimal Glacier Model approach with the improvement of Geographical Information System to obtain glacier geomorphological parameters. Then, after an accurate evaluation of climate contribution, temperature and precipitation are considered as climatic drivers of the glacier mass balance, which is the input of Minimal Glacier Model.
The development of this procedure starts investigating the dynamics and the future of two glaciers: Careser in Ortles-Cevedale group, Eastern Italian Alps, and the Rutor in Aosta Valley, Western Italian Alps.
Then, the core of this work is to apply Minimal Glacier Model with GIS approach on all glaciers of Greater Alpine Region with usable mass balance dataset. These results are also classified according to the size of glaciers and climate of Alps, to better understand some average behaviors according to future scenarios.
To drive the MGM on the historical period it is used for Careser and Rutor ERA-40 reanalysis climate dataset and, during last step, for all Greater Alpine Region glaciers it is used precipitation and temperature data coming from E-OBS dataset, the first high-resolution gridded dataset of daily climate observations over Europe. Then, as future conditions it is used Global Climate Models of Coupled Model Intercomparison Project Phase 5, also re-elaborated and downscaled by NASA Earth Exchange Global Daily Downscaled Projections project.
After the application of this model and the classification of these results, it is evident that all studied glaciers will lose at 2100 from 70-80% up to 100% of their initial length, and the most dramatic RCP 8.5 scenario will kill more glaciers than RCP 4.5. Then, the biggest will become medium or small glaciers and the actual medium and small glaciers will disappear following their climate fate.

KEY WORDS: Minimal Model, glacier, mass balance, climate, temperature, precipitation, GIS, future assessment

Riassunto

I ghiacciai montani e vallivi sono in rapido ritiro in tutto il globo, con particolare evidenza nell'Arco Alpino, dove una grande quantità di massa glaciale si è persa negli ultimi 50 anni a causa dei cambiamenti climatici e del riscaldamento degli ambienti di alta montagna.
L'obiettivo di questa tesi è la realizzazione di una semplice metodologia per riprodurre e prevedere il comportamento dei ghiacciai sottoposti alle fluttuazioni del clima usando parametri e dati facilmente recuperabili, al fine di poter applicare questa procedura su una grande quantità di ghiacciai.
In questo lavoro è stato adottato e sviluppato il Minimal Glacier Model affiancato da un'analisi GIS per il recupero dei dati geomorfologici. Per quanto riguarda il contributo climatico alla metodologia, come variabili di guida del bilancio di massa glaciale, vero input del Minimal Glacier Model, sono state considerate solo temperatura e precipitazione dopo un'attenta analisi statistica.
Lo sviluppo di questa procedura ha avuto inizio investigando innanzitutto la dinamica e il futuro di due ghiacciai, per provare le varie connessioni del metodo: il Careser nel gruppo Ortles-Cevedale, Alpi Orientali, e il Rutor in Val d'Aosta, Alpi Occidentali.
Quindi si è passati ad applicare il Minimal Glacier Model con l'approccio GIS correlato su tutti i ghiacciai dell'Arco Alpino che abbiano dati di bilancio di massa utilizzabili. Questi risultati sono poi classificati seguendo dimensione dei ghiacciai e clima delle Alpi, per meglio valutare i ritiri medi dei ghiacciai negli scenari climatici futuri.
Per guidare il Minimal Glacier Model nel passato del Careser e del Rutor è stato utilizzato il dataset di re-analisi climatica ERA-40, mentre nell'ultimo capitolo per riprodurre lo storico dei ghiacciai dell'Arco Alpino è stato utilizzato il dataset di osservabili ad alta risoluzione E-OBS. Infine, come condizioni climatiche future sono stati scelti i modelli di circolazione globale del clima nel progetto CMIP5. Questi dati sono stati scelti all'interno del progetto di downscaling dei modelli NASA Earth Exchange Global Daily Downscaled Projections.
Dopo aver ottenuto e classificato i risultati del modello sui ghiacciai dell'Arco Alpino, si è visto che i ghiacciai studiati perdono, alla fine di questo secolo, dal 70-80% fino al 100% della loro lunghezza iniziale al 2011. Ovviamente, nello scenario climatico futuro più drammatico RCP 8.5 è prevista la sparizione di più ghiacciai rispetto al più conservativo RCP 4.5. Si è concluso, dolo un'attenta valutazione del campione disponibile, che i ghiacciai attualmente più grandi potrebbero diventare medio-piccoli e gli attuali ghiacciai medi e piccoli potrebbero sparire, seguendo il loro destino climatico.

PAROLE CHIAVE: Minimal Model, ghiacciaio, bilancio di massa, clima, temperatura, precipitazione, GIS, previsioni future

Introduction

Mountains are sentinels of climate change, for their rapid response to environmental modifications (UN A/Res/62/196). The possibility of amplified warming in high-altitude regions and the associated notion of Elevation Dependent Warming (Rangwala and Miller, 2012), although dependent on the specific geographical area and mountain chain considered, is a topic of current interest and debate (Pepin et al., 2015). In high-altitude environments, mountain glaciers are rapidly retreating in most of the world (Nesje and Dahl 2000) with localized exceptions such as the Karakorum (Gardelle et al., 2012 and references therein). Glacier retreat is especially evident on the southern side of the European Alps, where large amounts of ice mass have been lost in the last fifty years (Paul et al., 2004).

To obtain estimates of future glacier conditions, quantitative descriptions of glacier dynamics are adopted. These vary from simple statistical, data-driven models used to describe the average behavior of an ensemble of glaciers (Bonanno et al., 2013), to simplified descriptions (Minimal Glacier Models sensu Oerlemans, 2001), and/or flow-line models (Oerlemans and Van der Veen 1984; Reeh, 1988), to a full three-dimensional description of the ice dynamics (Jouvet et al., 2009). The more complex models provide a detailed and realistic description of glacier dynamics, but also require a larger amount of input data and information. In case such information is not available, as it is often the case for most glaciers, it could be safer to resort to simplified descriptions that make best use of the existing data.

The term Minimal Glacier Model (MGM) indicates a class of models that do not explicitly describe the spatial dependence of the variables and develop a bulk description of the glacier in terms of glacier-averaged dynamical quantities that depend only on time. The MGMs are a simple but effective way of estimating glacier response to climate change and climate variability. In such approach, the main state variable is glacier length, L, depends on mean thickness and slope using a numerical experimentation with a Shallow Ice Approximation model (Oerlemans, 2001). The evolution of the glacier length is obtained from an integrated continuity equation driven by the glacier mass balance, as in more complex models.

In this work, we adopt a description based on the MGM approach and with the contribution of Geographical Information System GIS to set the parameters and initial conditions. By GIS analysis, we determined the glacier geomorphology from a Digital Elevation Model and we reconstructed the evolution with a multi-temporal analysis, drawing the flow lines accumulation-ablation, along which the MGM is applied.

Afterwards, after an accurate evaluation of climate contribution, in this approach temperature and precipitation are considered as proxies for the much more complex set of meteorological and environmental conditions which affect glacier dynamics and drive the mass balance input for MGM.

First, I used such enhanced MGM approach to investigate the dynamics of two important glaciers on the southern side of the Alps, namely the Careser glacier in Ortles-Cevedale group, Eastern Italian Alps, and the Rutor glacier in Aosta Valley, Western Italian Alps. After comparing the model results with the available data for the two glaciers under study, I tried to estimate the future behavior of these two glaciers.
To drive the MGM on the historical period I used for Careser and Rutor ERA-40 reanalysis, produced by the European Centre for Medium-Range Weather Forecasts (ECMWF). Then, for future climate conditions, I used the outputs of Global Climate Models (GCMs) from the Coupled Model Intercomparison Project Phase 5 (CMIP5) family (Knutti and others, 2013, Taylor and others, 2012), with specific focus on the CSIRO model (Jeffrey and others, 2012). I considered two Representative Concentration Pathways RCP 4.5 and RCP 8.5 to include the most dramatic and the most conservative scenarios still plausible (van Vuuren and others, 2011).
Then, the aim of my Ph.D research program is to apply MGM – GIS approach and climate drivers on all glaciers of Greater Alpine Region with usable mass balance dataset. The result of this development is the definition of classifications and average assessments of glacier terminus retreat up to 2100.
This development allows the elaboration of a simple and functional procedure to elaborate a large amount of glaciers, overcoming the lack of data or refined measurements on them.
To drive the historical mass balance of Greater Alpine Region (GAR) glaciers, it was used precipitation and temperature data coming from E-OBS dataset, the first high-resolution gridded dataset of daily climate observations over Europe, by the European Climate Assessment & Dataset (ECA&D) (Haylock et al.,2008). Then, to drive the MGM on GAR glacier for future climate conditions, I used the NASA Earth Exchange Global Daily Downscaled Projections (NEX-GDDP) dataset: downscaled climate scenarios for the globe that are derived from the GCM runs conducted under the CMIP5 (Taylor et al., 2012).
The work is structured as follows: chapter 1 illustrates the scientific background of glacier and climate change, chapter 2 presents the used fundamentals of modelling. Chapter 3 gives an overview and analysis of the meteorological and mass balance data used in this thesis, chapter 4 describes the first calibration of developed MGM on two glaciers, chapter 5 illustrates the development of a Geographic Resources Analysis Support System GRASS-GIS module that use MGM. Then in chapter 6 it is extended the application of our MGM approach on plausible GAR glaciers. Conclusions are the last paragraph.

Chapter 1: Glaciers and Climate Change

Study of glaciers is part of glaciology, the study of ice in all its forms. Like other branches of geophysics, glaciology is an interdisciplinary subject involving physicists, geologists, atmospheric scientists, crystallographers, mathematicians, and others. Investigators trained in all these disciplines have contributed in fundamental ways to our understanding of glaciers.
Glacier ice covers some 10% of the Earth's land surface at the present time and that the comparatively small glaciers on mountain areas were the first to attract attention, in both science and literature. Mountain glaciers have long served as natural laboratories for studying glacier processes.
They are also important elements of many landscapes; they release water, scour bedrock, cool the weather in summer, and advance down valleys or retreat into high basins. They command attention, in part, for their past and future influence on global climate and preserve an extraordinary record of past changes in Earth's climate and atmospheric composition (Paterson, 2010).

Glaciers

The name "glacier" refers to all ice bodies originating as accumulations of snowfall: mountain glaciers and icefields, small ice caps, continental ice sheets, and floating ice shelves (Paterson, 2010).
The mass of a glacier is composed by ice, various phases of snow, sediments, debris and water. Glacier is created on land and moves by gravity force, transferring mass from the upper region, where the accumulation process prevails, to the lower part, where the mass loss prevails. The firs sector is the Accumulation Area and the second ones is the Ablation Area; an imaginary line divides these areas, the Equilibrium Line Altitude.
Glaciers can be created where the snow can endure for years without completely melting. During this period, the metamorphosis of the snow generates the ice of glacier.
The most fundamental variables, which control this transformation, is the temperature, because it influences the way and the time to become ice. Within moderate regions and climate conditions, this transition occurs more rapid than Polar Regions, because of in the first scenarios there is change between melting and freezing, so the ice formation processes are helped, instead of the Polar Regions with temperature always under freezing threshold.

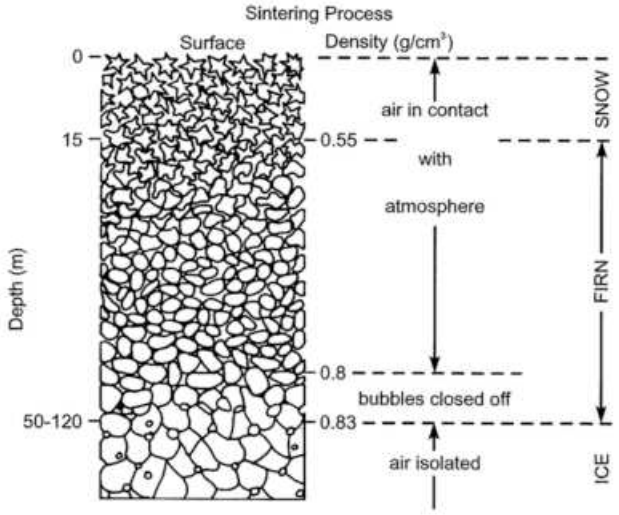

Figure 1: Transition scheme from snow to ice.

As in Figure 1, the snow under transition that survives an ablation season without melting is named firn. The density of snow, about 0,05 – 0,2 g/cm^3, increase to 0,4 – 0,83 g/cm^3, typical values of firn, under the pressure of snow and firn layers above.
This firn becomes ice when all the cavities, that allow the air circulation, are closed off and the air is isolated within bubbles. Its pressure becomes 0,83 – 0,91 g/cm^3 (Paterson, 2010; Benn and Evans, 1998).

Zones in a glacier

As seen previous, a glacier is essentially constituted by an upper accumulation sector and a lower ablation sector (Fig 2).
The "accumulation zone" was divided in different zones, according to their physical characteristics. Benson (1961), Müller (1962) and Paterson (2010) developed the idea of zones.
The upper zone is the "dry-snow zone", where no melting occurs, even in summer, because of the temperature is always below 0°C.

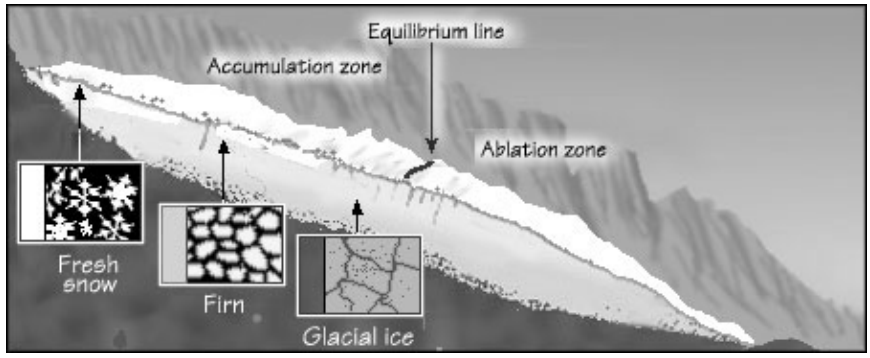

Figure 2: An Equilibrium Line Altitude divides accumulation area and ablation zone.

The “percolation zone” follows the first zone, divided by the “dry-snow line”: some surface melting occurs in this zone and water can percolate a certain distance into snow at temperatures below 0°C before refreezing. When it refreezes an ice layer and ice vertical channels are formed and a latent heat is released by physical process. The amount of meltwater produced during a summer normally increases with decrease of elevation. The point where, by the end of summer, all the snow deposited since the end of the previous summer has been raised to the melting temperature, is the “wet-snow line”, also the boundary with the next zone.
In the “wet-snow zone”, by the end of summer, all the snow deposited since the end of the previous summer has warmed to 0°C by refreezing processes. At lower elevations, however, so much meltwater is produced that the ice layers merge to a continuous mass, called superimposed ice. The term “superimposed-ice zone” defines the region with an annual increment of superimposed ice exposed at the surface. The “snow line” refers to the boundary between the wet-snow and superimposed-ice zones. The lower boundary is the “equilibrium line”, an important feature in mass-balance and glacier dynamics studies. Above it, the glacier has a net gain of mass over the year; below it, net loss.
The “ablation zone” is the area below the Equilibrium Line Altitude (ELA), where the glacier surface loses mass by the end of the year (Fig 2).
In a temperate glacier (as Alpine glacier), the ice is at melting point throughout, except for a surface layer, in which the temperature is below 0°C for part of the year. Temperate glaciers cannot have percolation zones because the temperature of part of the current snowpack and of deeper layers never reaches 0°C. In addition, the extent of any superimposed-ice zone is insignificant and the equilibrium line and snow line coincide on average. A temperate glacier thus has only wet-snow and ablation zones (Paterson, 2010)

Mass Balance

The distributed modelling of snow and ice mass balance is of scientific and practical interest, since it permits to better understand the processes involved in glacier hydrology and to predict glacier runoff under possible future climatic scenarios (Carturan et al., 2012). In addition, distributed glacier mass-balance data is an important component to interconnect different levels of observations, such as length change with climate.
An accelerated mass loss of mountain glaciers all over the world is reported in response to current atmospheric warming (WGMS, 2008; Cogley, 2009; Gardner et al., 2011). Knowledge about past and future changes in glacier mass balance at the mountain-range scale is crucial for assessing global impacts of glacier wastage.
Mass balance measurements are only available for very few of the more than 100.000 mountain glaciers worldwide and differences in mass balance between neighbouring

glaciers are more importantly controlled by glacier geometry than by regional climate variability (Huss, 2012).
The mass balance is the fundamental parameters to drive the glacier behaviour and evolution, because it describes the gain or loss of mass that it contribute on volume and glacier size.
Here it is described the fundamentals of mass balance process, based on the contributions of accumulation positive count and ablation negative one, measurement and archiving.

Accumulation processes

During the accumulation period (winter season for Alpine glaciers), there is a general increase of glacier layer due to snow deposition by solid precipitation. These transitions depend on the condition of snow: dry or moist. If the snow is dry, the metamorphosis is determined by the presence of a temperature gradient within the blanket of snow (Male, 1980; Gray and Male, 1981).
In this period most of re-distribution processes occur, due to the wind or avalanches. These two events increase their contribution with the rise of altitude, because it reduces the forest and vegetation and the force of wind intensifies its motion.
Another accumulation process is the inner refreezing of water during the ablation period. During the first part of the season, the melting water percolates inside and it can refreeze where the temperature is below 0°C. At the end, the freezing interests all the water inside the blanket of snow with its positive contribution on accumulation (Reijmer and Hock, 2008).

Ablation processes

The ablation refers to all the processes that allow loss of ice or snow mass.
The first one is the wind erosion, which redistributes the solid deposition and reduce the glacier surface. Then dry calving is also fundamental for mountain glaciers with high slope, because is the separation of blocks of ice from the glacier terminus.
The physical processes of ablation are melting, evaporation and sublimation. The loss of mass by these transitions occur on glacier surface or within the inner cavities. The melting is the most important contribution and the sublimation dominates at cold regions with dry air (e.g. Antarctica). These processes need an energetic input: the ablation occurs when the balance of energy on glacier surface becomes positive and the temperature reaches the melting point.
Summarize, after accumulation process during winter season, the winter snowpack is melted in late spring and early summer, and then the underlying ice is exposed to high air temperatures and a positive radiation balance throughout the summer.

Mass Balance formulation

The punctual mass balance is the mass variation during a certain time, as the algebraic sum of accumulation and ablation contributes. Generally, the mass balance period is between that two-time series within a year. The ablation season is the summer, where the summer surface of glacier with its impurities differs to the snowpack of accumulation contribution.

Figure 3 describes the two different counts to mass balance: ablation curve and accumulation curve.

The maximum value of volume-mass balance (b_w) is the winter balance; during spring the accumulation period ends and the ablation period starts. Then, during summer, the maximum melting creates the minimum summer volume-mass balance value (b_s).

The net mass balance is the total variation during the entire year, as the sum of winter balance and summer balance, or in other words the sum of the annual total accumulation (c_t) and annual total ablation (a_t);

$$b_n = b_w + b_s = c_t + a_t \qquad (1.1)$$

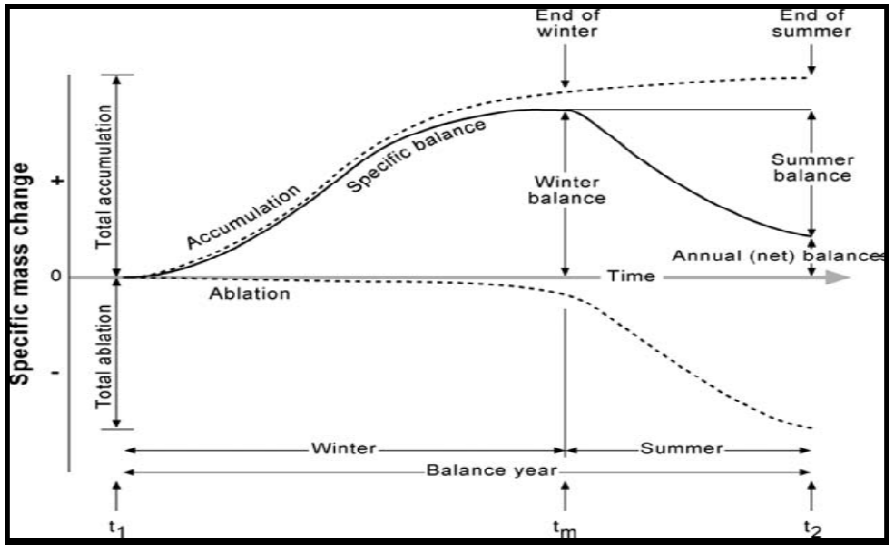

Figure 3: Trend scheme of annual net mass balance, a specific balance for one year.

The mass balance values are expressed by equivalent water height in meters or millimetres (m w.e. or mm w.e.) (Østrem and Brugman, 1991).

There are some assumptions to evaluate the mass balance:

- ✓ the beginning of the year is determined at 30th of September;
- ✓ on glacier surface there are the only considered processes, neglecting the inner accumulation (e.g. refreezing) or the melting of glacier basis.

Mass Balance measurements

Glacier mass balances can be measured several ways. The most common are (Dyurgerov and Meier, 2005):

- ✓ Geodetic and topography method: repeated measurements of the ice surface altitude every few years or few decades; these data on thickness changes, combined with glacier area and density, yield changes in mass (Fountain et al., 1997; Krimmel, 1999).
- ✓ Glaciological surface method: mass balance observations made directly in situ on the surface, which are summed over the glacier and over a year to get the glacier-wide mass changes, the net or annual balance. The measurements of balance is the variation of surface made by some wooden stakes, integrating the punctual values on altitude areas of glacier. This is the most accurate method, but it is also the most expensive and complicated to logistics or data elaboration (Østrem G. and Brugman M., 1991).
- ✓ Hydrological method: the measurements of mass balance as contribution of precipitation, de-fluxes and evaporation.
- ✓ Reconnaissance methods: it is based on the evaluation of the position of the ELA, estimating the ratio between accumulation and total area.

The surface-altitude method has recently become especially productive because of the development of laser altimeters that can be flown in aircraft using Global Positioning Systems (GPS) for spatial orientation (Echelmeyer et al., 1996; Arendt et al., 2002; Abdalati et al., 2001).

Also, is important the development of GIS analysis of Digital Elevation Models (DEMs) of the terrain, created by LIDAR, RADAR o cartography. Through DEMs, it is possible to reconstruct the evolution of glacier with a multi-temporal analysis and draw the contour lines of glaciers and their variation of surface elevations (Strigaro et al., 2015).

Nonetheless, most mass balance data from the world's glaciers have been obtained by traditional surface measurements.

Climate change

Climate is usually defined as the average weather, or more rigorously, as the statistical description in terms of the mean and variability of relevant quantities over a period ranging from months to thousands or millions of years. Weather describes the conditions of the atmosphere at a certain place and time with reference to temperature, pressure, humidity, wind, and other key parameters (meteorological elements), the presence of clouds, precipitation, and the occurrence of special phenomena, such as thunderstorms, dust storms, tornados and others. Climate in a wider sense also includes the associated statistics, such as frequency, magnitude, persistence, trends,

etc. Classically the period for averaging these variables is 30 years, as defined by the World Meteorological Organization. (Cubasch et al., 2013 WGI IPCC).

Climate change may refer to a change in average weather conditions attributed directly or indirectly to human activity, which is considered over long periods, typically decades or longer. Then refers to a change in the state of the climate that can be identified by changes in the mean and/or the variability of its properties (Cubasch et al., 2013).

Climate change commitment is defined as the future change to which the climate system is committed by virtue of past or current forcing. The components of the climate system respond on a large range of timescales, from the essentially rapid responses that characterise some radiative feedbacks to millennial scale responses such as those associated with the behaviour of the carbon cycle and ice sheets. Even if anthropogenic emissions were immediately ceased (Matthews and Weaver, 2010) or if climate forcing was fixed at current values (Wigley, 2005), the climate system would continue to change until it came into equilibrium with that forcing. Because of the slow response time of some components of the climate system, equilibrium conditions will not be reached for many centuries. Climate change commitment is indicative of aspects of inertia in the climate system because it captures the ongoing nature of some aspects of change (Cubasch et al., 2013).

Nowadays, the term climate change has become synonymous with anthropogenic global warming. Within scientific bibliography, global warming refers to surface temperature increases while climate change includes global warming and everything else that increasing GreenHouse Gas (GHG) levels will affect (Fig. 4).

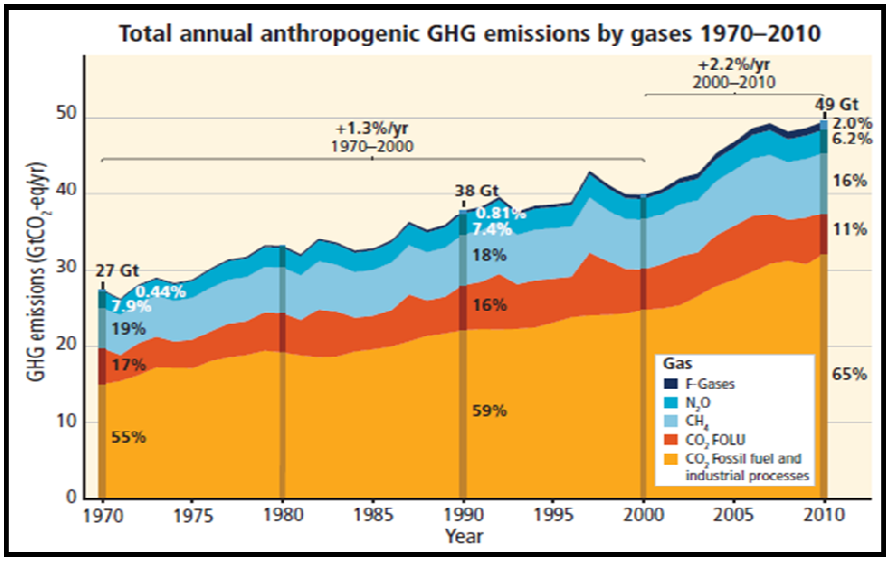

Figure 4: Total annual anthropogenic greenhouse gas emission ($GtCO_2$-eq/yr is Gigatonn of CO_2 equivalent per year), IPCC 5th report.

Evidences of climate change

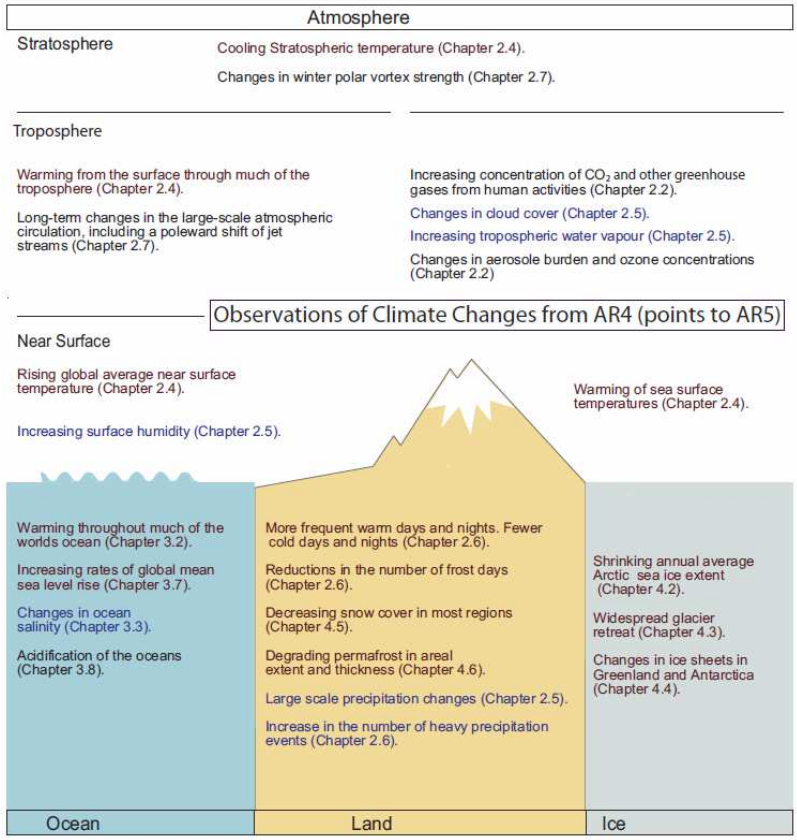

Figure 5: Overview of observed climate change indicators as listed in AR4. Chapter numbers indicate where detailed discussions for these indicators are found in AR5 (Temperature: red. Hydrogeological: blue. Others: black) (Cubasch et al., 2013).

The first line of evidence in assessing climate change is based on careful analysis of observational records of the atmosphere, land, ocean and cryosphere systems and is taken from a variety of sources that can be used to reconstruct past climates.

For earlier periods most of the evidence is indirect climatic changes inferred from changes in proxies, which is indicators that reflect climate, such as vegetation, ice cores, dendrochronology, sea level change, and glacial geology.

Nowadays, earth-orbiting satellites and other technological advances have enabled scientists to see the big picture, collecting many different types of information about our planet and its climate on a global scale.

There is incontrovertible evidence from in situ observations and ice core records that the atmospheric concentrations of GHGs such as CO_2, CH_4, and N_2O have increased substantially over the last 200 years (Fig. 4). In addition, instrumental observations

show that land and sea surface temperatures have increased over the last 100 years (Cubasch et al., 2013). Then the heat-trapping nature of carbon dioxide and other gases was demonstrated in the mid-19th century: there is no question that increased levels of greenhouse gases must cause the Earth to warm in response.
There are many indicators of climate change and a number of the key climate and associated environmental parameters are presented in Figure 5. These include physical responses such as changes in the following: surface temperature, atmospheric circulation and concentration of gas and particles, atmospheric water vapour, precipitation, severe events, mountains, glaciers, ocean and land ice, ocean acidification (ocean uptake of CO_2), and sea level (ocean warming + land ice melt) (Cubasch et al., 2013).

Glaciers

The mountain environment provide indications of global climate change, through phenomena such as the retreat of mountain glaciers, which are the best natural indicators of climate variations (UN A/Res/62/196, 2008).
Studying the worldwide retreats of many glaciers during the past few decades by experiments and modelling have led to a much improved understanding of the link between climate processes and glacier mass fluctuation (Oerlemans, 2001).
Glacier size is determined by a balance between snow inputs and melt output: as temperatures warm, glaciers retreat unless snow precipitation increases to make up for the additional melt; the converse is also true.
Variability in temperature, precipitation, solar radiation and subglacial hydrology can strongly determine the evolution of a glacier in a particular season. Therefore, one must average over a decadal or longer time-scale and/or over many individual glaciers to smooth out the local short-term variability and obtain a glacier history that is related to climate (Cubasch et al., 2013).
Warming of the climate system is unequivocal (Fig. 6) and since the 1950s, many of the observed changes are unprecedented over decades to millennia. Each of the last three decades has been successively warmer at the Earth's surface than any preceding decade since 1850. The period from 1983 to 2012 was likely the warmest 30-year period of the last 1400 years in the Northern Hemisphere, where such assessment is possible.
In Figure 6, the correlation between the increase of surface temperature and the glacier retreats is shown by the representation of a sample of 20 glaciers length around the world.

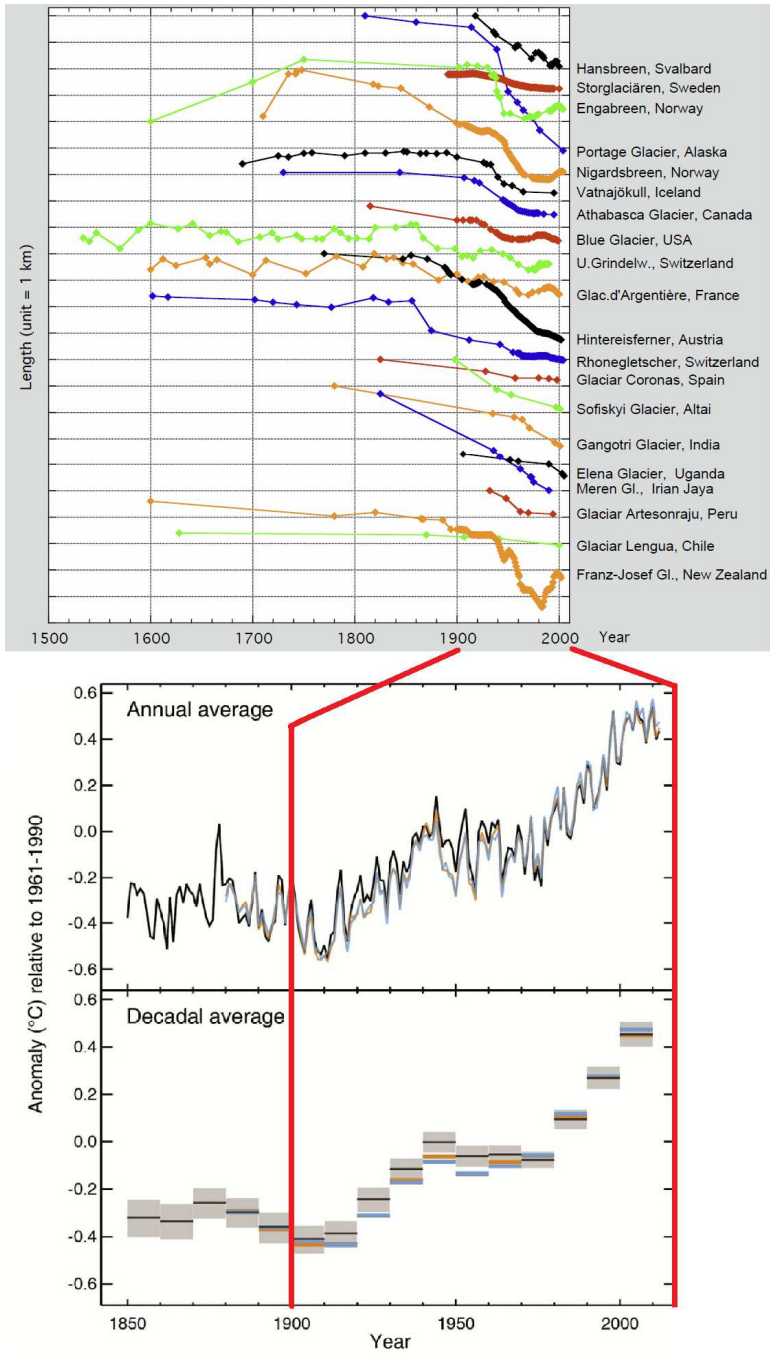

Figure 6: A selection of 20 glacier length records (Oerlemans, 2005), which are compared with the observed globally averaged combined land and ocean surface temperature anomaly.

Due to the increase of temperature and radiation, Alpine glaciers lost 35% of their total area from 1850 up to the 1970s, and almost 50% by 2000. Total glacier volume around 1850 is estimated at some 200 km³ and is now close to one-third of this value. (Zemp et al., 2006).
The terminus retreat is usually directly related to the mass balance of a glacier (Villa et al., 2007). Both, glacier mass balance and glacier length change should be applied in combination for worldwide glacier and climate system monitoring. Climate and glacier fluctuations over a specific period can be viewed as composed of a linear trend on which smaller scale fluctuations are imposed. Although many records of mass balance are short, as many records of glacier length are much longer, and can be used to provide information on climate variability (Haeberli, 1995; Oerlemans, 1994).

Study Area

The study area of this project is the Greater Alpine Region (G.A.R.), located between 5–16° E and 43–48° N as in Figure 7. The GAR includes the entire territory of Switzerland, Liechtenstein, Austria, Slovenia and Croatia, and the Alpine sector of France, Italy, Germany, Czech Republic, Slovakia, Hungary and Bosnia, covering 724.000 Km² of surface.

Figure 7: Geographic location of Greater Alpine Region within the Southern area of Europe: [5°-16°] E, [43°-48°] N.

The significant study area is a sub-region of GAR, excluding the territories without mountains and glaciers: the European Alps range from the Mediterranean Sea level to a maximum altitude of 4.810 m a.s.l. at Mont Blanc summit in the western part of the Alps.
The Alps are arcuate in shape at their western end they extend 250 km North South. Their orientation is West-East through Switzerland, where the ranges are less than 100 km in total width, and through Austria where they broaden to 150 km, but are

subdivided by pronounced longitudinal valleys (master thesis Zemp, 2006; Barry, 2013).
The altitude is the most characteristic and important among the factors that can affect the mountain climate. The air density and temperature tend to decrease with altitude. Instead, the thermal excursion increases because of the increasing heat capacity of the air, because it is rarefied. The topography plays a key role in determining the local climates, especially with the steepness of the slopes and exposure to climatic factors. These factors governing the distribution of the absorption of solar energy and precipitations.
The Alpine region include many mountain and valley glaciers: they start from South-West, with the Saint-Sorlin and Sarennes Glaciers, through the Central glaciers with Jamtal glacier to Northeast, with Vernagtferner and Wurten glaciers of Golberg Group (Fig. 8).

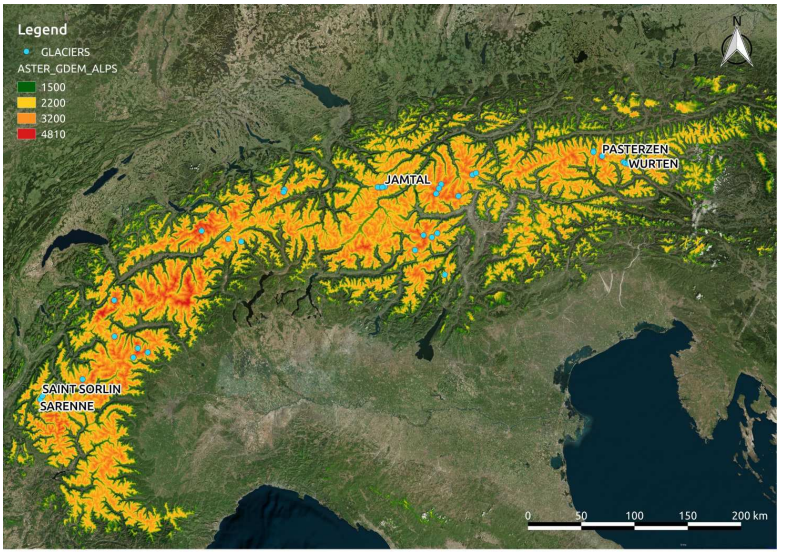

Figure 8: Distribution of glaciers (azure dots) on GAR with useful data to the analysis (Digital Elevation Models rendering).

In this region it is possible to study the climatic condition with the archived long series of whether variables, within some parameters were registered from the 18th century.
I focused my attention on the available mass balance data of Alpine glaciers, up to 2011. I obtained these series searching for databases (WGMS) and internet catalogues and I chose the glaciers with at least 8 years of mass balance values (blue dots of Fig. 8), as listed in Table 1.

Glaciers		Position		Mass balance values		
Name	N° ID	Lat E	Long N	N° of year	Initial Year	Final Year
Sarennes	SAR1	45,133	6,133	61	1951	2011
Hintereisferner	HIN2	46,800	10,758	59	1953	2011
Kesselwandferner	KES3	46,858	10,791	59	1953	2011
Saint_Sorlin	SAS4	45,160	6,160	55	1957	2011
Stubacher_Sonnblick	STU5	47,132	12,596	53	1959	2011
Silvretta	SIL6	46,852	10,077	52	1960	2011
Griesgletscher	GRI7	46,438	8,330	50	1962	2011
Vernagtferner	VER8	46,876	10,818	48	1965	2012
Grosser_Aletsch	ALE9	46,503	8,019	45	1951	1995
Careser	CAR10	46,450	10,700	45	1967	2011
Plattalva	PLA11	46,833	8,989	39	1951	1989
Limmerenfirn	LIM12	46,813	8,977	35	1951	1985
Argentiere	ARG13	45,943	6,998	36	1976	2011
Pasterze	PAS14	47,099	12,697	25	1980	1997
					2005	2011
Wurten	WUR15	47,039	13,005	29	1983	2011
Fontana_Bianca	FON16	46,484	10,771	25	1984	1988
					1992	2011
Jamtal	JAM17	46,858	10,160	23	1989	2011
Basodino	BAS18	46,416	8,481	20	1992	2011
Ciardoney	CIA19	45,518	7,390	20	1992	2011
Filleck	FIL20	47,130	12,600	17	1964	1980
Gebroulaz	GEB21	45,298	6,628	17	1995	2011
Pendente	PEN22	46,966	11,225	16	1996	2011
Grand_Etret	GRE23	45,476	7,219	14	2000	2013
Sforzellina	SFO24	46,348	10,513	14	1987	2000
Kleinfleiss	KLE25	47,053	12,947	13	1999	2011
Timorion	TMR26	45,552	7,274	13	2001	2013
Vog.Ochsenkar	GOL27	47,042	12,970	12	1989	2000
Lagol	AGL28	46,151	10,861	12	2002	2013
Malavalle	MAL29	46,951	11,183	10	2002	2011
Ochsentalergl	OCH30	46,852	10,105	9	1991	1999
Vermuntgl	VRM31	46,853	10,131	9	1991	1999
Ruitor	RUI32	45,648	7,001	9	2005	2013
Langtaler	LAN33	46,789	11,019	8	1963	1970
Lunga_Vedretta	LUN34	46,467	10,612	8	2004	2011

Table 1: List of sample of Alpine glacier, with their positions and the description of the available mass balance datasets.

To study the climate of GAR, I used three gridded data sets of observations CRU, E-OBS and HISTALP and mass balance series of 32 glaciers (Tab. 1) compiled by the World Glacier Monitoring Service (WGMS), covering the period 1950-2013 (as explained in Chapter 3).

In general, the climate of the Alpine region is characterised by a high degree of complexity, due to the interactions between mountain ridges and the general circulation of the atmosphere, which result in features such as gravity wave breaking, blocking highs, and Foehn winds. A further cause of complexity inherent to the Alps results from the competing influences of a number of different climatological regimes in the region, namely Mediterranean, Continental, Atlantic, and Polar (Beniston, 2005; Zampieri et al., 2013).

Moreover, accumulation of masses of snow, constantly converted into the ice mass of glaciers, also maintains a variation of very different climates within the narrow space

between the valley floor and the upper ridges of the surrounding mountains. Its most important function is to govern the water supply of the regions, which are crossed by the water streams that start from the Alps. During the end of autumn, winter and spring, nearly all the moisture that is precipitated is stored in the form of snow. This snowpack gradually diffused in the course of the succeeding summer and even in the hottest and driest seasons the reservoirs accumulated during a long accumulation period of years remain available to sustain the regular flow of the greater streams (Huss et al., 2010; Marzeion and Nesje, 2012; Balocco master thesis, 2015).

Importance of Alpine Glaciers

Nowadays glaciers cover about 10% of land area, and about only 1% of the land ice is located outside the Arctic and Antarctic Area, even though they represent only a very small part of the ice on Earth.

The glaciers of the Alps have a big local importance related to environmental or microclimatic and economic factors. They are an important element of the Alpine environment from different points of view. First of all their value is linked to a geologic-naturalistic function. Then, in our history, in densely populated mountain areas, as the Alps, glaciers also appear as an important character in myths, legends and tales. From another point of view, Alpine glaciers have an economic value linked to a touristic function (trekking or alpine paths, winter and summer ski, etc…) and to hydropower production. Sure enough freshwater stocked in glacial bodies acts as a lung for artificial basins by releasing water during the summer season, when it is needed both for hydropower production and for irrigation. (Villa, 2007).

Chapter 2: Fundamentals of modelling

First, I will start making a clarification to the usability of this model. The following MGMs is applicable if the glacier is free of debris, because a glacier covered of some kinds of debris and rubble follows different dynamics. The covering interrupts the normal accumulation, the average flux accumulation area-ablation area and the usual melting processes. Then the application of MGM is not allowed on debris-covered glaciers, such as the Miage glacier (Western Alpine glaciers, Monte Bianco - Graie Alps).

Minimal Glacier Model

In a minimal model approach, the glacier evolution is obtained from integrating an appropriately averaged continuity equation (Oerlemans, 2001). For alpine glaciers, the equation for the total ice volume V is

$$\frac{dV}{dt} = B_s \tag{2.1}$$

where B_s is the total surface mass balance rate. The glacier volume V is given by the product of the mean width W, the mean ice thickness H_m and the glacier length L. MGMs assume a diagnostic relationship between glacier length and thickness (Oerlemans, 2011):

$$H_m = \frac{\alpha_m}{1+\nu s} L^{1/2} \tag{2.2}$$

where s is the mean bed slope and α_m and ν are empirical constants. If the bed slope is set to zero, the mean thickness varies with the square root of the glacier length, in agreement with a perfect plasticity assumption.
For simplicity, here we take the width W to be constant along the glacier (Oerlemans, 2011), although the model can be easily extended to the case of a non-constant width. With such assumptions, volume changes are entirely determined by length changes. After simple manipulations, and according to Oerlemans (2001), we obtain an evolution equation for L:

$$\frac{dL}{dt} = \left(\frac{3\alpha_m}{2(1+\nu s)} L^{1/2} - \frac{\alpha_m \nu}{(1+\nu s)^2} L^{3/2} \frac{\partial s}{\partial L} \right)^{-1} \frac{B_S}{W} \tag{2.3}$$

Assuming a mass balance profile that depends linearly on altitude, one obtains:

$$B_S = W\beta\int_0^L \left(H(x)+b(x)-E\right)dx = \left(H_m+\bar{b}-E\right)\beta W \qquad (2.4)$$

where $\bar{b}$ is the mean bed elevation, E is the equilibrium line altitude (ELA) and β is the mass balance gradient along the glacier.
A simple representation of the bed elevation *b(x)*, useful for the glaciers considered here, is a simple concave bed:

$$b(x) = b_0 e^{-x/x_l} = b_0 - s(L)\cdot L \qquad (2.5)$$

where b_0 is the maximum elevation of glacier's head and x_l is the length scale that determines how quickly the height of the bed decreases. From this, one can obtain an expression for the length-dependence of the mean slope, to be used in eq. 2.3:

$$\frac{\partial s(L)}{\partial L} = -\frac{b_0\left(1-e^{-L/x_l}\right)}{L^2} + \frac{b_0 e^{-L/x_l}}{x_l\, L} \qquad (2.6)$$

The above equations fully define the minimal model adopted here. Limitations and possible extensions are mentioned in the discussion section.

Numerical method for results

Equation 2.3 has the form:

$$\frac{dL}{dt} = f\{L, P_j\} = y'(x,y) \qquad (2.7)$$

Here P_j is a set of parameters that vary in time and represent the "forcing" of the model glacier.
The results of this model can be obtained with many numerical solutions: one of the most refined methods is the Runge-Kutta of integrating ordinary differential equations (Hamming, 1986).
Given $y(x_n) = y_n$ and h = 1 year the time-step, the R-K scheme is:

$$
\begin{aligned}
k_1 &= hf\left(x_n, y_n\right) \\
k_2 &= hf\left(x_n + \frac{h}{2}, y_n + \frac{k_1}{2}\right) \\
k_3 &= hf\left(x_n + \frac{h}{2}, y_n + \frac{k_2}{2}\right) \\
k_4 &= hf\left(x_n + h, y_n + k_3\right) \\
y_{n+1} &= y_n + \frac{1}{6}\left(k_1 + 2k_2 + 2k_3 + k_4\right)
\end{aligned}
\tag{2.8}
$$

In geometric terms, at the point $\left(x_n, y_n\right)$ is applied the slope k_1/h to examine the slope one-half step forward. Then using this new slope k_2/h, it is sampled the slope in $\left(x_n, y_n\right)$ one-half step forward. This latest slope k_3/h is used to evaluate the last k_4/h. Finally, the four slopes are averaged, using weights $\frac{1}{6}, \frac{2}{6}, \frac{2}{6}, \frac{1}{6}$ to obtain $\left(x_n, y_n\right) \rightarrow \left(x_{n+1}, y_{n+1}\right)$. The method has an error proportional to h^5.

Climate forcing of Minimal Glacier Models

The input data of MGMs are the mass balance gradient β along the glacier and the equilibrium line altitude *E*. The mass balance gradient (Oerlemans, 2011) depends on the net mass balance $\dot{b}$ as

$$
\beta = \frac{d\dot{b}}{dz} = \frac{\dot{b}}{\bar{h} - E} \tag{2.9}
$$

where *dz* is the altitude variation and $\bar{h}$ is the mean elevation

$$
\bar{h} = H_m + b_0 - \frac{L \cdot s}{2} \tag{2.10}
$$

and we assumed a homogeneous gradient along the glacier.

In cases where measurements of the net mass balance $\dot{b}$ and *E* are available, the MGMs can be directly driven by these variables. In most cases, however, one has to parameterize the mass balance and the *E* fluctuations in terms of variations in their climatic drivers (Chapter 3).

Simplified MGM without ELA

Considering that the purpose of this work is the elaboration of a procedure to evaluate the behaviour of a large amount of glaciers, I had to take into account that some parameters are difficult to retrieve.
One of these variables is the equilibrium line altitude, because within the glacier databases there are not a completely and usable series of *E* values year by year.
Therefore, I applied the MGMs without including an *E* input owing to the lack of data. The simplified model is then useful to overcome the insufficient data availability, substituting eq. 2.3 and eq. 2.4 with:

$$\frac{dL}{dt} = \dot{b}L\left(\frac{3\alpha_m}{2(1+\nu s)}L^{1/2}\right)^{-1} \qquad (2.11)$$

Eq. 2.11 contemplates the net mass balance $\dot{b}$ as climate input and the glacier length *L*, the surface slope *s* and the thickness parameter α_m as morphological conditions.

Method to evaluate glacier thickness

In the MGMs, the parameter ν in eq. 2.2 was fixed at the standard value for valley glaciers (Oerlemans, 2011), as ν = 10. The other parameters, as surface slope *s* or maximum altitude b_0 are obtained from the glacier properties.
As far as scientific literature is concerned (Oerlemans, 2011), the value of the parameter α_m in eq. 2.2 is often set to $\alpha_m = 3 m^{1/2}$ for valley glaciers and ice sheets. However, given that all the Alpine glaciers had a particular behaviour, if the morphological input data are available, I can estimate α_m using eq. 2.2 and the expression for the bed slope along the flow line.
Eq. 2.2 requires the knowledge of the ice thickness H_m. We obtained these values with an approach that considers a constant basal shear stress along the flow line of the glacier and estimates the ice thickness along the central flow line (Linsbauer and others, 2012):

$$H_m = \frac{\tau}{f\rho g \sin(\gamma)} \qquad (2.12)$$

where *f* = 0.8 is the shape factor, related to the lateral drag on a glacier through friction at the valley walls and the general form of the glacier cross section (Paterson, 1994). ϱ = 900 kg m^{-3} is the ice density, *g* = 9.81 m s^{-1} is the gravity acceleration, γ is the glacier surface slope along the flow line and τ is the basal shear stress.

The basis for this parameterization scheme is the estimation of maximum and minimum altitude (h_{max}, h_{min}). The mean altitude is defined as $\bar{h} = \frac{h_{\max} + h_{\min}}{2}$ and the elevation range is $\Delta h = h_{\max} - h_{\min}$. The value of τ is obtained from an empirical relationship between τ and Δh, according to a polynomial regression (Haeberli and Hoelzle, 1995):

$$\begin{cases} \tau = 0.005 + 1.598\Delta h - 0.435\Delta h^2 \; \Delta h \leq 1600m \\ \tau = 150kPa \;\; \Delta h > 1600m \end{cases} \qquad (2.13)$$

Then, using eq. 2.11, I applied the results on the mean ice thickness with the length and altitude evaluation from morphological values, and I can estimate the average a more accurate values of α_m, useful for MGMs.

GIS module for glacier parameters

The interconnection between MGM algorithms and GIS analysis was produced collaborating with Dr. Matteo Mattavelli, Ph.D candidate in my group of research, to set the MGMs parameters and initial conditions (Strigaro et al., 2015; Mattavelli Ph.D thesis, 2016).

A huge quantity of morphometric and morphologic parameters of several glaciers are collected by different remote sensing instruments, such as satellites and UAV, and by in-situ measurements. Such morphometric parameters provide detailed information to calibrate and validate glacier models.

We determined the glacier geomorphology from a DEM using a GIS: we reconstructed the evolution of glacier with a multi-temporal analysis and we draw the flow lines that follow the accumulation-ablation dynamics, along which the model is applied. The algorithms were developed to extrapolate from DEMs, in a GIS environment, all the features needed to calibrate the Minimal Model (Fig. 9).

This algorithm is developed with QGIS tools, using several libraries and the interoperability of different open source software such as GDAL, GRASS, and SAGA. The procedure requires, as inputs, DEMs, POLYGONs and FLOW LINEs and we obtain all the morphological parameters and initial condition for the MGMs, such as maximum and minimum elevation, altitude range along the flow lines, mean slope and its variations, and flow line length.

These parameters are useful to start the iterative process and to calibrate the results on actual values. Moreover, we validate the simulated results by comparing the numerical outputs with the length values from past measurements.

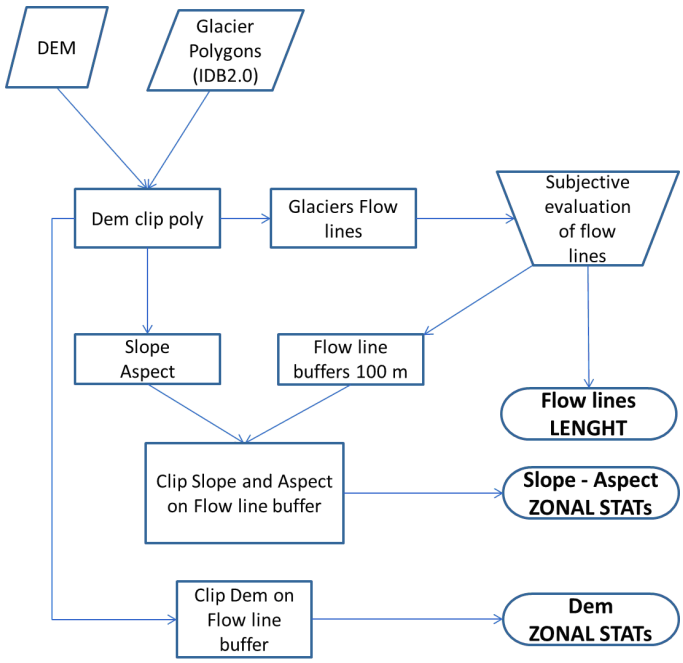

Figure 9: GIS algorithm used to calibrate MGMs boundary and initial condition (Strigaro et al., 2015).

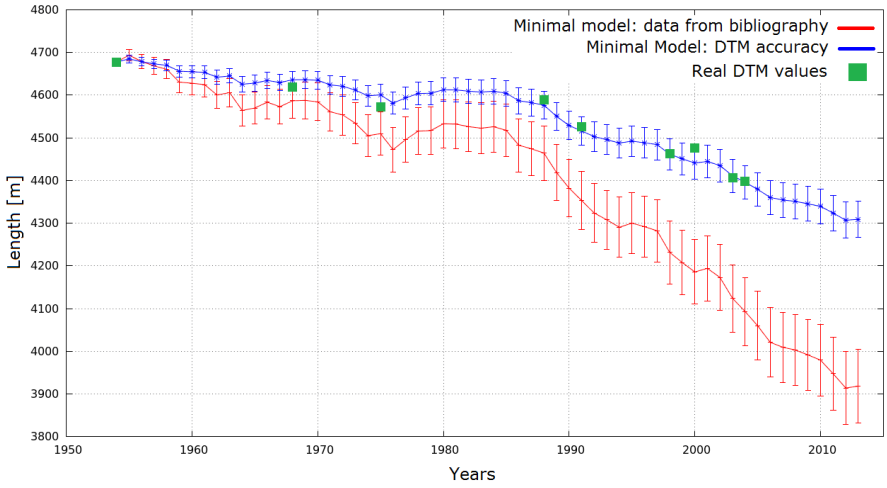

Figure 10: Comparison between model results. Light blue dots represent the lengths measured by DEMs, the blue line represents the simulated results by GIS calibration and the red one is the simulated results with data from databases.

In this way, the GIS analysis of glacier flow line could increase the accuracy of MGMs (or of more refined glacier models). As shown in Figure 10, from the calibration of Rutor glacier (western Italian Alps, Val d'Aosta), keeping the same starting point, the accuracy of the simulated values obtained from the model calibrated with the DEM

analysis is much better than the accuracy obtained using bibliographical or standard parameters.

Minimal Glacier model programming

First of all MGM algorithm was developed by FORTRAN programming code, to better communicate with the previous version, released by Daniele Peano (Peano D. master thesis, 2011). I had formulated a complete algorithm that consist of MGM core, thickness evaluation with previous method, application of mass balance input and error estimation.
At a later stage, I had to convert all the sections from FORTRAN to Python language (Appendix A). This is due to have a more versatile and dynamic code.
For example, using Python code with html and javascript environments, in collaboration with Dr. Daniele Strigaro, Geomatic DISAT laboratory, we developed the MGM algorithm for use via web on the website (Fig. 11):

http://geomatic.disat.unimib.it/mgm.

According to the appropriate guide at web site, user can upload input glacier parameters to set the initial and contour conditions. Then he can upload the climate dataset (choosing temperature/precipitation series or the mass balance set directly). In closing, after the compiling the MGM algorithm, user can download .csv file with MGM results, composed by three columns: referring years, length simulations and their errors.

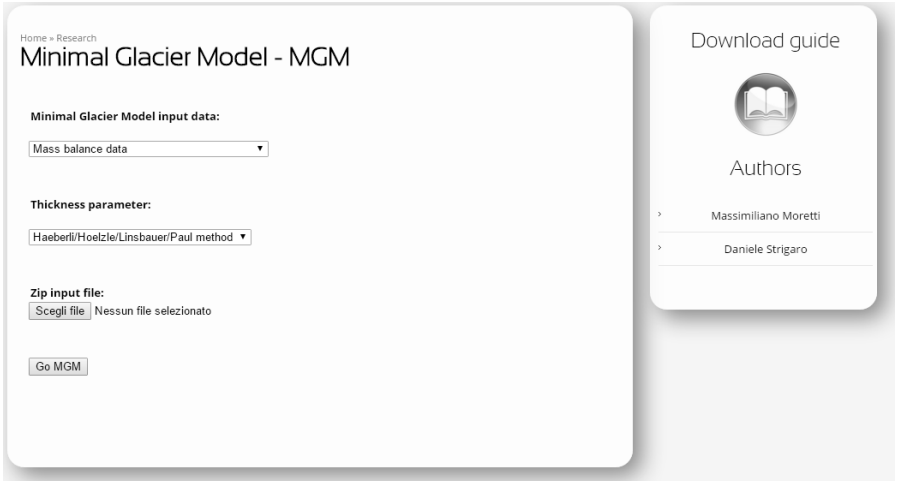

Figure 11: User mask of MGM web site http://geomatic.disat.unimib.it/mgm.

Chapter 3: Mass balance and climate forcing

This chapter illustrates the relation between the mass balance of a glacier and the climate forcing which drives the accumulation and melting processes.
In his approach, temperature and precipitation are considered as proxies for the much more complex set of meteorological and environmental conditions, which affect glacier dynamics. For instance, incoming solar radiation and cloudiness can play an important role, but are ignored because we wanted to evaluate a simplified empirical model that uses only temperature and precipitation (the most commonly available data extending back to 1950).
To use the climate dataset and drive the Minimal Glacier Models, we before analysed precipitation and temperature data coming from three different data sets: CRU, E-OBS and HISTALP. There are few mass balance models as far as scientific literature is concerned, which are based on gridded data sets. Some used HISTALP data set to reconstruct inter-annual mass balance variability of glaciers in the Alps. Our work represents the first that contemplates the use of CRU and E-OBS data sets to model climate influence on glacier mass balances in the Alps.
Then choosing the best observational dataset, we can evaluate the best fitting function, which relate the temperature and precipitation fluctuation with the mass balance.
Afterwards, to drive the MGM for future climate conditions, I used the NASA Earth Exchange Global Daily Downscaled Projections (NEX-GDDP) dataset for RCP 4.5 and RCP 8.5
This step of my Ph.D thesis is made by the collaboration with three bachelor and master thesis candidate. First, I was the co-tutor of Sali to recover and study the mass balance data (Sali bachelor thesis, 2015). Then I collaborated as co-tutor of Maffezzoni to study the climate trend of Alpine Region, related to the geomorphological characterization of GAR glaciers (Maffezzoni master thesis, 2015). During my Ph.D thesis, I also collaborated with master thesis of Balocco, Dr. J. Von Hardenberg and Dr. E. Palazzi recovering past and future climate data, to evaluate the goodness of these datasets and to study the transfer function between mass balance and climatic variables (Balocco master thesis, 2015).
The aims of this step are:

- ✓ the definition of the correct procedure to drive the glacier mass balance with the contribution of climate variables;
- ✓ the classification of the studied glaciers according to climate, mass balance, position and geomorphological parameters to have a first grouping to condition the final results of MGMs.

Mass balance dataset analysis

Every year a glacier collects ice from snowfall mainly during winter and loses ice by melt and other processes mainly during summer, as seen in Chapter 1. If the gains and losses are not equal, the volume of the glacier will change over time. The cumulative difference between income and expenditure gives the account of the net balance. On many glaciers the budget fluctuates over an annual cycle are measured with some methods described in Chapter 1. The integrated change over this cycle determinates whether a glacier expands or shrinks from one year to the next. Mass balance is a critical factor in the relation between glaciers and climate, subject of widespread interest (Oerlemans and Reichert, 2000; Paterson, 2001; Vincent, 2002; Braithwaite, 2006; Huss, 2012; Six and Vincent, 2014).
In this step, I considered with Sali the mass balance series of 50 glaciers within GAR, reached by WGMS database and other atlas or internet archives. Then, there are 4 French glaciers, 21 Italian glaciers, 11 Swiss glaciers and 14 Austrian glaciers. For each element, beyond the mass balance, I had to determine the geographic position, minimum and maximum elevation, slope and surface orientation.
Then I spatialized the glaciers to allow a classification by longitudinal sector: I divided them into 4 sector, to have a sufficient statistical contribution to our analysis and to characterize each sector with a same climate forcing condition.
For each area, I evaluated the net mass balance and the cumulate trend over the entire archived period, formulating an average trend of annual net mass balance of our sample of data and a gradient estimation of fluctuations.

Western Alps

Starting from the left side of the Alps, the first sector is the Western Alps, which include the Delfinato, Graie and Pennine mountains.

Figure 12: Western Alps, 15 glaciers.

There are 15 glaciers, divided into France (4), Italy (9) and Switzerland (2) (Fig. 12). In particular, Sarennes and Saint Sorlin at Delfinato, Gebroulaz and Rutor at border Italy-France, the Monte Bianco chain with Toula, Argentiere, Pre de Bar and Petit Grapillon, the Gran Paradiso Massif with Grand Etret, Timorion and Ciardonè, the Monte Rosa with Findelen and Indren and then Gries glacier near the followed sector.

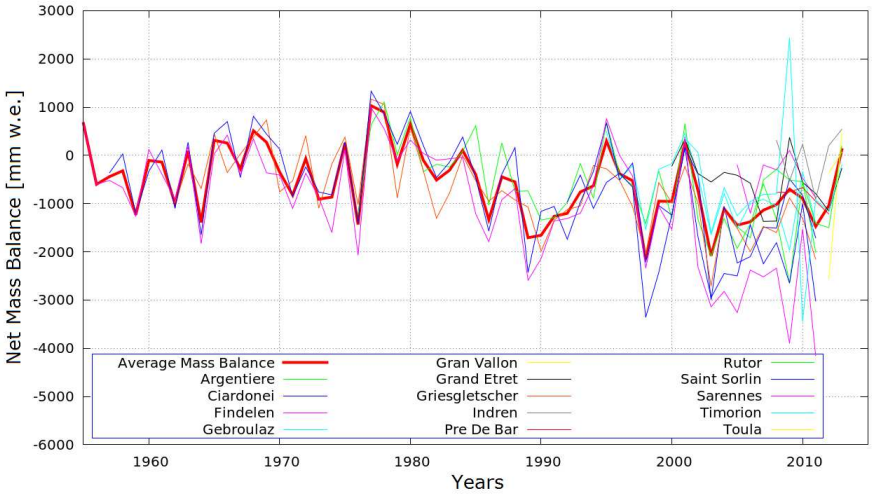

Figure 13: Net mass balance of Western glaciers, with their average trend.

The Figure 13 represents all the net mass balance of the Western glaciers, with the average trend values. The longest series are Sarennes (since 1949), Saint Sorlin (since 1957) and Argentiere (1976).

The mass balance trend of Western glaciers are generally negative. We can evidence that the Sarennes has the worst conservative behaviour, due to its geographic position (the most Southern glacier of GAR) not so far from the Tyrrhenian Sea, its inferior altitude and the exposure to the South. Sarennes lost about 60 m of water equivalent since 1949 and had a significant mass fragmentation. In addition, Gries, at highest altitude, shows a significant retreat due to its lower tongue (Kappenberger, 2009). The most conservative glaciers are within the mountain range of Valle d'Aosta, as Grand Etret.

We can distinguished two different periods with different gradient of net mass balance: the range of negative balance before 1984 is between -100 and -350 mm/year, then after 1984 the balance trend becomes about -800 and 1400 mm/year.

Central Alps

The Central Alps includes the Bernesi, Glaronesi and Western Retiche Alps, with 16 glaciers: 9 of them are in Switzerland, 3 in Italy and 4 in Austria (Fig. 14).

Figure 14: Central Alps, 16 glaciers.

The Tsanfleuron, Raetzli, Gross Aletsch, Rhone and Basodino glaciers are at Bernesi Alps; the Glaronesi Alps include Limmern, Plattalva and Pizol and the Eastern Silvretta group have Silvretta, Klostertaler, Ochsentaler, Jamtal and Vermunt glaciers. On the southern flank, there are the small Italian glaciers: Suretta, Campo Nord and Lupo. This is the most populous sector with a good temporal series.

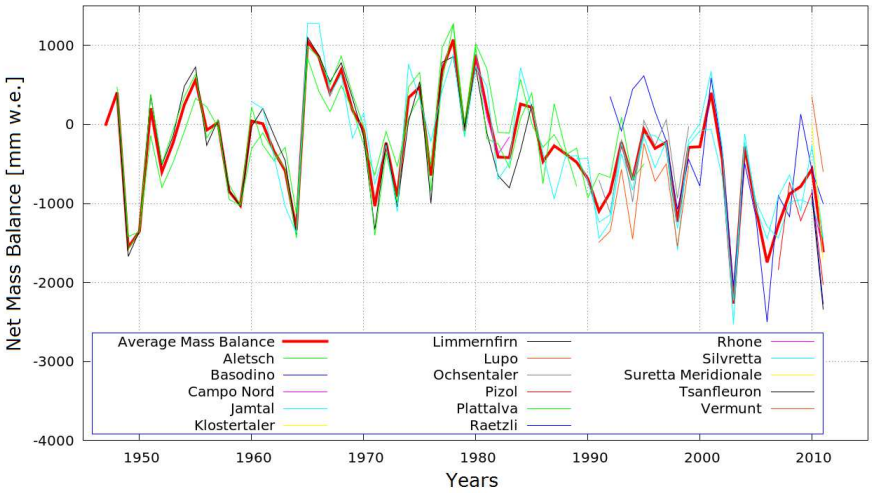

Figure 15: Net mass balance of Central glaciers, with their average trend.

From Figure 15 is evident a strong coherence of those mass balance, despite the wide area and the difference in altitude and exposure. The average values follow the fluctuations with a good approximation. The longest series are Aletsch, Limmern and Plattalva, since 1948, and Silvretta since 1960.

We can evaluate three different period of gradient behavior: the first negative trend starts from 1947 and ends with the negative fluctuation of 1964; the second period is characterized with an accumulation trend that finishes at 1985, a significant positive peak; the third one is in agreement with the other sectors and presents a negative

trend. As values, the average gradients are -380 mm/year for the first period, + 162 mm/year for the second and -683 mm/year for the last period.
Then, Central glaciers show a good agreement of their mass balance datasets in view of the heterogeneity of the altitudes and morphology: we can underline the homogeneity of the climate conditions.

Central-Eastern Alps

The followed sector is the Central-Eastern, between the Southern Retiche and the Eastern Alps, with its 11 glaciers from which 7 glaciers are Italian and 4 Austrians (Fig. 16).

Figure 16: Central-Eastern Alps, 11 glaciers.

There are 3 different groups, recognizable in Figure 16: the Ortles-Cevedale and Adamello groups with Sforzellina, Careser, De la Mare, Vedretta Lunga and Fontana Bianca glaciers; the Eastern Venoste Alps where there are the 4 Austrian glaciers Hintereisferner, Kesselwandferner, Vernagtferner and Langtalerferner; the Stubai Alps with Malavalle and Vedretta Pendente.

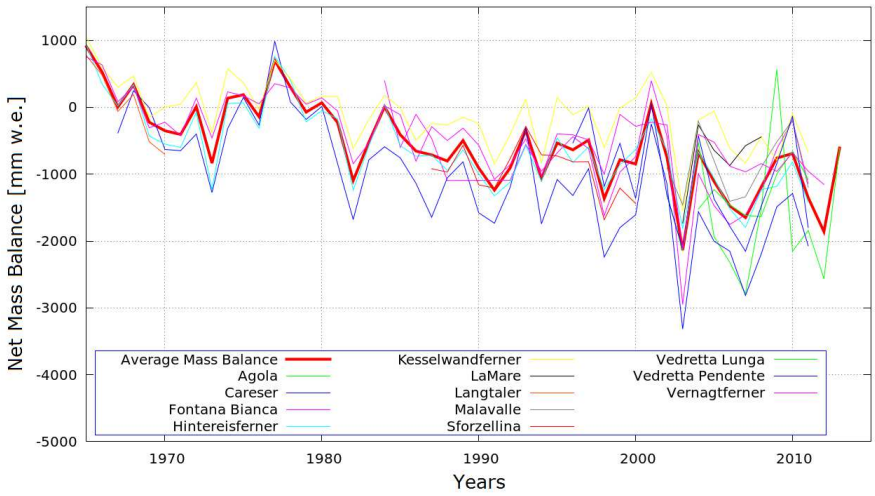

Figure 17: Net mass balance of Central-Eastern glaciers, with their average trend.

In this sector, the Careser glacier has the longest series of Italian glaciers (since 1967) and we can evaluate three Austrian glacier with very intresting mass balance series, good size and high elevation: Hintereisferner, Kesselwandferner (since 1954) and Vernagtferner (since 1965).

From Figure 17 is evident that the entire group of glaciers have a heavy negative behavior and the Careser is the less conservative of this sector.

A peculiarity is the evolution of Hintereisferner, Kesselwandferner and Vernagtferner: the first is the less conservative, the second the most conservative and the third one has the mass balance similar to the average trend. In conclusion, in spite of their proximity and similar climate conditions, they have different maximum altitude and minimum altitude, which diversify the climate forcing on their surfaces and their mass balance trends.

Eastern Alps

In this sector, there are 7 glaciers, only 1 at Italy and 6 Austrian glaciers (Fig. 18). All these glaciers are at Noriche Alps: the Western Ries glacier (subset of Pusteresi Alps) and Filleck, Sonnblick, Pasterze, Goldberg, Kleinfleiss and Wurten.

Figure 18: Eastern Alps, 7 glaciers.

We can recognize (Fig. 18) two principal groups: the Goldberg group (Kleinfleiss, Wurten, Voc.Ochsenkar) and the Sonnblick with Filleck. These last two glaciers were a unique body of ice and they have a very similar mass balance values. Eastern glaciers are smaller than 2 Km^2, except the Pasterze. These shapes and size contribute to generate their preservative and coherent trends, exposed to continental streams.

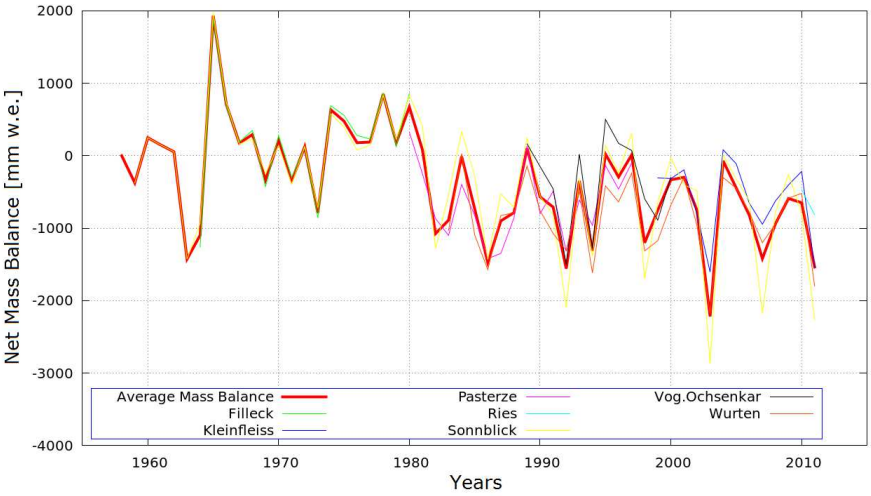

Figure 19: Net mass balance of Eastern glaciers, with their average trend.

In this sector (Fig. 19), we can have distinguished two different periods: the first has a moderate accumulation and ends at the peak 1981 and the follow is characterized of an important melting. From the 1958 to 1981, the average gradient is about +121 mm/year, whereas at period 1982 – 2011 is about -750 mm/year. The most negative glacier is the Pasterze glacier, with -1193 mm/year from 2004 to 2011.

Climate dataset of the GAR region

Gridded datasets for temperature and precipitation

	Res. °	Start and end date		Reference
		Temperature	Precipitation	
HISTALP	0.08°	1780 – 2008	1801 – 2003	Auer et al. 2007
CRU v. 3.22	0.50°	1901 – 2013	1901 – 2013	Harris et al. 2014
E-OBS v. 10.0	0.25°	1950 – 2014	1950 – 2014	Haylock et al. 2008

Table 2: Characteristics of the three gridded datasets used to study the climate of the GAR region. Res. = Resolution (degree).

In collaboration with Balocco (Balocco master thesis, 2015), we analysed three gridded datasets widely used in climatology covering the GAR region, to apply climate forcing on mass balance. These datasets are summarized by Table 2 with their resolutions, start and end date.

HISTALP consists of monthly-homogenised records of temperature and precipitation for the GAR with resolution of 0.08° x 0.08°. The longest series of temperature extend back to 1780, precipitation to 1800 (Auer et al., 2007).

CRU dataset is provided by the Climate Research Unit (CRU), University of East Anglia, Norwich, and contains information on observed surface air temperatures and precipitation overland on a 0.5° x 0.5° (Harris et al., 2014).

Haylock et al. (2008) describe E-OBS as the first high-resolution gridded data set of daily climate over Europe. The European Climate Assessment & Dataset (ECA&D) contains daily land station observations throughout Europe and the Mediterranean. The data is provided by National Meteorological Services, Universities as well as by other data providers. The station series are then blended with those from nearby stations and the Global Telecommunication System (GTS) to create series that are as long as possible. In addition, homogeneity checks are done and climatology are calculated. Daily observations were compiled for precipitation and minimum, maximum and mean surface temperature, covering the period 1950–2006. Although the final grids produced in the data set were spaced with a resolution of 0.25° x 0.25°.

To compare these data sets, as they have different resolutions, Balocco remapped their monthly values from their original resolution to the coarsest grid, defined by CRU (0.5° x 0.5°).

Gridded analysis: summer temperature

As we can see from Figure 20, all data sets agree and show a significant positive trend. CRU, E-OBS and HISTALP show mean values of trend 0.24 ± 0.05° C/10y, 0.23 ± 0.06° C/10y and 0.28 ± 0.02° C/10y. Approximately, this trend is equivalent to an increase in temperature of 1.4° C/50y in the GAR region over the last 6 decades (Balocco master thesis, 2015).

As far as scientific literature is concerned, the values of trend in summer air temperature is pointed out on average 1.02 °C to 1.10 °C warmer during the period 1991 – 2010, than the base period 1961 – 1990 in the Alps (Braithwaite et al., 2013). Also is advised that climate change in the Alps during the 20th century has been characterized by increases in minimum temperatures of over 2° C (Beninston, 2000).

This temperature increase follows the global warming and is slightly larger than the global trend reported at 2013: the IPCC point out the values of trend about 0.18 ± 0.03° C/10y during the period 1951-2012.

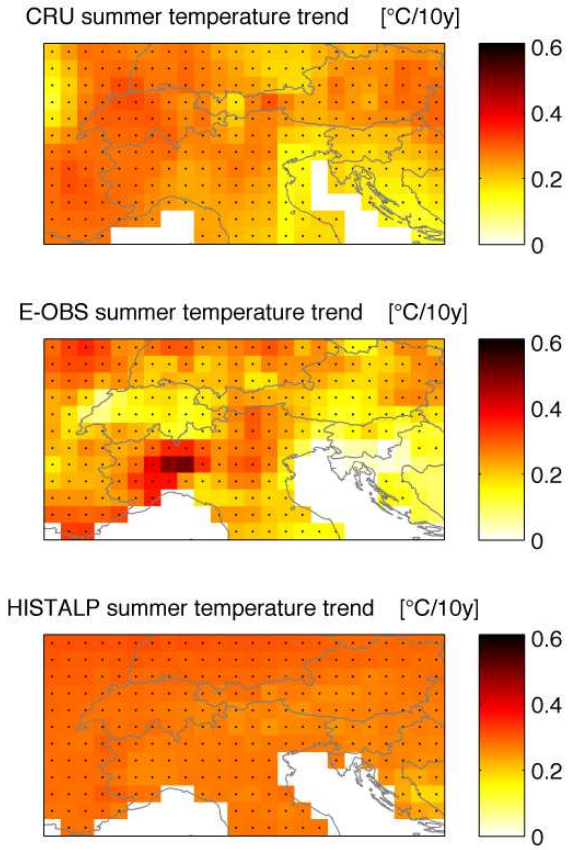

Figure 20: Summer temperature trends, May - September, over the GAR region (1950 - 2008), (Balocco master thesis, 2015).

Gridded analysis: winter precipitation

Analysing Figure 21, we can see a trend of winter precipitation with a Southeast - Northwest gradient. NW sectors is affected by a positive trend in precipitation, while SE sectors seem to show a negative trend (Balocco master thesis, 2015). There is a division between Northern and Southern sectors of the GAR, with positive and negative trends respectively, which represent a first different climate contribution to Alpine glaciers.

As far as scientific literature is concerned, it is possible to find a description of a significant decrease of summer precipitation on the Southern flank and a not always significant increase in the North of the Alps. The precipitation trends in the GAR are very sensitive to the choice of the time window considered. In fact, the actual contribution in precipitation comes from autumn, winter and spring period (Brunetti et al., 2006).

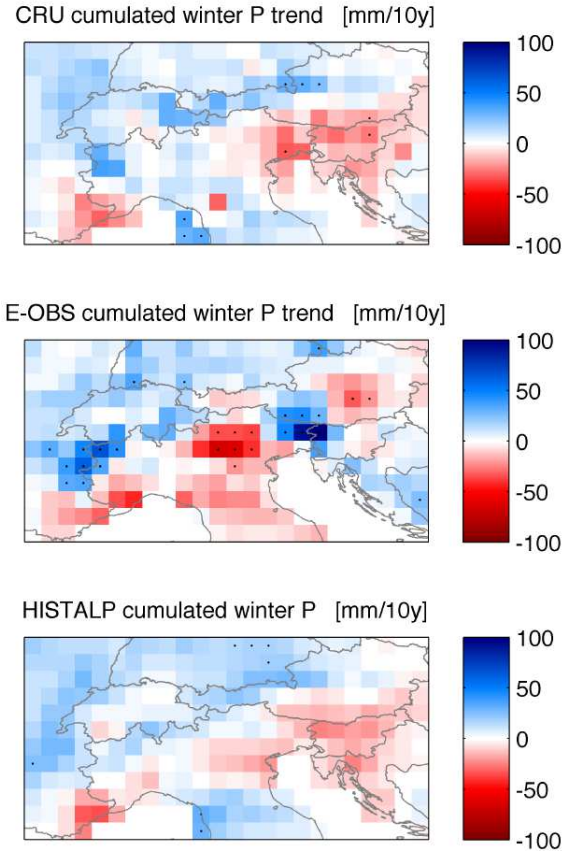

Figure 21: Winter precipitation trends September - May, over the GAR region (1950 - 2003), (Balocco master thesis, 2015).

Another research regards different short time period for winter precipitation: for period 1901 – 1990 it is shown a positive trend in precipitation in the NW sector during

winter and a negative trend during autumn in the South Alps (Schmidli et al., 2002). On the other hand, other studies focused their attention on climate variability in the western Italian Alps and found that no significant trend is present in this region (Casty et al., 2005, Durand et al., 2009).
Nonetheless, Figure 21 evidences more differences between E-OBS and the other two datasets than between CRU and HISTALP. The more significant trends in precipitation of E-OBS is probably due to the high density of the stations in these regions that, with an inaccurate homogenization, may cause noise during the interpolation and downscaling of gridded data. These "noised" pixels are outside the location of our studied glaciers, and then this dataset is useful to our analysis.

Models for mass balance functions

Now the analysis of the response of glacier mass balances to climate forcing variables is fundamental to create a function that relate the climate variables to the input values of MGM.
After an accurate evaluation of climate contribution, in our approach, temperature and precipitation are considered as proxies for the much more complex set of meteorological and environmental conditions, which affect glacier dynamics. For instance, incoming solar radiation and cloudiness can play an important role, but are ignored because we wanted to evaluate a simplified empirical model that uses only temperature and precipitation (the most commonly available data extending back to 1950).
To drive the results with the empirical models, it was used precipitation and temperature data coming from three different data sets: CRU, E-OBS and HISTALP. As far as scientific literature is concerned, there are few mass balance models, which are based on gridded data sets. Some used HISTALP data set to reconstruct inter annual mass balance variability of glaciers in the Alps; nobody used CRU and E-OBS before our project (Balocco master thesis, 2015).

Best method for mass balance function

Then the aim is to find the relations that link the series of summer temperature and winter precipitation to mass balance, and therefore assessing climate sensitivity of glacier behavior. We focused the investigation on 13 glaciers with more than 30 years of data during the period 1950-2013 to have a more robust statistical analysis.
The analysis tested different models to relate mass balance variability to summer temperature and winter precipitation, using Akaike Information Criterion. The AIC is a measure of the relative quality of statistical model for a given set of data, referred to other models and not evaluates the absolute value of a hypothetic model. The chosen model is the one that minimizes the Kullback-Leibler distance between the model and the truth. AIC is founded on information theory and gives a relative estimate of the

information lost when a given model is used to simulate the process that generates the results. It is as a criterion that seeks a model that has a good fit to the truth but few parameters to generate this fit (Burnham, 2003).
In addition, Balocco ensured that no significant statistical structure is left out of the model, in other words the stochastic component residuals of the model must be Gaussian, did not show a trend and was non-autocorrelated in time.
The starting point is the assumption that mass balance can depends on combinations of temperature and precipitation:

$$\dot{b} = f\left(T, T^2, P, P^2, TP\right) \qquad (3.1)$$

where $\dot{b}$ is mass balance, T is mean summer temperature and P is cumulated winter precipitation. Generally, from Balocco thesis, the best model to be considered in explaining mass balance variability $\dot{b}_i$ is the model that linearly combines summer temperature $T_{s,i}$ and winter precipitation $P_{w,i}$ (Balocco master thesis, 2015):

$$\dot{b}_i = aT_{s,i} + bP_{w,i} + c \qquad (3.2)$$

A most parsimonious model using only temperature as predictor also showed high performance. As far as the significance of the T and P predictors is concerned, T is always a significant predictor, while P is non-significantly different from zero only for some glaciers. Due to this consideration and to the analysis of the weights of precipitation and temperature in the eq. 3.2 mass balances of the glaciers considered seem to be mainly influenced by temperature rather than by precipitation. This means that, if summer temperature keeps rising at present rate, mass balance of Alpine glaciers will be increasingly negative (Balocco master thesis, 2015).

Final climate application and results on GAR

During the work of the master thesis of Maffezzoni, we analysed the different behaviours of climate dataset on GAR to classify them according to summer temperature and winter precipitation trends.

Classification North-South

The geographical position is the most important factor of alpine glacier's health (Evans, 2006), and although dominated by winds from the west, the alps are unusual in comparison with other mid-latitude regions, where strong linear gradients are found as precipitation diminishes away from west coasts for example in the Western Cordilleras of America (Østrem et al., 1981; Evans, 1990). This happens because Alps

receive precipitation and winds from various direction (Frei. C. and Schär. C., 1998) and the differences is due to east–west elongation of the Alps, their curvature, and the generation or revival of cyclonic systems on the Po Plain on their southern flank (Cantu, 1977).

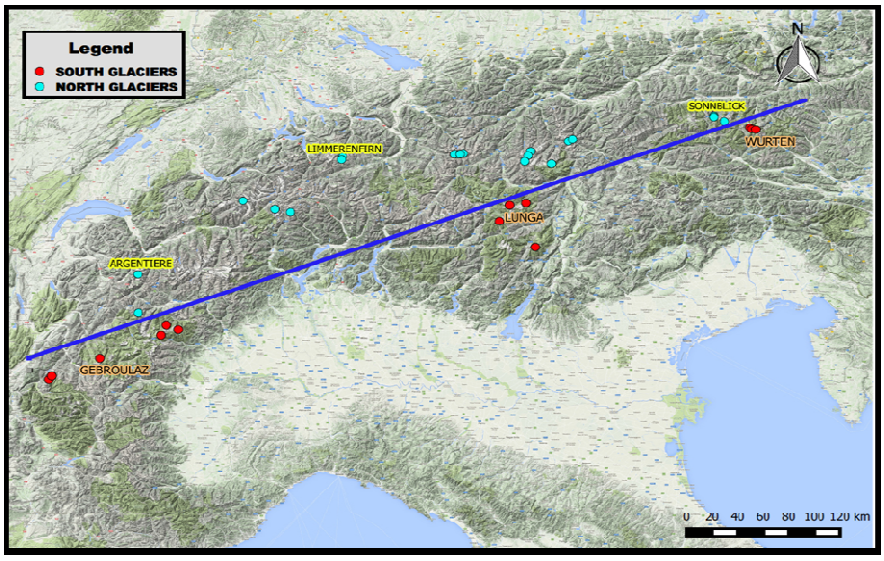

Figure 22: The Alpine glaciers are divided into two different groups by transect (blue line): Southern glaciers, red dots, and Northern, light blue dots (Maffezzoni master thesis, 2015).

Moved by this climate knowledge and, as seen before, by a different precipitation gradient between Northern and Southern glaciers, we divided our sample into two classes, by a simple manually digitized transect (Fig. 22): North glaciers above transect and South Glaciers under. This transect is angle as the curvature of the Alpine chain.
Then, we started using the two categories of glaciers, that are divided by transect, to individuate some particular cluster distributions, some marked trends or some differences between them. We focused our attention on the correlation between two different kinds of mainly dependences of glaciers: climate and topography (Oerlemans, 2001).
We analysed the Alpine glaciers with E-OBS climate data, to classify different behaviors. Because of the extreme natural system variability and the reduced number of analysable glaciers, we did not make other classifications under those to obtain a significant statistic.

Winter precipitation: Northern and Southern glaciers

Winter precipitation series in Figure 23 (November – March) of Northern glaciers show irregular trends, within a range from 200mm/season to 1400mm/season. These trends follow the same oscillation frequencies with similar up and down tendency.

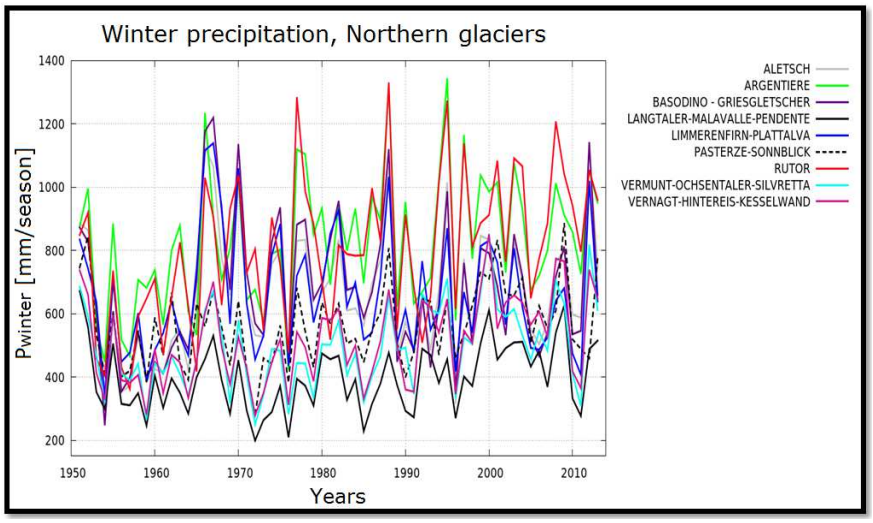

Figure 23: Winter precipitation of Northern Glaciers, 1951-2013.

The average rainfall of entire Northern group shows a positive gradient of about +120 mm/season. Within this sector, the Northwestern glaciers, as Argentiere and Rutor, usually have a larger amount of precipitation, about 800 mm/season, then others. The glaciers of Central Alps, as Vermunt or Pendente, have the lowest rainfall accumulations, under 500 mm/season.

The winter precipitations trends for Southern glaciers are irregular and span from 50 mm/season to 1300 mm/season (Fig. 24).

Considering the average rainfall of entire sector, the trend line shows a positive gradient of about +120 mm/year as Northern sector. The South-Western Glaciers, as Sarennes, Grand Etret and Timorion, received the greatest precipitations with an average of 700 mm/season. The Southeastern glaciers, as Wurten and Vog. Ochsenkar, get about 550 mm/season. The glaciers situated in the Central Alps, as Lagol and Fontana Bianca, received not more than 400 mm/season with minimum around 50 mm/season during the period 1995 – 2000.

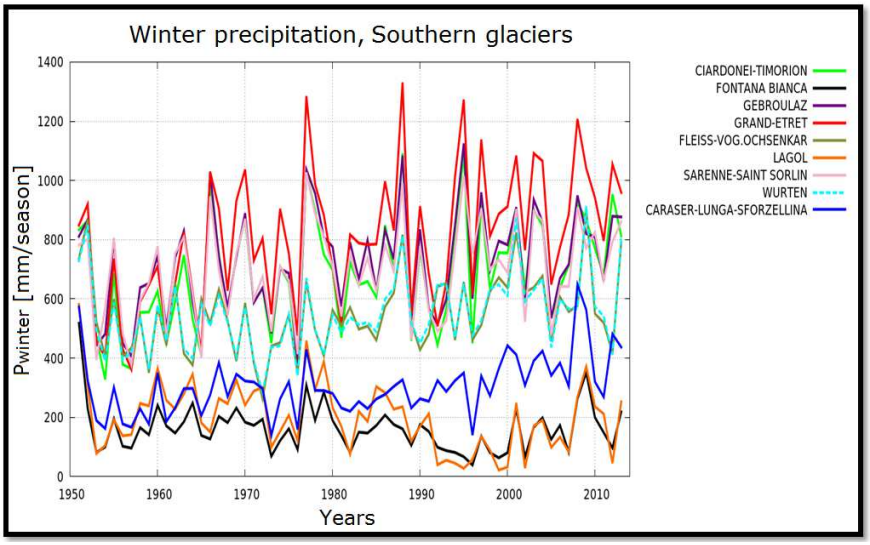

Figure 24: Winter precipitation of Southern Glaciers, 1951-2013.

In Figure 25, we compared the average cumulative precipitation of studied glaciers on the longitudinal position. There are 3 different clusters: North-Western and South-Western glaciers (violet circle) received more precipitations, around 750 mm/season, than Eastern glaciers (orange circle), 550 mm/season. The Central glaciers have the littlest amount of precipitation, under 100mm/season, and between Northern and Southern glaciers there is a gap of about 200 mm/season or more.

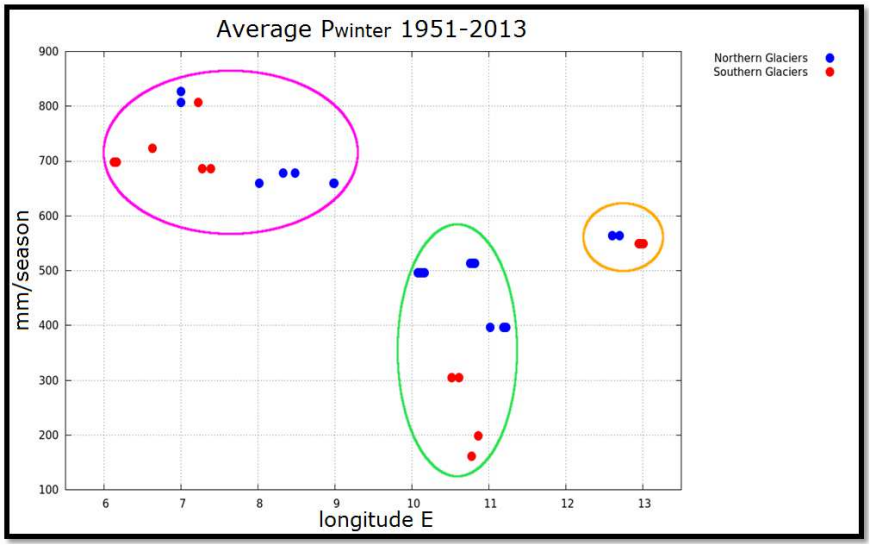

Figure 25: Average seasonal cumulative precipitations, period 1951 - 2013. Blue dots are Northern glaciers and red dots are Southern glaciers.

Typical weather situation about precipitation

Because of the geographical position of the Alps (arc from France to Eastern Austria and Italy), they include oceanic, continental, polar, Mediterranean and, on occasion, Saharan influences as a climate crossroads of them (Beniston, 2006). The Alpine arc is also dominated by wind streams from West and is subjected to the influence of many air masses of different nature, receiving precipitation from various directions (Frei, Schär, 1998).

There are two most important meteorological conditions: convective and advective weather situations. Convective situation is not controlled by macroscale pressure systems and usually occurs when high-pressure cells or low-pressure cells are far away from the Alps, therefore local differences in temperature will cause small high and low pressure zones, with local winds and rainfall. Advective situations is caused by a macro-scale wind, which is generated by large pressure systems: for example, a high pressure over the Azores and a low pressure over Iceland generate Westerlies.

Generally, advection is applied to a horizontal movement of air over several hundred km and we can observe two kinds of precipitations: cyclonic precipitation, that is formed when two masses of air of different temperature, humidity and density meets, or orographic precipitation, when airflows over the mountain ascend and cool down (Fig. 26).

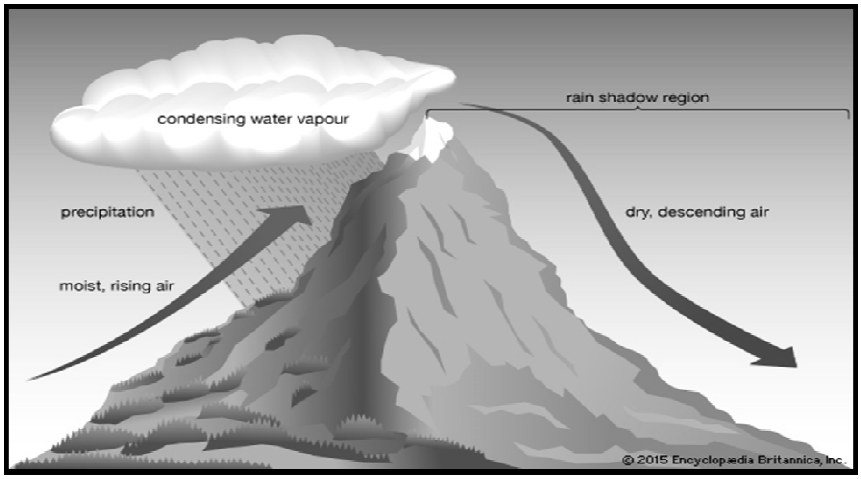

Figure 26: Orographic precipitation is produced when moist air is lifted as it moves over a mountain range. As the air rises and cools, orographic clouds form and serve as the source of the precipitation, most of which falls upwind of the mountain ridge. (Encyclopaedia Britannica, 2015).

Now we want to explain the different behavior of precipitation on the Alps (Maffezzoni master thesis, 2015).

The west winds blow more than 50% of the year over the Alps. This weather regime is important, related to precipitation: humid air flows in high altitude from the Atlantic towards Europe. Then polar front waves with low pressure cells drift over Central Europe. When the low pressures (Extratropical Cyclone) come from North-West or

North (Fig.27), the rainfall are higher on the W-NW of the Alps than on the S-SE, because of the orographic precipitation (Fig. 26).
Sometimes, several cyclonic systems from the Mediterranean Sea flow across Tyrrhenian Sea and Po plain and strike their precipitations on the South-South Eastern flanks of the Alps.
We can conclude that entire Alpine arc is subject to the influence of Atlantic or Mediterranean storm and the Western Alps are the most influenced by both these weather situations, because of their proximity. It could be the reason why the West sector of GAR receives the highest amount of winter precipitation (Fig. 25).

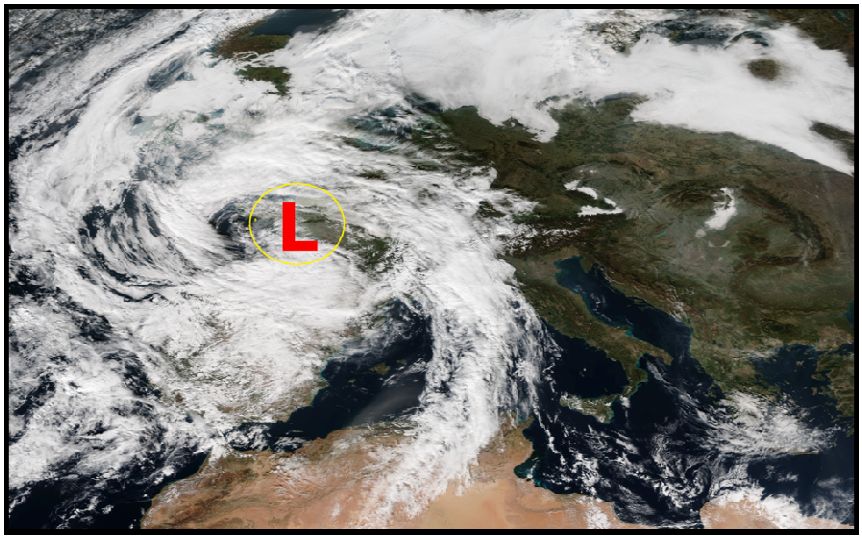

Figure 27: Extratropical Cyclone moves from the France to East. This situation generates a warm front over Western Alps.

However, typically from November to April, another baric situation occurs over the Europe when Azores anticyclone lies in the Northwest of Europe, creating low pressures near or over Adriatic Sea (Fig. 28). It becomes source of precipitations which affecting the Eastern sector (South and North flanks) of the Alps (Fig. 25), not so different to the Wester contribution.

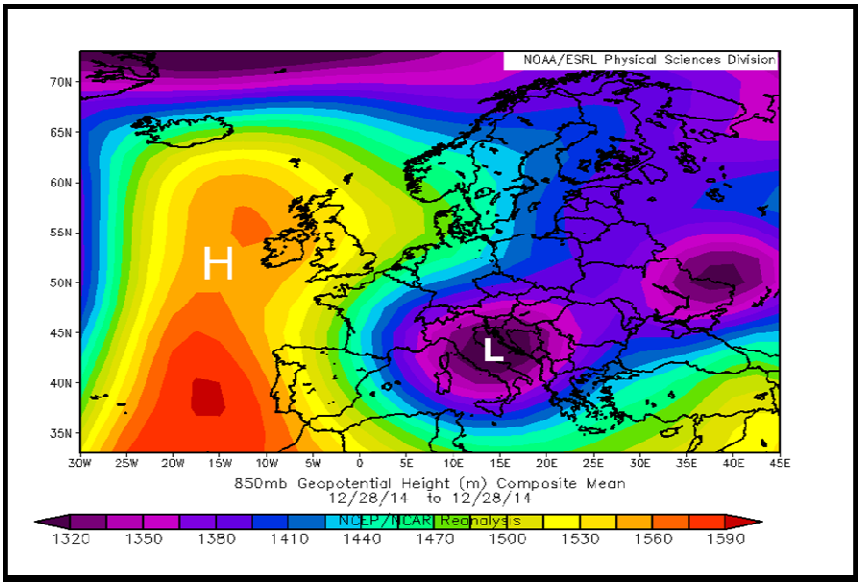

Figure 28: High pressure over Great Britain and Low pressure over Adriatic Sea that creates precipitations over Eastern sector.

In conclusion we can obviously notice that Central glaciers less influenced by both situations, but we observed in Figure 25 that exists an important gap between North and South glaciers. This is due to the "snowfall shadows" of the Southern glaciers because their protected geographical position within mountain chains. On the other side, when sometimes low-pressures come from Baltic or North Sea, the Central Northern Alps receive important orographic precipitations.

Summer temperature: Northern and Southern glaciers

Summer temperatures (May – September) of Northern glaciers show irregular and coherent trends, within a range from 2 °C to 14 °C (Fig. 29). Considering the average temperature, during the decade 1970 – 1980 there was a general decrease with a followed an increase trend with positive gradient of about 1,5 °C. The sector with Vernagtferner, Hintereisferner and Kesselwandferner usually have the lowest temperature, the Central glaciers were around 6.5°C and 8°C before and after 2000 respectively and the Weastern glaciers, as Aletsch, Argentiere, Basodino, Griesgletscher, Limmernfirn and Plattalva show the highest temperature, about 11°C during the last 13 years.

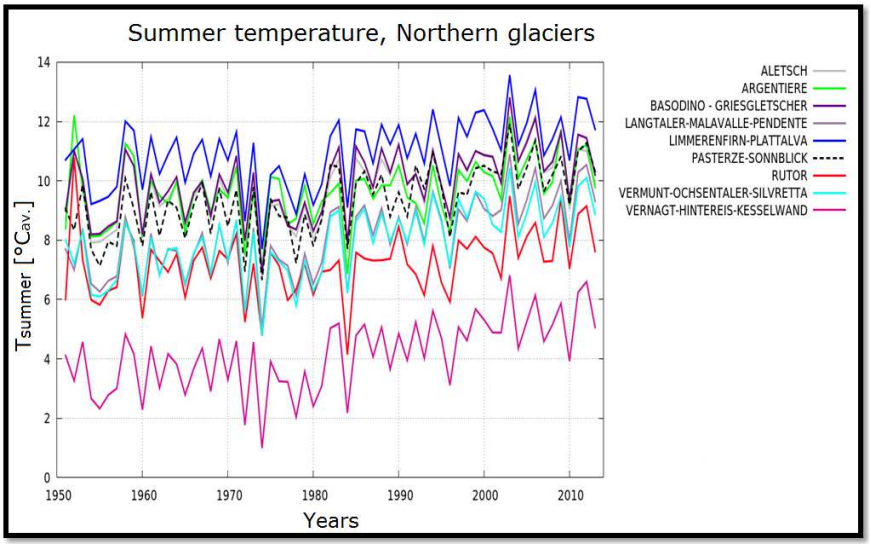

Figure 29: Summer temperature of Northern Glaciers, 1951-2013.

Focusing on Southern glacier, we can see an irregular but coherent trend span within 4 °C and 20 °C, with two important gap (Fig. 30). It is visible a low decrease during 1970 – 1980 and a followed increase of about 2 °C as before.

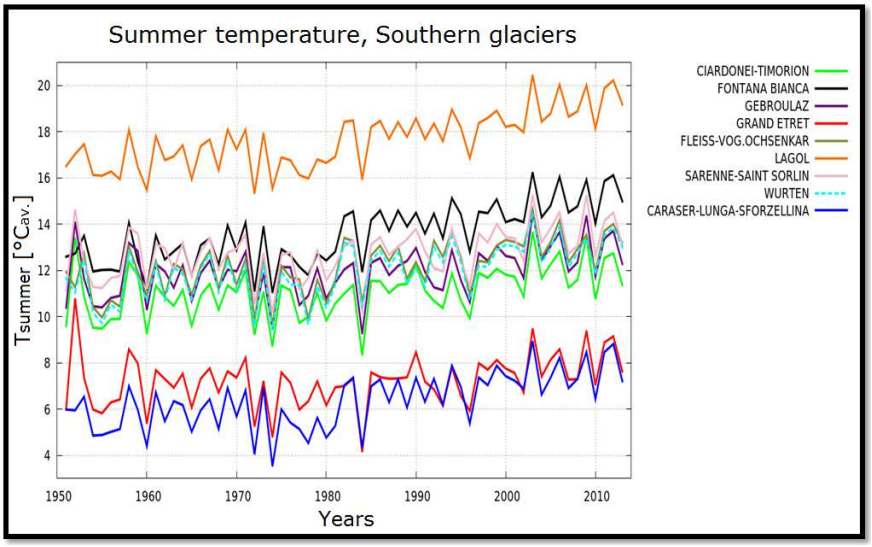

Figure 30: Summer temperature of Southern Glaciers, 1951-2013.

Lagol glacier is the most Southern with the highest temperature and the glaciers with the lowest temperature are the Central ones, as Careser, Vedretta Lunga e Sforzellina.

Typical summer temperature condition

Calculating the average seasonal temperature during 1951 – 2013, we can see a quite different behavior between Northern and Southern glaciers, divided by an imaginary line at 11 °C (Fig. 31).

This different behavior is due to the proximity of Southern glaciers to the subtropical zone and subtropical anticyclones, which are hot air masses, influence them. In addition, the temperatures also decrease starting from the West side, due to the location of high pressure over the Alps.

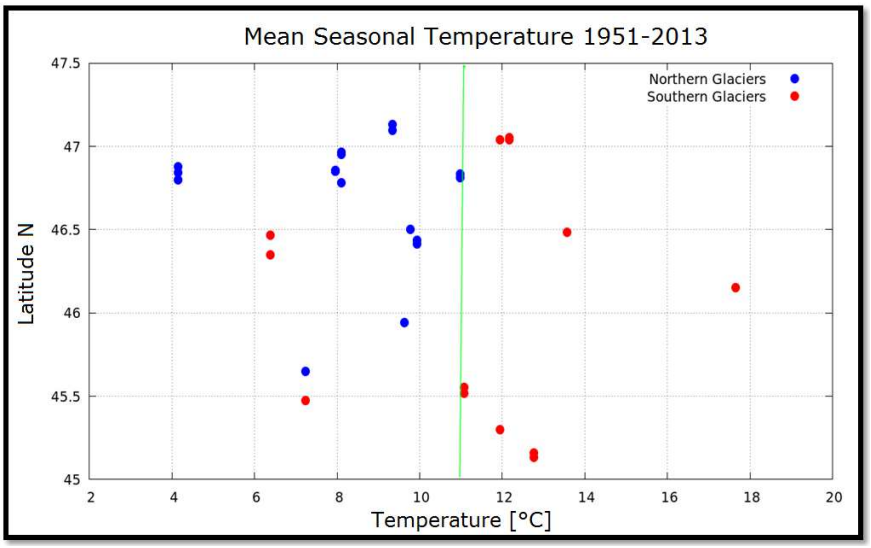

Figure 31: Average seasonal temperature, period 1951 - 2013

In fact, during summer period both Azores and North African anticyclone usually place their maximum geopotential height closer to the Western Alps (Fig. 32). From here, the air temperatures follow a dynamic high pressure that diminishes towards the Central Alps and the temperatures are highest over West than East sector (Fig. 33) (Lolis et al., 2002; Bartzokas, 1989).

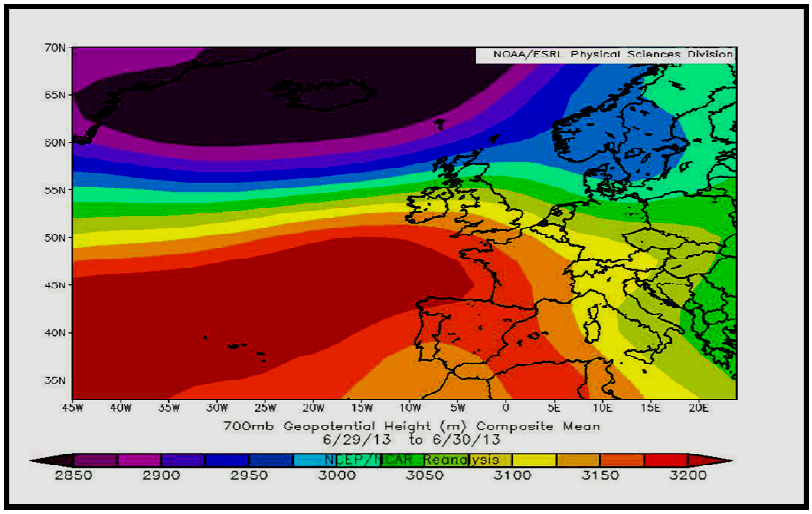

Figure 32: 700 hPa (3000 meters) Geopotential Height Maps. The Anticyclone over the Azores with tongue extended towards west Europe to Western Alps.

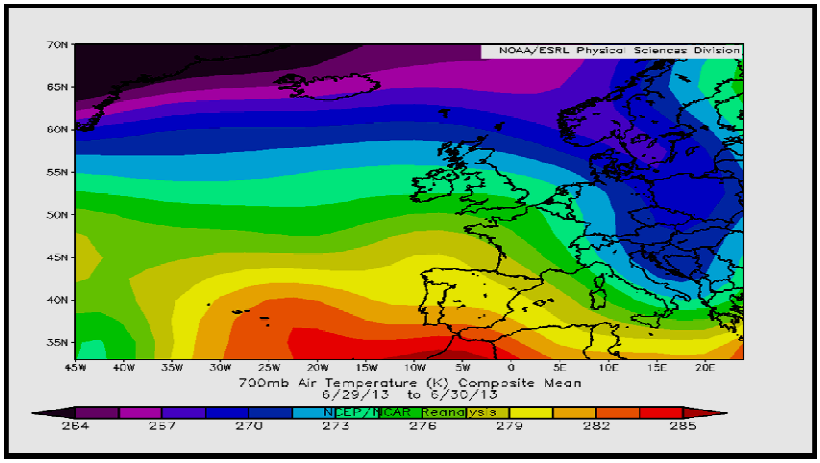

Figure 33: This map is the same as Figure 32, referring to the temperature at 770 mb height.

Future climatic dataset

Therefore, we analysed the mass balance dataset and the climate dataset of the period 1951 – 2013, and we defined the mass balance transfer function driving by climate forcing. These are the elements as statistical basis to prepare the future evolution of Alpine glaciers.

Afterwards, to drive the MGM for future climate conditions, I used the NASA Earth Exchange Global Daily Downscaled Projections (NEX-GDDP) dataset: 11 terabytes of data predicting temperature (Fig. 34) and rainfall.

This data is comprised of downscaled climate scenarios for the globe that are derived from the General Circulation Model (GCM) runs conducted under the Coupled Model Intercomparison Project Phase 5 (CMIP5) (Taylor et al., 2012) and across two greenhouse gas emissions scenarios known as Representative Concentration Pathways (RCPs) (Meinshausen et al. 2011).

The CMIP5 GCM runs were developed in support of the Fifth Assessment Report of the Intergovernmental Panel on Climate Change (IPCC AR5). The NEX-GDDP dataset includes downscaled projections for RCP 4.5 and RCP 8.5 from the 21 models and scenarios for which daily scenarios were produced and distributed under CMIP5 (Table 3). The purpose of these datasets is to provide a set of global, high resolution, bias-corrected climate change projections that can be used to evaluate climate change impacts on processes that are sensitive to finer-scale climate gradients and the effects of local topography on climate conditions.

Model ID	Institution ID	State
ACCESS1-0	CSIRO-BOM	Australia
bcc-csm1-1	BCC	China
BNU-ESM	BNU	China
CanESM2	CCCMA	Canada
CCSM4	NCAR	USA
CESM1-BGC	NSF-DOE-NCAR	USA
CNRM-CM5	CNRM-CERFACS	France
CSIRO-Mk3-6-0	CSIRO-QCCCE	Australia
GFDL-ESM2G	GFDL	USA
GFDL-ESM2M	GFDL	USA
inmcm4	INM	Russia
IPSL-CM5A-LR	IPSL	France
IPSL-CM5A-MR	IPSL	France
MIROC5	MIROC	Japan
MIROC-ESM-CHEM	MIROC	Japan
MIROC-ESM	MIROC	Japan
MPI-ESM-LR	MPI-M	Germany
MPI-ESM-MR	MPI-M	Germany
MRI-CGCM3	MRI	Japan
NorESM1-M	NorCC	Norway

Table 3: List of GCM conducted under the CMIP5 and downscaled for the NASA NEX-GDDP dataset.

The demand for downscaling of GCM outputs arises from two primary limitations. First, most GCMs are run using resolution grids with cell sizes of a few degrees or hundreds of km, which limit their ability to capture the spatial details in climate for regional or local analyses. Second, the GCMs may produce projections that are globally

accurate but locally biased in their statistical characteristics when compared with observations.

The Bias-Correction Spatial Disaggregation (BCSD) method used in generating the NEX-GDDP dataset is a statistical downscaling algorithm specifically developed to address these current limitations of global GCM outputs (Wood et al., 2002; Wood et al., 2004; Maurer et al., 2008; Thrasher et al., 2012). The algorithm compares the GCM outputs with corresponding climate observations over a common period and uses information derived from the comparison to adjust future climate projections so that they are (progressively) more consistent with the historical climate records and, presumably, more realistic for the spatial domain of interest. The algorithm also utilizes the spatial detail provided by observationally derived data sets to interpolate the GCM outputs to higher-resolution grids.

The spatial resolution of the dataset is 0.25 degrees (~25 km x 25 km). Each of the climate projections includes the periods from 1950 through 2005 (Retrospective Run) and from 2006 to 2099 (Prospective Run) (Fig. 34).

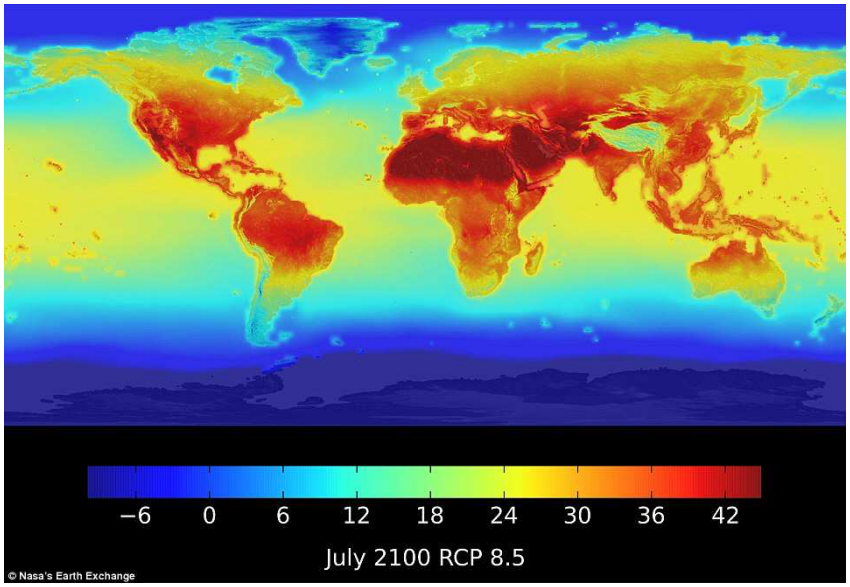

Figure 34: Maps of maximum temperatures (°C) produced using NASA new climate projection data set for RCP 8.5. In North Africa, the Middle East and northern India maximum temperature will exceed 45°C by 2100 (NASA's Earth Exchange http://nex.nasa.gov).

In conclusion, I chose the E-OBS historical dataset to apply the transfer function (eq. 3.2) and to drive the mass balance records with a climate forcing, comparable with the resolution of these GCM from NEX-GDDP dataset (about 0.25° x 0.25° as in previous paragraphs).

Chapter 4: First calibration of MGM

Adopting a description based on the MGM approach and improved by an intensive use of GIS information, I want to calibrate this procedure investigating the dynamics of two important glaciers on the southern side of the Alps, namely the Careser glacier in Ortles-Cevedale group, eastern Italian Alps, and the Rutor glacier in Aosta Valley, western Italian Alps. The Careser glacier has a complicated shape and history; we will discuss discrepancies between model outputs and observations, which provide relevant information on the glacier dynamics.
After comparing the model results with the available data for the two glaciers under study, we estimate the future behaviour of these two glaciers. I used the climatic drivers provided by a set of General Circulation Model (GCMs) participating in the Climate Model Intercomparison Project 5 effort (CMIP5) (Knutti et al., 2013; Taylor et al., 2012) without downscaling analysis as explained in the previous paragraph. I also estimated the uncertainty and the reliability of the glacier projections by using the ensemble of model runs provided by the CSIRO-Mk3.6 model (Jeffrey et al., 2012), also available from CMIP5.
This is the preparatory work of first and second year, formulating the correct algorithm of MGM by using Fortran and Python programming languages (Appendix A) to interconnect the GIS analysis and the suggested applications (MGM on-line Chapter 2, and r.glacio.model Chapter 5) (Strigaro et al., 2015).

Study cases and available dataset

Careser Glacier

The Careser glacier (Vedretta del Careser, 46°27'08.45" N 10°42'42.63" E) is located on the right side of Val di Pejo, called Val de la Mare, eastern Italian Alps (Fig. 35a).
This glacier is part of a catchment lying in the southern part of the Ortles-Cevedale massif, which includes the artificial lake Careser and generates the Noce River. The Careser glacier begins at the pass between Marmotta peak and the three Venezia peaks (about 3330m a.s.l. and 3390m a.s.l.).
The Careser glacier is the residual accumulation area of a much wider glacier that exhibited a well-developed valley tongue during the Little Ice Age. Mass balance and Equilibrium Line Altitude (ELA) measurements have been carried out since 1967 and the data series, the longest one for the Italian Alps, continues up to today without interruption (Zanon, 1982; Carturan and Seppi, 2007, 2009; Carturan et al., 2009a, 2012, 2013).

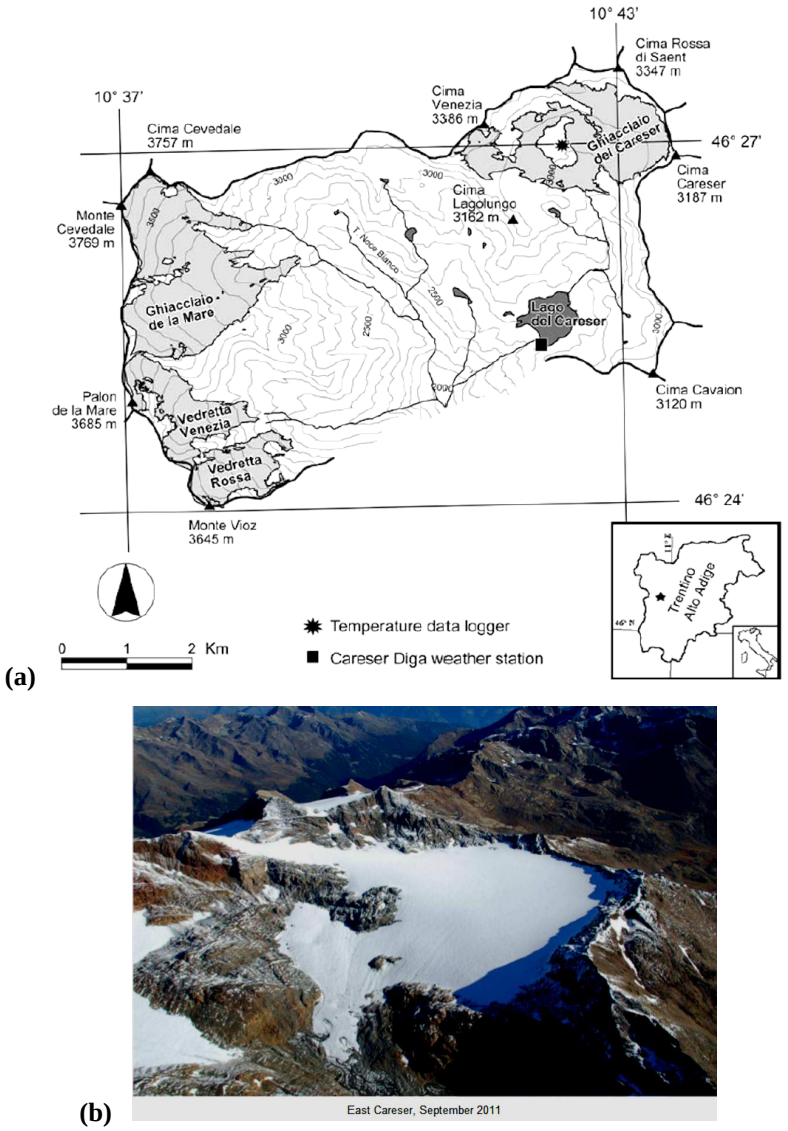

Figure 35: (a) Geographical setting of Careser glacier in Val de la Mare, Pejo (TN); (b) Eastern part of the Careser glacier, representing 90% of the total glacier area at 2011 (photo by TESAF – unipd).

A strongly negative mass balance (Fig. 36a) in the last decades resulted in huge morphological changes of the glacier. Positive feedbacks contributed to accelerate the ablation processes and the fragmentation of the ice body. In 2012, 90% of the remaining glacier area was located in the eastern part of the Careser (Fig. 35b). From 1981, the ELA was mostly above the highest elevation of the glacier, with just a few exceptions (Fig. 36b). Currently, the Careser glacier has no accumulation area and its complete extinction is thus expected within a few decades, as discussed below.

In addition to glaciological data, two weather stations have been operated in Val de la Mare since the 1920s: Careser Diga (2605m a.s.l.) and Cogolo (1200m a.s.l.), recording 2m air temperature and precipitation.

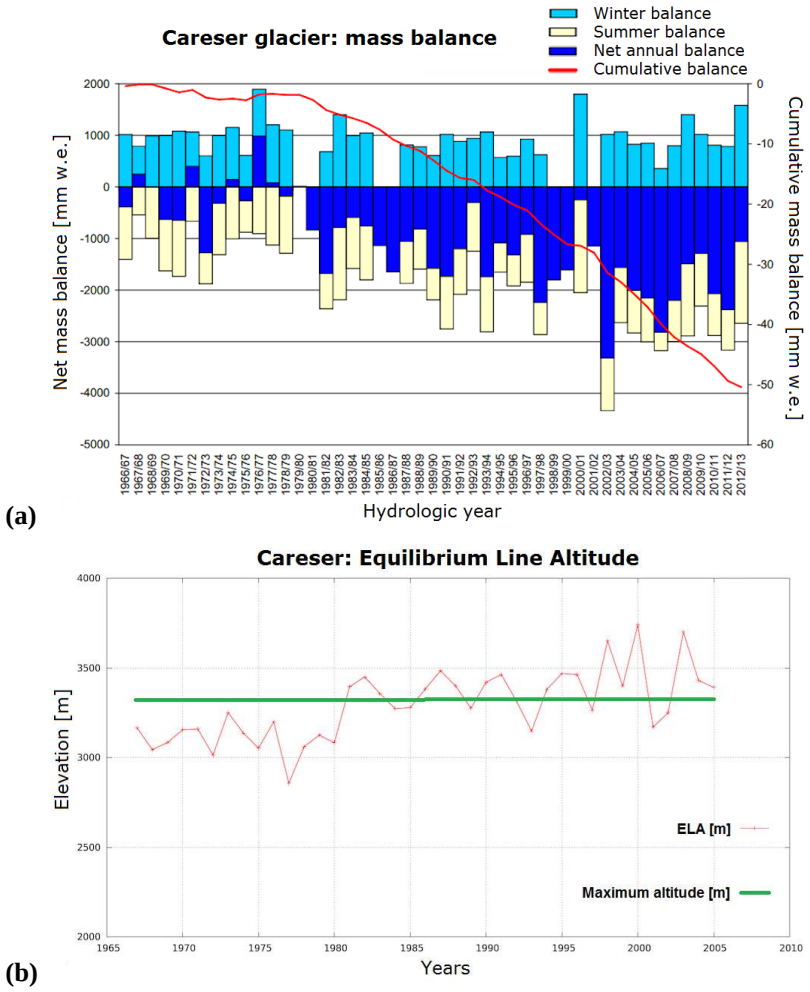

Figure 36: Available data for the Careser glacier: (a) cumulative and net seasonal mass balance; (b) Equilibrium Line Altitude, compared with the maximum elevation of the glacier.

Rutor glacier

The Rutor glacier (45°37'54.35" N 7°00'50.32" E) is located in the Rutor Massif, La Thuile Valley (Val d'Aosta) in North-Western Italy (Fig. 37a). The Rutor is one of the largest glaciers in the Italian Alps, with a surface area of 8.5 square kilometres. It has an approximately rectangular shape and a rather flat surface morphology.

(a)

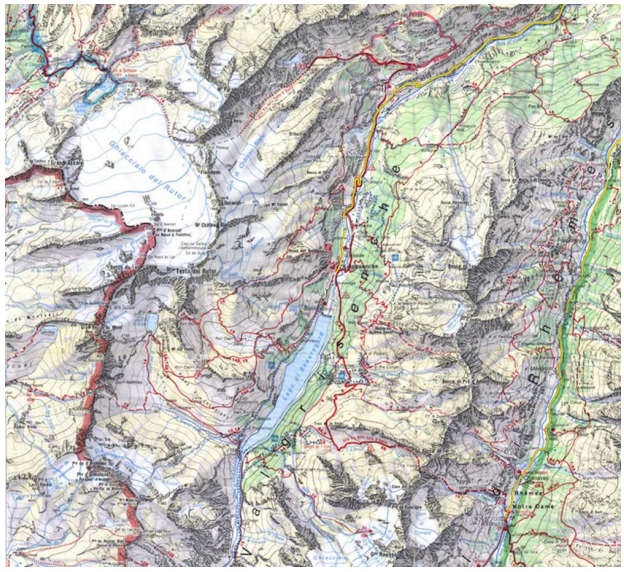

(b)

Figure 37: (a) Geographical setting of the Rutor glacier in La Thuile Valley (AO); (b) Rutor glacier, NW view.

The Rutor glacier faces mainly North-West, with an altitude range between 3440 m a.s.l. and about 2450 m a.s.l. (Fig. 37b). The Rutor is bound South-Westerly by the French/Italian border, to the South by the Testa del Rutor peak and the Saint Grat Dessus and Moriond Dessus glaciers, to the East by the Doravidi group, Tsassè Blanc Glacier, and Flambeau and Invergneures glaciers, and to the West by the Grande Assaly Glacier. In the Rutor valley, many natural lakes occupy the cavities left by the retreating glacier front and they are filled mostly with glacial meltwater and sediments, converging in the Rutor torrent downstream. The position of the glacier snout has been surveyed, albeit not regularly, by the Italian Glaciological Committee since the beginning of the last century, 1916 (Villa et al., 2007, 2008). The Rutor mass balance has been measured since 2004.

GIS analysis and model parameters

Careser glacier

For the Careser glacier, a large amount of maps and cartography/geomorphology studies are available. As a result, several DEMs were created, using data collected by remote sensing techniques and land surveying starting from 1933. The last product is a DEM with resolution 2x2m, derived from a Lidar aerial survey in 2007 (Carturan et al., 2013). Using DEMs, the evolution of polygons, contour maps and size of the glacier were reconstructed. Figure 38 shows the flow line obtained with the accumulation-ablation dynamics on the eastern region, the last surviving area of the glacier.

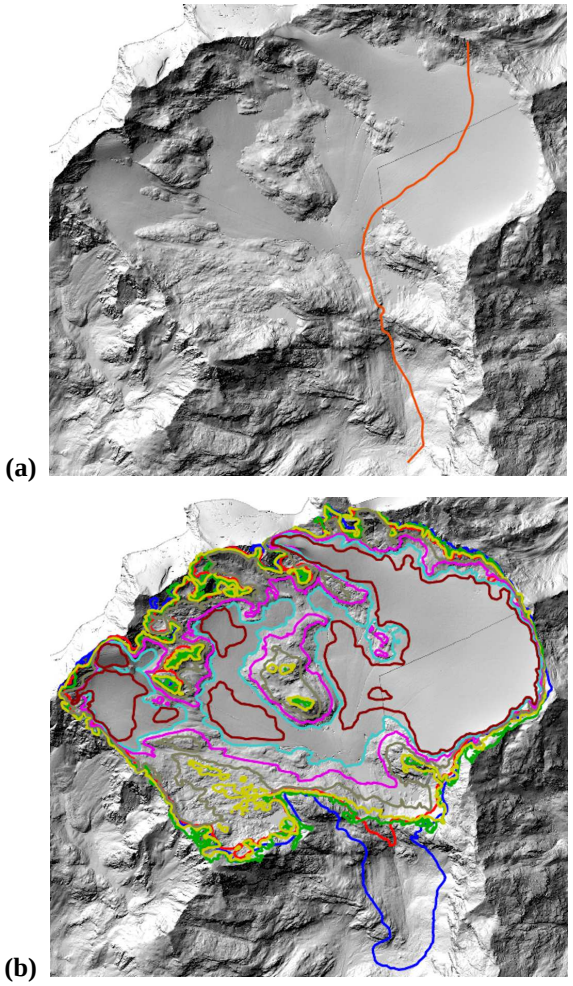

(a)

(b)

Figure 38: DEM analysis of Careser glacier (Carturan and others, 2013): (a) flow line derived from contour maps and used to implement the minimal model; (b) different polygons of the outer glacier limit, from 1933 to 2012.

In the glacier model, the parameter ν in eq. 2.2 was fixed at the standard value for valley glaciers (Oerlemans, 2011), as ν = 10. The other parameters for the Careser glacier are obtained from the glacier properties and are s = 0.16 and b_0 = 3320 m.
As far as scientific literature is concerned, the value of the parameter α_m in eq. 2.2 is often set to $\alpha_m = 3 m^{1/2}$ for valley glaciers and ice sheets. However, given that Careser glacier had a particular behavior and accurate historical input data are available, we estimate α_m combining eq. 2.2 and eq. 2.10, with elevation range values from the DEM analysis of about Δh = 388m. The average value is $\alpha_m = (3.4 \pm 0.1)\ m^{1/2}$ for the Eastern flow line of the Careser glacier.

Rutor glacier

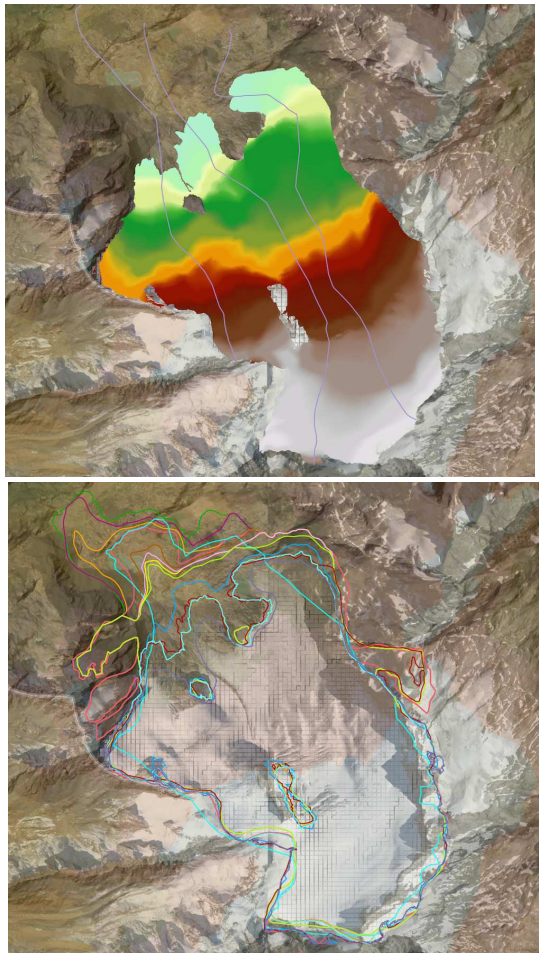

Figure 39: DEM analysis of Rutor glacier: (a) identified flow lines; (b) different polygons of the outer glacier limit, from LIA to 2004 (Villa and others, 2007).

From the morphological point of view, the Rutor glacier is characterized by the "Vedette del Rutor" ridge, which develops in SE-NW direction (Fig. 37b). This ridge

divides the glacier into two regions, each one with its own dynamics and fluxes. The conjunction of these fluxes is visible in the lower part, just below the "Vedetta Nord" outcrop where a medial moraine can be recognized (Villa and others, 2008). From DEMs, we identified three different flow lines that characterize the dynamics of this glacier (Fig. 39a).
As done above for the Careser, we estimated all the necessary parameters for the Rutor glacier simulation. The slope measurements from the 2003 by DEMs are s = 0.22 as the average value, s = 0.23 for the eastern flow line, s = 0.26 for the central flow line and s = 0.32 for the western flow line. The other parameter values are $\nu = 10$ and $b_0 = 3440$ m. The parameter α_m was separately estimated for the eastern and middle-western regions, owing to the differences in length, slope and elevation range. I estimated the values $\alpha_m = (4.3 \pm 0.5)$ $m^{1/2}$ for the Eastern region, $\alpha_m = (4.0 \pm 0.5)$ $m^{1/2}$ for the Central region and $\alpha_m = (5.6 \pm 0.5)$ $m^{1/2}$ for the Western region.

Climate drivers

To drive the minimal model on the historical period, we used the ERA-40 reanalysis, as explained in Chapter 3. These meteorological observations span the period from September 1957 to August 2002. The ERA-40 data have a spatial resolution of about 120 km in the area of interest (Uppala et al., 2005).
To drive the models for future climate conditions, we used the outputs of Global Climate Models (GCMs) from the CMIP5 family, with specific focus on the CSIRO model, without the downscaling development of NASA project (Chapter 3) and according to the RCP 4.5 scenario of radiative forcing and the RCP 8.5. Table 4 reports the climate model outputs used in this preparatory step; I selected only those models with spatial resolution finer than 2 degrees, to better interconnect the future climate driver with the resolution of ERA-40 re-analysis dataset.

CSIRO

The CSIRO-Mk3.6 climate model was used to prepare a joint CMIP5 submission in a partnership between the Commonwealth Scientific and Industrial Research Organisation (CSIRO) and the Queensland Climate Change Centre of Excellence (QCCCE) (Table 4).
The CSIRO Mark 3.6 global climate model is based on a coupled atmosphere–ocean model with dynamic sea-ice and a soil–canopy scheme with prescribed vegetation properties. This experiment also included an interactive aerosol treatment and an updated radiation on environment scheme. The modifications in model physics were limited to those required to use CMIP5 forcing datasets (Jeffrey et al., 2012). I used ten runs of CSIRO model, to provide an ensemble of simulated future glacier behaviors and to analyse the response of MGM on a single kind of model, with its ensemble of different statistical runs.

Model ID	Resolution LonxLat° Lev	Institution ID	Reference
ACCESS1-0	1.875x1.25L38	CSIRO-BOM	Bi et al., 2013
ACCESS1-3	1.875x1.25L38	CSIRO-BOM	Bi et al., 2013
bcc-csm1-1-m	1.125x1.125L26 (T106)	BCC	Wu et al., 2013
CCSM4	1.256x0.9L27 (T63)	NCAR	Meehl et al., 2012
CESM1-BGC	1.25x0.9L27	NSF-DOE-NCAR	Hurrell et al., 2013
CESM1-CAM5	1.25x0.9L27	NSF-DOE-NCAR	Hurrell et al., 2013
CNRM-CM5	1.40625x1.40625L31 (T127)	CNRM-CERFACS	Voldoire et al., 2013
CSIRO-Mk3-6-0	1.875x1.875L18 (T63)	CSIRO-QCCCE	Rotstayn et al., 2012
EC-EARTH-r8i1p1	1.125x1.121 (T159)	EC-EARTH	Hazeleger et al., 2012
HadGEM2-AO	1.875x1.25L60	MOHC	Martin et al., 2011
HadGEM2-CC	1.875x1.25L60	MOHC	Martin et al., 2011
HadGEM2-ES	1.875x1.25L38	MOHC	Bellouin et al., 2011
MIROC5	1.40625x1.40625L40 (T85)	MIROC	Watanabe et al., 2010
MPI-ESM-LR	1.875x1.875L47 (T63)	MPI-M	Giorgetta et al., 2013
MPI-ESM-MR	1.875x1.875L95 (T63)	MPI-M	Giorgetta et al., 2013
MRI-CGCM3	1.125x1.125L48 (T159)	MRI	Yukimoto et al., 2012

Table 4: CMIP5 models used in this work. Their resolution is higher than 2 degrees.

Model validation results

Careser glacier

Length variation measurements for the Careser glacier started in 1933, with the oldest DEMs acquired from a topographic map, while mass balance and ELA measurements started in 1967 (Carturan et al., 2013).

Figure 40 shows the results for the glacier length provided by the minimal model, driven by the measured values of the mass balance and ELA. The error bars are estimated by propagating the uncertainty on the input variables and parameters.

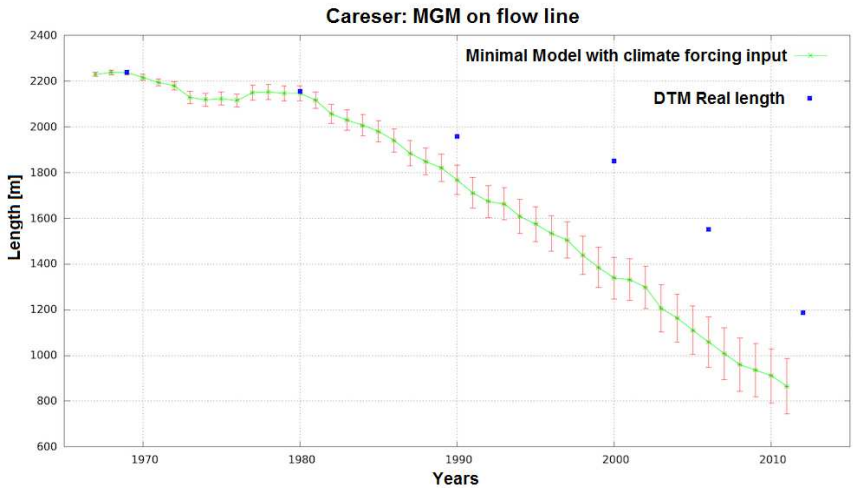

Figure 40: Results of the minimal glacier model for the Careser glacier mass balance, compared with the DEM length variations. ELA data were used as input.

The comparison of simulated with measured lengths clearly indicates the slow-down of the front retreat since about 1980; in this period, the melting predicted by the model is larger than the observed one. After 2000, the decrease in modelled and observed lengths parallel each other.

In the last 20 years, the Careser glacier has shown a passive retreat everywhere, with the disappearance of the mid-western region, which is fully dominated by ablation. The rapid mass loss and fragmentation of this region make it difficult to estimate the mass balance contribution from this area.

On the Careser glacier, the fluid-dynamical contribution is essentially turned off in the last thirty years. The break-up of the accumulation-ablation dynamics, the rise of widespread glacier thinning and the drift velocity of mid-western ice reduces the speed of front retreat, as shown in Figure 40. These processes create a peninsula of stationary ice, shown in Figure 41, which is included and protected by two drops, upwards and downwards. This ice peninsula is a flat strip with a slope of about 8-10% and an area of 300x800 m^2. At the end of this little region, there is also a slight rise on the ridge of the promontory.

This situation masks the actual condition of the flow line and the actual length variations of the glacier front. The ice thickness in this peninsula was sufficient to slow down the false front variations by glacier dynamics up to 2000, when there was a change in retreat speed (Fig. 40) when the thickness exceeded a threshold that allowed for the recovery of the dynamical retreat.

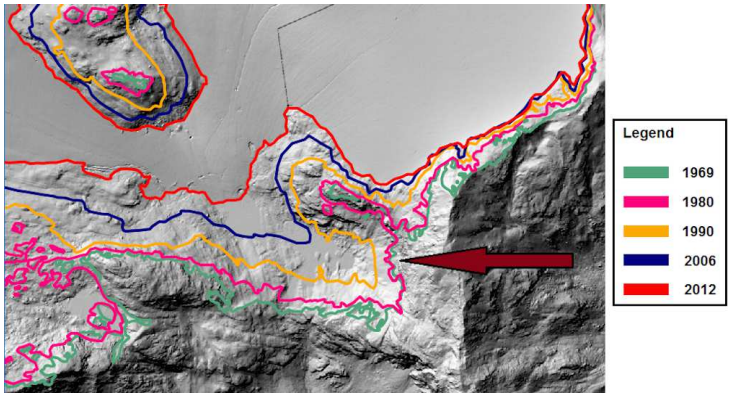

Figure 41: Enlarged DEM view of the Careser front between 1969 and 2012. The arrow indicates the stationary ice peninsula.

According to this observation, we applied the minimal model starting from 2000, to simulate the last decade.

As shown in Figure 42, these results are close to the observed dynamics of the glacier front, indicating that the actual ablation in the eastern region of Careser was well reproduced by the model dynamics. The discrepancy between the data and the model in the period 1980-2000 is thus due to the special, non-fluid-dynamical behavior of Careser glacier in this period.

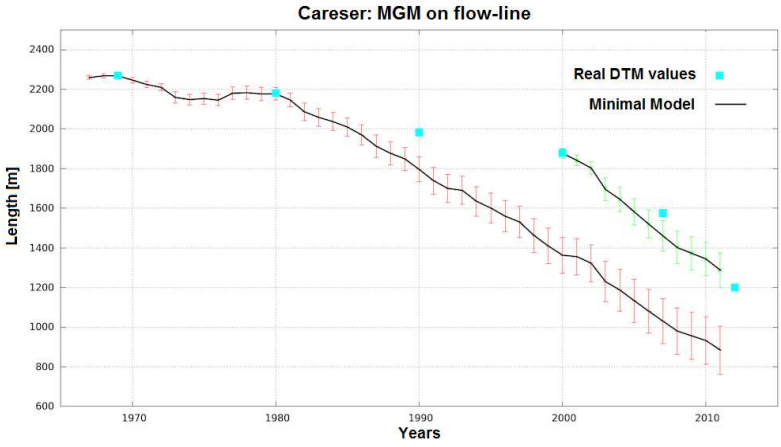

Figure 42: Minimal model applied to the Careser glacier for the period after 2000, using the observed values of the mass balance and ELA as inputs to the model.

Rutor glacier

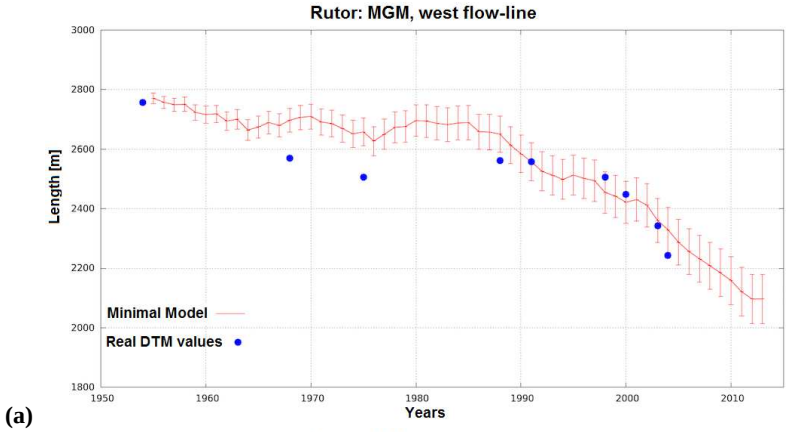

(a)

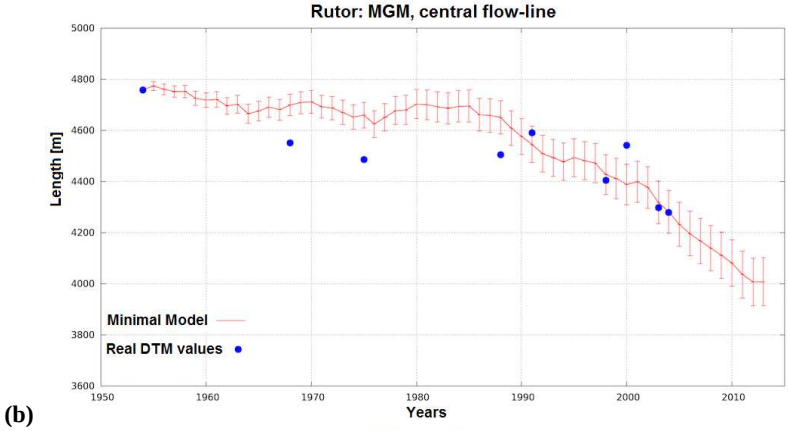

(b)

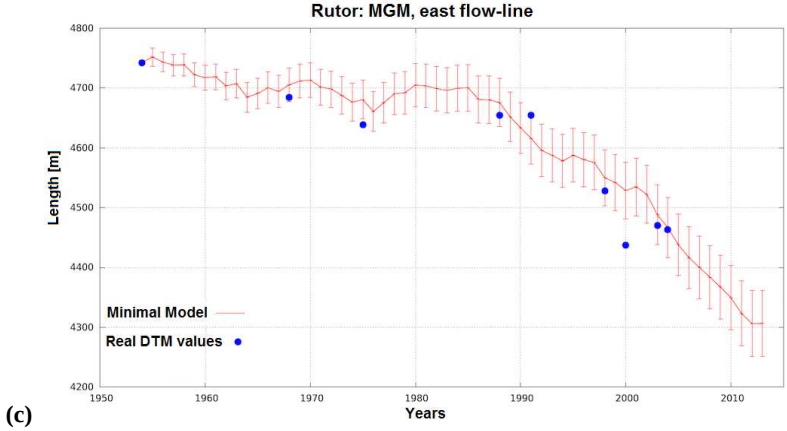

(c)

Figure 43: Glacier length simulated by the minimal glacier model for the Rutor glacier, compared with DEM length variations. The measured mass balance is used as a model input. The panels refer to: a) western, b) central and c) eastern flow lines.

Variations in the surface area of Rutor glacier were studied from its maximum expansion in the Little Ice Age to the present, through a combination of ground surveys, digital techniques and pre-existing data time series (Villa et al., 2007). For the Rutor glacier, we applied the minimal model without including an ELA input owing to the lack of data (eq. 2.9).
The model results reported in Figure 43 are in good agreement with the measured values, obtained from the DEM analysis. The Rutor glacier is a system with an active dynamics without mass fragmentation, and the terminus variations follow the standard glacier evolution.

First approach to future behavior

To illustrate the future glacier behavior, we drove the minimal glacier model by the GCM ensemble CMIP5 and by the CSIRO ensemble as climate forcing, focussing on the emission scenarios RCP 4.5 and RCP 8.5.
Uncertainty in climate model projections is often characterized by the measure of spread across an ensemble of simulations (Tebaldi and Knutti, 2007; Knutti at al., 2013). The results depend on the range covered by the distribution of the responses and, assuming that all the models are independent, we used the spread of the different solutions to indicate the forecast range.

Careser glacier

All the length assessments are cut off at 200 m, because the uncertainty bars are of the order of 200 m, thus any estimate beyond this minimum threshold is not significant. Moreover, when a glacier become too small, it can be entirely covered by debris and its volume is mixed up with rubble, distorting its dynamics.
The minimal model – CMIP5 combination was applied from 2006 to 2100. The 16 climate models (Table 1) highlight a significant resolution on the local climate of Ortles-Cevedale and Val de La Mare (Figure 44).
The glacier behavior simulations using an ensemble of 10 different runs of the CSIRO model for the [2006-2100] period are similar to those obtained with the CMIP5 ensemble and are not shown. On average, all model simulations indicate that by 2040 the Careser glacier will have a length smaller than 200 m (glacier disappearance). The ensemble spread indicate glacier disappearance in a range between 2035 and 2055, for both RCP 4.5 and RCP 8.5.

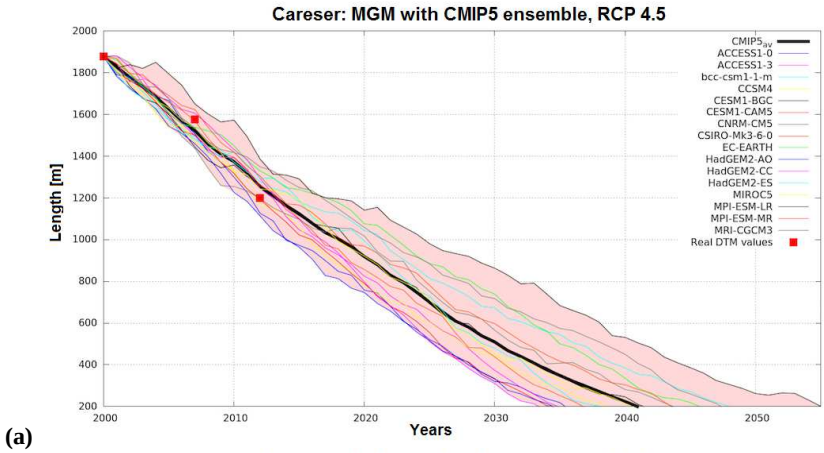

(a)

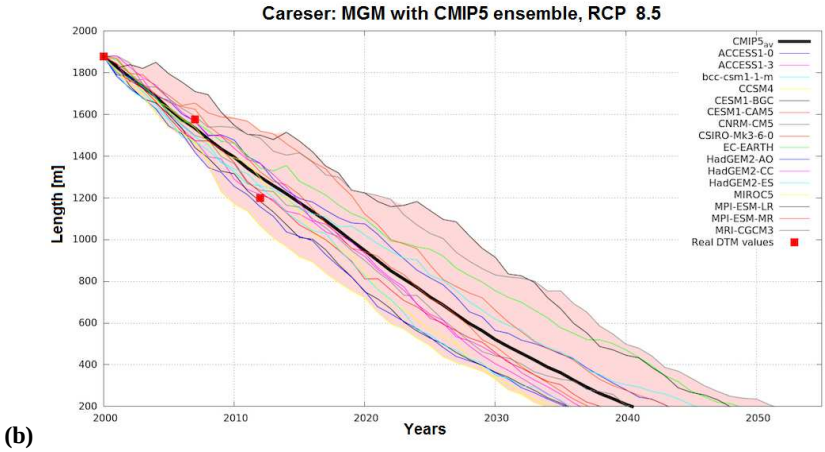

(b)

Figure 44: Minimal model-CMIP5 results for Careser glacier: a) RCP 4.5 scenario; b) RCP 8.5 scenario.

Rutor glacier

Figure 45 shows the results for the Rutor glacier length in the RCP 4.5 and RCP 8.5 scenarios, using as a driver the climate outputs of the ensemble of CMIP5 models on the longest flow line.

Table 5 reports the initial lengths in 2004, the forecasted lengths in 2100 in the two scenarios RCP 4.5 and RCP 8.5 and the related uncertainties (1σ deviation of the ensemble).

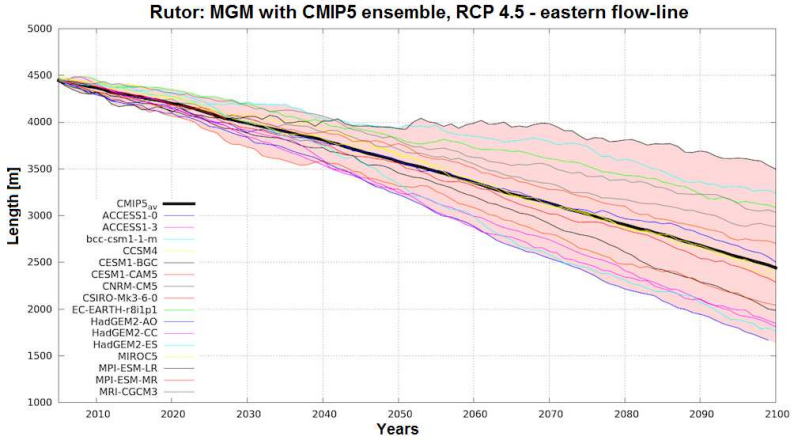

(a)

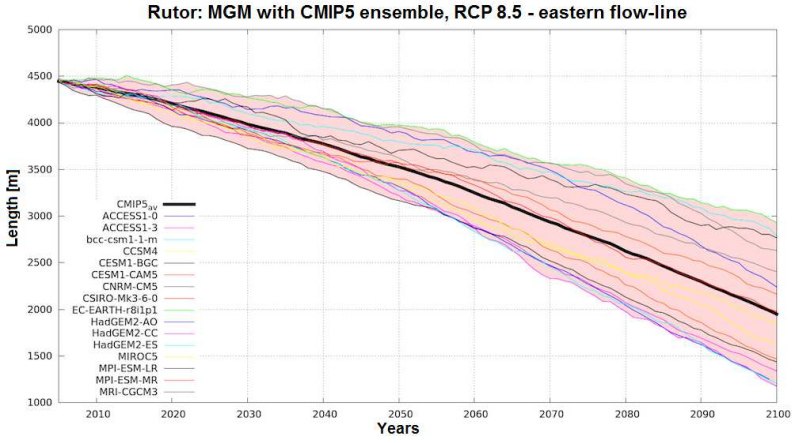

(b)

Figure 45: Minimal model results, driven by CMIP5 models in a) RCP 4.5 and b) RCP 8.5 on the longest flow lines (eastern).

GCMs	Emission scenarios	Flow line	Initial length at 2004 [m]	Final length at 2100 [m]	Standard deviation (1σ)
CMIP5	RCP 4.5	West	2243,70	953,68	346,13
	RCP 8.5			676,76	347,08
	RCP 4.5	Central	4279,97	2067,35	614,53
	RCP 8.5			1560,23	639,81
	RCP 4.5	East	4463,48	2441,99	579,86
	RCP 8.5			1950,45	623,82
CSIRO	RCP 4.5	West	2243,70	978,79	214,49
	RCP 8.5			781,95	252,16
	RCP 4.5	Central	4279,97	2177,99	381,73
	RCP 8.5			1761,82	460,54
	RCP 4.5	East	4463,48	2494,89	360,98
	RCP 8.5			2153,21	445,57

Table 5: Results of the minimal model forecasts, driven by the ensemble of CMIP5 models for the RCP 4.5 and RCP 85 scenarios.

Summary on first application of MGM

In this chapter, I investigated the dynamics of the Careser and Rutor glaciers, and built a GIS-based minimal model to identify the glacier flow lines and describe changes in glacier length along them. For this purpose, I used DEM analysis with an iterative GIS module (Mattavelli Ph.D thesis, 2016). The glacier model was driven either by the observed mass balance and ELA values, or by the mass balance and ELA values estimated from summer temperature and winter precipitation. From the comparison between the simulated and observed values, we first validated the modelling set-up on the historical period using a climate driver from ERA-40, and we then used the drivers provided by an ensemble of CMIP5 simulations to estimate the glacier behavior in future decades.

Careser glacier

The Careser glacier displays a strongly negative mass balance and it is characterized by positive feedbacks that accelerated the ablation and fragmentation of the ice body. In the last two decades, the ELA was usually above the highest elevation of the glacier. Glacier dynamics was basically stopped for several years and the Careser underwent constant ice melting which reduced the glacier thickness. Interestingly, the minimal model provided good match to the observed glacier behavior in two periods,

respectively before about 1980 and after about 2000, when the glacier was dynamically active. After the dynamical crisis in the 1980-2000 interval, during the last decade it was observed the recovery of the flow line retreat in the East region and a good match between observed and simulated fluctuations was again obtained. Simulations of future behavior indicate the disappearance of Careser glacier around 2040-2050, for both the RCP 4.5 and RCP 8.5 scenarios.

Rutor glacier

The Rutor glacier has considerable size and it displays a rather regular and lively dynamics. We applied the minimal model to the most evident flow lines. The different flow lines display a different degree of retreat under future scenarios. The western flow line (the shorter one), has a range of retreat from about 1300m in RCP 4.5 to 1600m in RCP 8.5. The central and the eastern flow lines show a similar decrease, of about 2100m and 2500m in RCP 4.5 and RCP 8.5 respectively.

Intermediate conclusion on MGM-GIS approach

Overall, the use of a minimal glacier model combined with GIS information is a simple but effective way of simulating glacier response to climate change and climate variability, provided the glaciers are still responding in a dynamical way. Fragmentation and local melting, as happened to the Careser glacier between 1980 and 2000, clearly hamper the application of a dynamically based model.

Chapter 5: r.glacio.model

The aim of this work is to integrate the Minimal Glacier Model in a Geographic Information System Python module in order to obtain a spatial representation of glacier retreat. This module can be useful for the scientific and glaciological community in order to evaluate glacier behavior, driven by climate forcing.
I collaborated with Dr. Daniele Strigaro, scientific assistant of Geomatic Laboratory of DISAT department, University of Milano-Bicocca. He created the platform of this module, called r.glacio.model, in a GRASS GIS environment using Python programming language combined with different libraries as GDAL, OGR, CSV, math, etc. I wrote the functions of MGM, climate connection with mass balance, thickness evaluation and error assessment, using Python.
The module is applied and validated on the Rutor glacier because it is very large and features rather regular and lively dynamics. The simulation is calibrated by reconstructing the 3-dimensional dynamics flow line and analysing the difference between the simulated flow line length variations and the observed glacier fronts coming from ortophotos and DEMs. The approach devised in r.glacio.model can be applied to most alpine glaciers to obtain a first-order spatial representation of glacier behavior under climate change.

Implementation of MGM into GRASS GIS

Flow line

The glacier flow line depends on similar factors. The general pattern of the ice flow is determined by the net budget between accumulation and ablation of the ice mass driven by the morphology of bedrock and the gravity force. The balance velocity is a parameter that describes this behavior (Waddington, 1998) and can be calculated from directions of ice flow using ice thickness and slope map (Huybrechts et al., 2000).
The flow line reconstruction is usually used in addition to a basic topographic analysis, in particular to model the erosion and the deposition in complex terrain. In this context, the flow line can be estimated by various algorithms, that are based on morphological factors from which the flow depends. Some of these parameters are slope angle, slope length, aspect and the upslope contributing area. Downhill flow lines merge in valley and can be used for the extraction of the channels (Mitasova et al., 1996).
Therefore, in glaciology the flow line is the vector, which describes the flow of mass between the accumulation area at the top of glacier and the ablation area at the bottom. It is possible to digitalize the glacier flow line as a vector line in a GIS environment from top to bottom.

Module development

At the beginning, I implemented the MGM as a python script without the use of a spatial analysis. Then, Dr. Daniele Strigaro applied a 2D and 3D approaches to spatialize the MGM.

The module r.glacio.model is developed using Python programming language (www.python.org) as a raster module for Geographic Resources Analysis Support System (GRASS GIS), an open source GIS software.

The joint of MGM and GIS is made using the Python libraries: GDAL and OGR for raster and vector analysis respectively, Numpy and Math for scientific computing, CSV to read and write input and output data and some other GRASS GIS modules that can be called into a Python environment easily.

The module r.glacio.model is developed starting from a standard geomorphological terrain analysis. First, r.slope.aspect is used to calculate the slope raster map, which contains slope values stated in degrees of inclination from the horizontal (Hofierka et al., 2009), from a Digital Elevatio Model (DEM). Then the mean slope of the glacier on a buffer area around the line and the range altitude as the difference between maximum and minimum elevation is calculated for each feature of the vector flow line layer. This data is used as input in the core equation of the module coupled with the mass balance data read from a CSV file. The vector line of flow line is cut according to the annual length variations, as model output. The last flow line length, at the end of the mass balance record, is used to create a vector and a raster layer with all the futures, come from the starting flow line.

Moreover, some features are added to increase the usability of r.glacio.model: 1) the possibility to calibrate the model using the α_m parameter by the comparison between simulated and real results on historical glacier behavior; 2) a method to allow the use of this module in case of lack of data as follows in the next sections.

Essential data required by r.glacio.model

Raster maps, geomorphological parameters and climate variables represent the user input of r.glacio.model.

- ✓ DEM/DTM: One of the inputs of this module is the raster digital surface of the glacier morphology. The more accurate the better it is, because slope raster map and other processes derives from it. DEM/DTM must not have the presence of artefacts.
- ✓ Glacier bound: this vector polygon identifies the contour line of the glacier.
- ✓ Flow line: this vector line is useful to identify the glacier dynamics and calibrate MGM outputs.
- ✓ Mass balance data: these values must be formatted in a csv file tab that is divided into two columns: 1) the referred year; 2) the mass balance value in meters of water equivalent (m w.e.). A percent value of mass balance error must be included.

- ✓ Thickness parameter: the float value named α_m, must appear. This feature is fundamental in order to calibrate the model results.

The main result of this module is a flow line in raster and vector format.

- ✓ Output as text: the simulated values of glacier evolution are written on a text file presenting a simple support to the user in managing the output data.

Module on Rutor glacier

Available DTMs of Rutor glacier

The followed data sets are used to analyse the geospatial glacier retreat of the Rutor flow lines using r.glacio.model:

- ✓ DTM at 1954 to calibrate the model up to 2012;
- ✓ flow lines and bound of the Rutor glacier;
- ✓ set of mass-balance data;
- ✓ error % about DTM elevation data and mass-balance data.

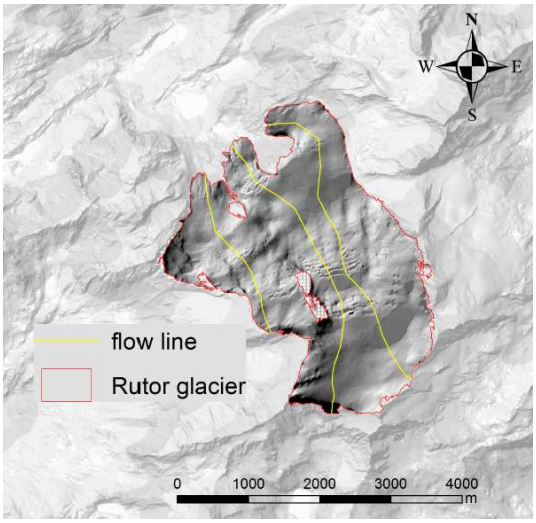

Figure 46: The three flow lines digitalized for the Rutor glacier.

The DTM at 1954, provided by the Earth and Environmental Sciences Department (DISAT) of the university of Milano-Bicocca, is obtained from a reconstruction of the past behavior of the Rutor glacier (Orombelli, 2005), with a resolution of 10 meters. On the other side, the DTM 2008 is a terrain model with a high accuracy and resolution (2 meters). The 2008 DTM comes from LIDAR data acquired by the Valle d'Aosta Italian region.

One of the most important parts of this work is the evaluation of the flow lines on the individual glacier branches. After an accurate analysis regarding the principal existent algorithms, the flow lines are retrieved using GIS software and then corrected manually (Fig. 46), as in Chapter 4.

East, center and west sections with three different behaviors have been identified to explain the Rutor glacier dynamic. Thus, different parameters must be chosen to calibrate the retreat of every flow line.

Calibration setting

A careful calibration was made starting from the data described above. The mass balance is the driving force for any glacier because its increase or decrease is strongly correlated in a variation of the shape of the glacier. This data comes from different analyses made on glaciers and in order to set the model the α_m parameter, present inside the algorithm, must be set up to made a calibration.
To show the sensitivity of the model to α_m, r.glacio.model is performed setting different values of this parameter for each flow line. In Figure 47 are represented these results to better understand how the model behavior change set the other variables: mean glacier slope, flow line length and mass balance set of data (1976-2013).

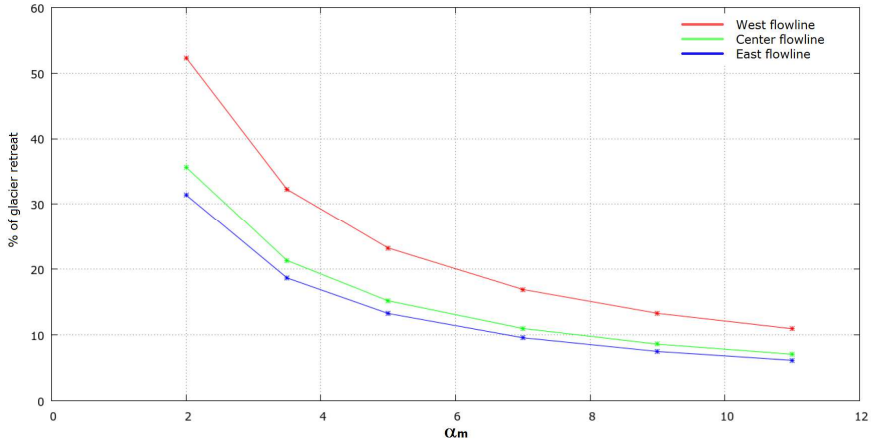

Figure 47: α_m vs % of length retreat. Starting length: 2360m for the western flowline, 4500m for the central flowline and 4667m for the more eastern.

There is a great dependency between the value of α_m and the velocity of the glacier retreat. Higher values mean less velocity in the length retreat and lower values are related to more sensitivity in the process of lost glacier mass. Moreover, the starting length of flow line is strongly correlated to the glacier dynamic. According to the eq. 2.9, the glacier variation is related to the input length by a factor of ½:

$$\frac{dL}{dt} \propto L^{1/2} \qquad (5.1)$$

Then, higher value of initial length creates greater variation than small initial length. However, this comparison concerns the absolute values of glacier length and variation. Figure 47 is based on relative amount of retreat, and it shows that higher values of

flow line length mean minor percentage of retreat referring to the beginning, than the lower values of flow line length. Therefore, the small glacier disappear faster than glaciers with large size.

Results

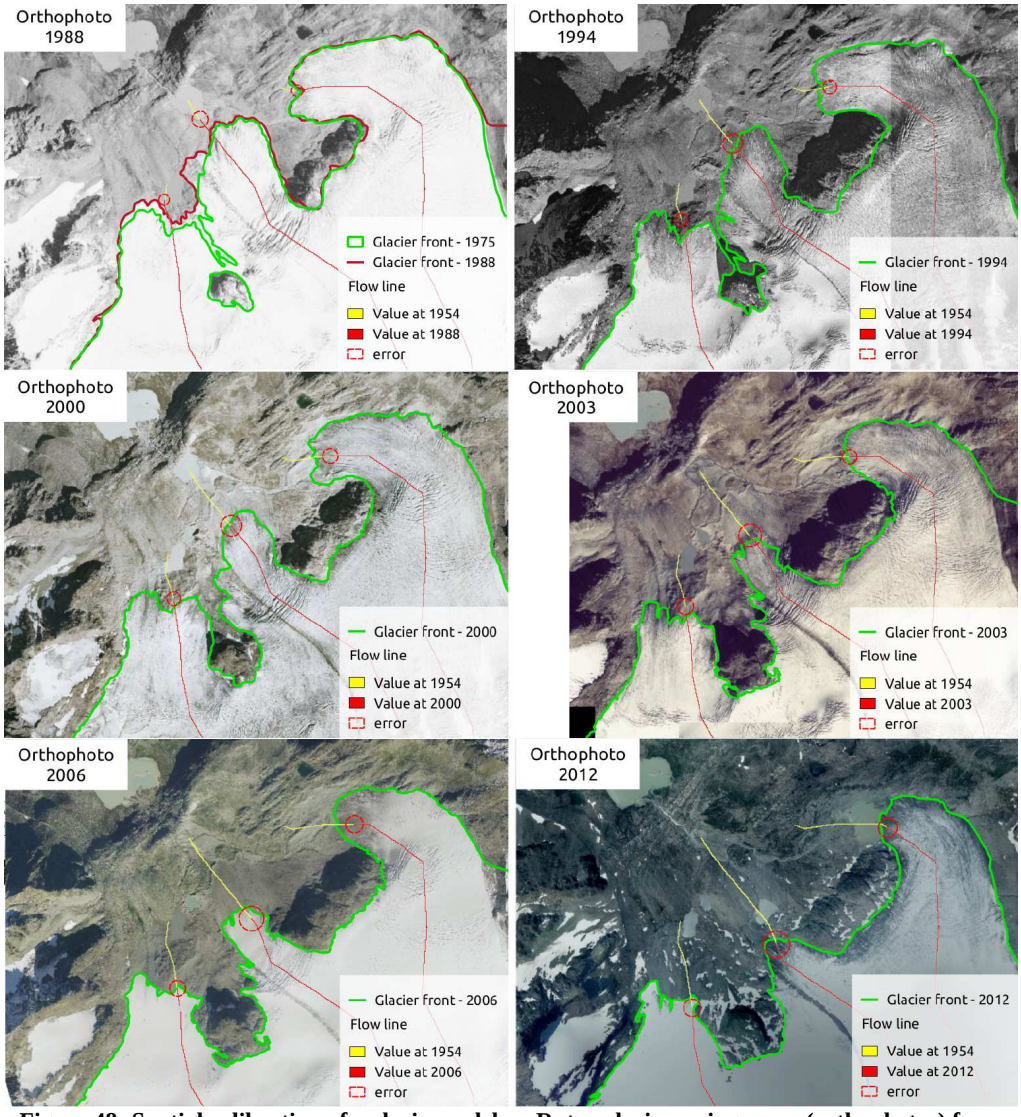

Figure 48: Spatial calibration of r.glacio.model on Rutor glacier, using maps (orthophotos) from 1988 to 2012 (Strigaro et al, 2015).

The MGM is calibrated on Rutor glacier from 1952, the first available and reliability DTM (Orombelli, 2005), to 2012, the newer georeferenced data of glacier extension.
A value of α_m parameter for each flow line is used to perform a calibration of the length variations, comparing the result with six orthophotos. These orthophotos are available through a Web Map Service (WMS) from the national geoportal (www.pcn.minambiente.it) for 1988, 1994, 2000, 2006 and 2012; in addition, orthophotos for 2003 are referred to the flight made by the Valle d'Aosta region. The most recent set of orthophotos is used to find the best geospatial fitting, while the previous were used to control the behavior during the target period in order to find the best parameter settings.
In Figure 48 are showed the results of the comparison between 1975 and 2012. The first picture highlights the mid-80s increase because the glacier in 1988 has the same front as in 1975. At the beginning of the calibration, the most problematic flow line is the middle one, because we can see in front of this tongue the presence of a glacier lake that can have an effect in the increase of the melting of ice. The 1994, on the other hand, shows a general well-fitting analysis. The western flow line, however, has a good fit because this tongue is forked due to morphological characteristic of the bedrock. The absence of the geophysics affects the elaboration because it is impossible to predict rock mass formation. Considering a mean front variation, the simulated flow line error includes the actual front position. 2000, 2003, 2006 show very similar results with a good correlation between simulated and expected position of the glacier front. Finally, the last step in 2012 is the final step of our calibration and it confirms the initial hypothesis.

Future developments of r.glacio.model

According to this work, in the near future, other improvements are expected. First, an automatic extrapolation of the flow line using some geomorphological algorithms or developing a new algorithms based on some simplified flow line extrapolations (Le Bris and Paul, 2013). Furthermore, the algorithm can be improved to increase the accuracy of the results introducing a geomorphological analysis during the flow line calculation process per year. In this way, new surrounding conditions can be retrieved year by year and the output of the main equation will change. Finally, the r.glacio.model will be applied on available glaciers in the entire Alpine chain to evaluate the alpine glacier general movements.

The source code is released on the GRASS-Addons repository under a Gnu Public License (GPL) v3 to create the possibility of external improvements and suggestions, but also to release a simple tool that can be used by the glaciological and scientific community to assess future glacier fluctuations (Strigaro et al., 2015).

Chapter 6: results and classifications

In this last chapter, I show the simulated results of the application of MGM on GAR glaciers, assessing response to climate scenarios up to 2100.
As explained before, I chose the MGM with the implementation of GIS approach to retrieve geomorphological parameters as initial and boundary condition of studied glaciers. Then, I used climate variables come from E-OBS dataset to drive MGM during past period and define the parameters of the eq. 3.2 to obtain mass balance from meteorological values. The future climate assessments come from the NASA NEX-GDDP dataset.
These results are observed as cumulated retreats or annual variation and the goal of this evaluation is the classification of glacier future behaviors according to the previous analysis, for example:

- ✓ the geographical sectors who divide the mass balance trends;
- ✓ the climate effects on GAR according to precipitation and temperature behaviors;
- ✓ the geomorphological structures of glaciers.

Using E-OBS dataset

As seen in Chapter 3, I chose to start my analysis during this Ph.D work with E-OBS high-resolution gridded dataset, because of its spatial resolution of 0.25 degrees (~25 km x 25 km), comparable with the grid dimension of the Prospective Run of NASA NEX-GDDP dataset of future meteorological conditions, with its goodness and reliability of observed data. (Haylock et al., 2008). From E-OBS, I extracted from the nearest grid point to the coordinates of each glacier.

Pre-processing of data

A preliminary analysis of the used data is necessary before doing any kinds of elaborations, to control and prepare the object of the followed process. I this procedure is necessary to verify the E-OBS series of summer temperature and winter precipitation.
First, I verified the absence of eventually missing values that can create a lot of problem when E-OBS value are compared with mass balance dataset. During this phase, I can state that the dataset is complete without lack of values.
Then I had to focus my attention on the independent variables to evaluate particular statistic distributions, for example not-normality, not-linearity, not-additivity, asymmetry or heteroscedasticity (variable with no uniform variance). The transformation of a variable is the way to resolve these effects and:

- ✓ stabilise the variance;
- ✓ linearize the relation between the variables;
- ✓ normalize the distribution;
- ✓ create solid model.

I decided to work with standardized climatic variables because reduces the influence of systematic errors.
It is the case of precipitation values that are the sum of the mm of rainfall during the winter season of 1951 – 2013. Because of their multiplicative structure (Fig. 49a) it is important to linearize the cumulative structure and I applied the log-transformation:

$$P_i^t = \log(P_i) \tag{6.1}$$

on precipitation values for each pixels (glaciers) during the historical period.
After the single transformation, it is also necessary that each independent variable of eq. 3.2 are comparable during a multivariate processing, overcoming the high variance, the different kinds of variables, the different scale of measurements or the contribution of other hide variables. Therefore, to create homogenized variables, I had to scale my datasets.
During the previous transformation, the *i*-value depends only on the corresponding original value and on the used operation. Instead, the *i*-scaled value depends on the corresponding original value, on the used scaling and on some statistic parameters of these variables, such as average, standard deviation, minimum or maximum values.
I chose the auto-scaling, the most common scaling used to homogenise a variables of a multi-variate analysis. The results are obtained subtracting the mean from each value and then dividing the result for the standard deviation, which are referred to a reference period:

$$\tilde{T}_i = \frac{T_i - \overline{T}_{rif}}{\sigma_{rif}} \tag{6.2}$$

$$\tilde{P}_i = \frac{P_i^t - \overline{P}_{rif}^{\,t}}{\sigma_{rif}^{\,t}} \tag{6.3}$$

The auto-scaling of temperature and precipitation values create a dataset with null arithmetic mean and unit variance:

$$\begin{aligned} \overline{\tilde{P}} &= 0 \cdots\cdots V(\tilde{P}) = 1 \\ \overline{\tilde{T}} &= 0 \cdots\cdots V(\tilde{T}) = 1 \end{aligned} \tag{6.4}$$

The resulted probability distribution functions are represented with the histograms of Figure 49 and Figure 50 for precipitation and temperature respectively.

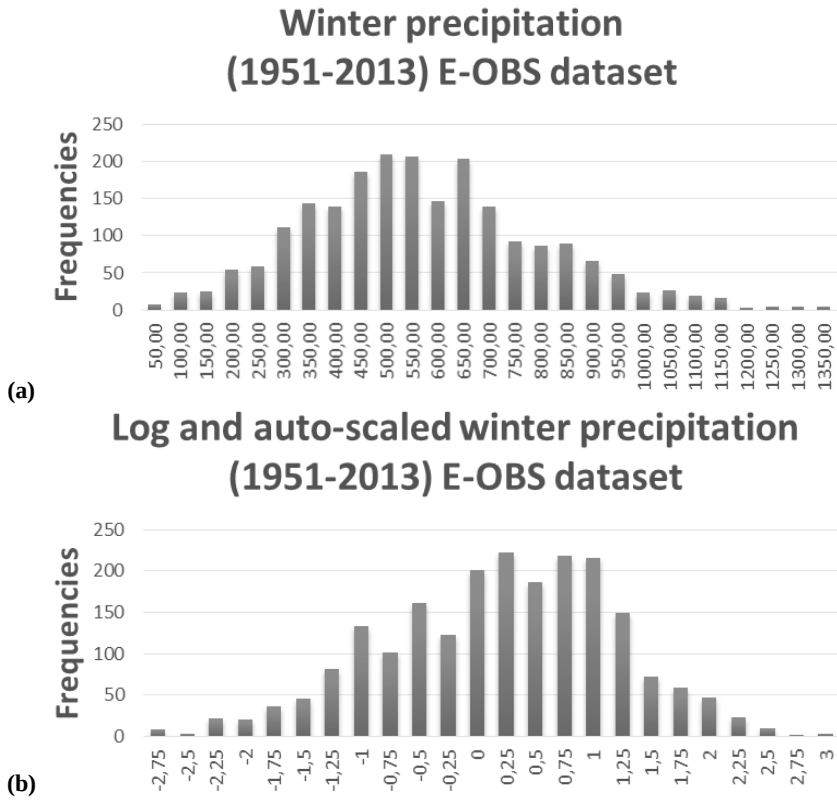

Figure 49: Histograms of winter precipitation values: (a) cumulative seasonal data (sum of winter months) and (b) after log-transformation and auto-scaling.

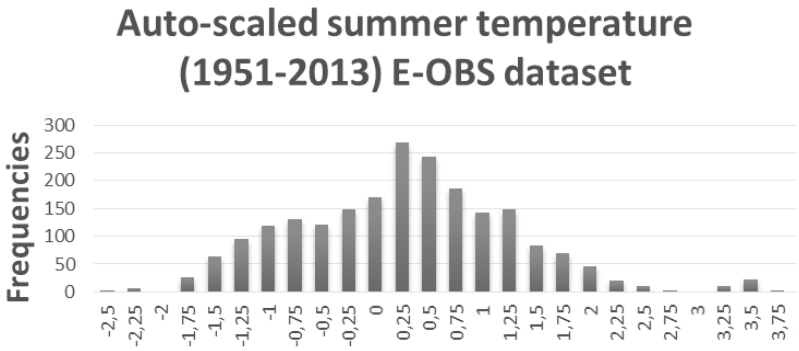

Figure 50: Histograms of summer temperature values after auto-scaling.

To evaluate this P.D.F. it was made the Kolmogorov-Smirnov test that tries to determine if the sample data is a good fit with a distribution. Here I applied the K.S. test to evaluate the comparison with the normal distribution, referring this test with relate critical values. Then the P.D.F.s are equipped with the Skewness and Kurtosis

values, which are descriptors of the shape of the distribution. The first represents the level of asymmetry of the Gaussian distribution: if skewness is positive the distribution is said left-skewed, instead if skewness is negative right skewed. The Kurtosis is the measure of the taildness, in other words if the data are peaked, positive value, or flat, negative value, relative to a normal distribution.
Al these parameters are listed in Table 6. First, the K.S. tests show the goodness of the P.D.F. with a normal distribution. The Skewness values define that precipitation is lightly tailed on the left and temperature is lightly tailed on the right. The Kurtosis values show that the temperature are more peaked than the precipitation distribution.

P.D.F. summer temperature Fig. 50	**P.D.F. winter precipitation** Fig. 49b
K.S. test $0{,}025 < 0{,}030_{critical}$	**K.S. test** $0{,}020 < 0{,}036_{critical}$
Skewness = 0,26	**Skewness** = - 0,24
Kurtosis = 0,17	**Kurtosis** = - 0,36

Table 6: Parameters of the histograms that represent the probability distribution functions of auto-scaled temperature and precipitation series: K.S. = Kolmogorov-Smirnov test, Skewness, Kurtosis.

Sensitivity of mass balance to climate fluctuation

The components of the used transfer function (eq. 3.2) are the dependent values of mass balance and the two independent series of temperature and precipitation. To understand the sensitivity of the dependent mass balance, I had to relate in Figure 51 an overview of summer temperature, winter precipitation and mass balance series for all the glaciers under study.
Temperature and precipitation are extracted from E-OBS (as explained before) with a grid resolution of about 25 x 25 km. Some glaciers lie within the same grid point with the same climatic settings. Mass balance dataset derives from the WGMS or internet archives (Chapter 3) with at least 8 years of data.
Then, in Figure 51 are represented the different series of data: temperature, precipitation and mass balance datasets are standardized (as in previous paragraph) with auto-scaling method to compute regressive models and to compare the relative contribution to the dependent variable.
Observing Figure 51 is clearly a positive trend of temperature since the 80s instead of a not visible trend in precipitation in this region. According to the increase of temperature values, it is possible to notice a negative trend in mass balance. Furthermore, another important future is highlighted: temperature ensemble shows minor spread around the drawn averaged value than the precipitation group. This means that temperature has a higher spatial coherence in variation, compared to precipitation.
Finally, I can underline the evident signal of year 2003. During hydrological period 2002 – 2003 there were an extraordinary warm summer, represented by an evident

positive peak, and a quite drier winter, the negative signal during precipitation series. Therefore, this characteristic year is distinguished of a strongly coherent negative mass balance.

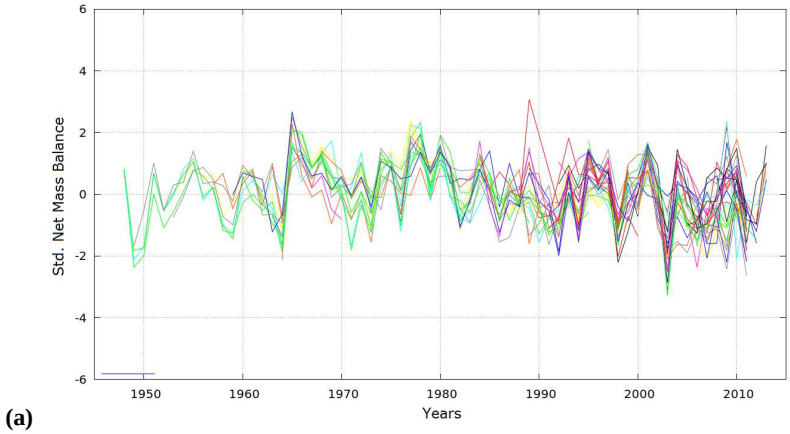

(a)

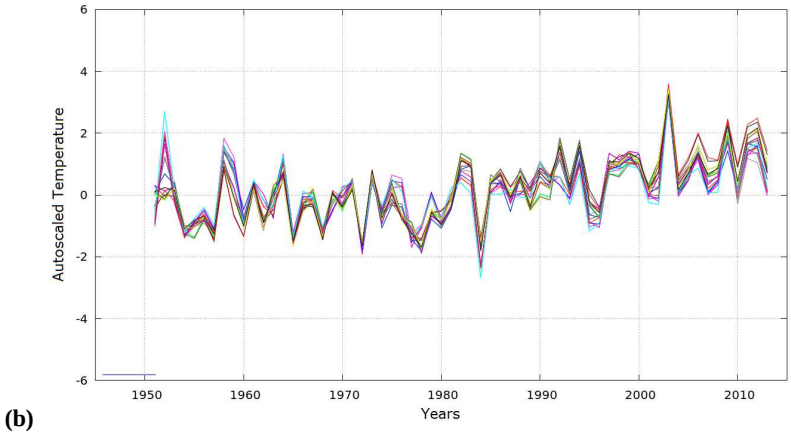

(b)

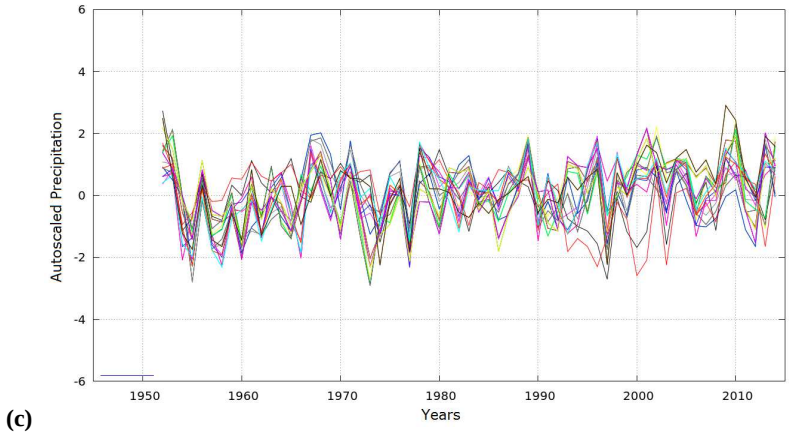

(c)

Figure 51: Comparison between: (a) Mass Balance series of glaciers, (b) summer Temperature (May - September) and (c) winter Precipitation (November - March) extracted from the nearest grid point (E-OBS data set) of each position of glaciers.

Parameters of mass balance function

Summer period for temperature values

As seen in Chapter 3, the most delicate explanatory value is temperature. Sure enough, studying the weights of precipitation and temperature we observed that the mass balance is mainly influenced by temperature rather than by precipitation (Balocco master thesis, 2015).

For this reason, I focused my attention to the choice of the summer period on which I had to calculate average temperature.

Using E-OBS dataset, I analysed and scaled data from five different amounts of summer months: May – September, June – September, May – October, June – October and July – October. Then I apply eq. 3.2 to obtain the different series of multivariate parameters related to the cited period, correlating the coefficient of determination R^2 to indicate how well the statistical model fits the dataset.

Observing Figure 52, we can see the histogram of the R^2 values for each glacier and for each summer period (different colours). The period 5 – 10, 6 – 10 and 7 – 10 have the worst statistical fit, thus excluding October contribution. With the support of Table 7, I can compare in detail the range with May – September (5 – 9) and June – September (6 – 9).

Using eq. 3.2 I had to analysis the E-OBS summer temperature choosing the May – September monthly contribution.

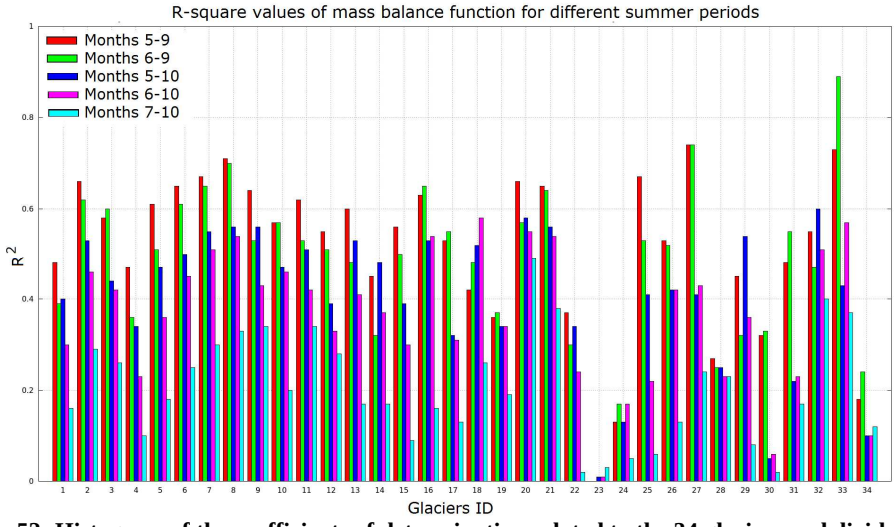

Figure 52: Histogram of the coefficients of determination related to the 34 glaciers and divided by 5 different colours who identify the different considered period.

R–square *R-square corr.*	Summer months				
	5 - 9	**6 - 9**	**5 - 10**	**6 - 10**	**7 - 10**
Average glaciers 1 - 34	0,51 0,44	0,48 0,41	0,41 0,31	0,36 0,27	0,20 0,09
Average glaciers 1 – 22	0,56 0,50	0,50 0,46	0,45 0,40	0,40 0,35	0,22 0,16
Average glaciers 24 – 34	0,46 0,31	0,46 0,31	0,32 0,13	0,30 0,10	0,17 -0,06

Table 7: R^2 analysis. There are listed the average R^2 of 34 glaciers and divided in two groups without the 23th glacier (Grand Etret). This table reports the R^2 and the R^2 corrected values.

Mass balance function on GAR

Using E-BOS dataset of winter precipitation (November – March) and summer temperature (May – September) and using the mass balance dataset as seen in Chapter 3, I applied the eq. 3.2 on each glacier of our 34 ensemble, using linear multivariate regression analysis to estimate the coefficients of that equation.

$$\dot{b}_i = aT_{s,i} + bP_{w,i} + c \qquad (3.2)$$

With the support of Table 8 and Figure 53, R^2 values define that Grand Etret (glacier n° 23) has not a statistical definition because of its null R^2. Then I had to remove the Grand Etret glacier from the ensemble of studied glacier within our sample.

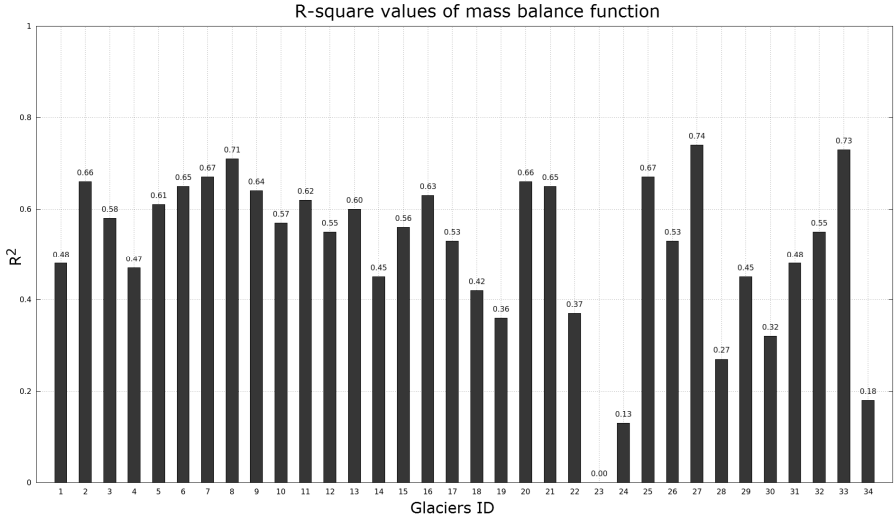

Figure 53: Histogram of the coefficients of determination related to the 34 glaciers, come from the regression analysis with E-OBS dataset.

ID	Glaciers	a	b	c	R^2
SAR1	Sarennes	-781,43	261,34	-889,72	0,48
HIN2	Hintereisferner	-484,29	115,63	-520,89	0,66
KES3	Kesselwandferner	-355,49	114,68	-68,63	0,58
SAS4	Saint_Sorlin	-704,66	250,34	-607,20	0,47
STU5	Stubacher_Sonnblick	-706,71	189,53	-234,10	0,61
SIL6	Silvretta	-645,70	274,22	-210,47	0,65
GRI7	Gries	-606,63	281,88	-641,61	0,67
VER8	Vernagtferner	-435,08	87,89	-292,06	0,71
ALE9	Grosser_Aletsch	-472,53	159,46	-172,65	0,64
CAR10	Careser	-633,60	88,82	-903,90	0,57
PLA11	Plattalva	-491,75	294,38	-192,44	0,62
LIM12	Limmern	-462,03	249,03	-192,70	0,55
ARG13	Argentiere	-681,42	235,18	-547,11	0,60
PAS14	Pasterze	-394,41	49,22	-607,94	0,45
WUR15	Wurten	-428,26	166,19	-672,86	0,56
FON16	Fontana_Bianca	-608,15	159,67	-237,25	0,63
JAM17	Jamtal	-453,89	314,03	-592,38	0,53
BAS18	Basodino	-604,39	413,57	-22,33	0,42
CIA19	Ciardoney	-587,22	198,60	-945,70	0,36
FIL20	Filleck	-623,55	292,65	44,31	0,66
GEB21	Gebroulaz	-483,46	404,83	-586,30	0,65
PEN22	Pendente	-520,16	125,74	-579,01	0,37
GRE23	Grand_Etret	28,71	-24,78	-526,66	0,00
SFO24	Sforzellina	-196,02	20,41	-832,69	0,13
KLE25	Kleinfleiss	-493,02	216,95	-221,36	0,67
TMR26	Timorion	-392,30	210,58	-454,91	0,53
GOL27	Goldberg	-653,62	160,94	-87,29	0,74
AGL28	Agola	-238,28	504,61	-1112,26	0,27
MAL29	Malavalle	-330,71	126,52	-539,33	0,45
OCH30	Ochsentalergl	-360,74	178,89	-258,96	0,32
VRM31	Vermuntgl	-440,33	315,41	-735,30	0,48
RUI32	Ruitor	-385,71	667,50	-963,60	0,55
LAN33	Langtaler	-671,21	171,70	-538,95	0,73
LUN34	Lunga_Vedretta	146,13	-111,15	-1294,78	0,18

Table 8: List of coefficients come from the linear regression analysis applying eq. 3.2 on each glacier under study. 'a' is the temperature parameter, 'b' is the precipitation parameter and 'c' is the intercepts. All these glaciers have the R^2 values of the linear regression.

Analysis of residuals

An important way of checking whether the goodness of a regression, is to check the residuals of a regression. The residual is the difference between the observed value of the dependent variable and the predicted value by the model. Each data point has one residual and both the sum and the mean of the residuals of a sample of data must be equal to zero.

Ideally all residuals should be unstructured, namely the regression analysis has been successful in explaining the essential part of the variation of the dependent variable. If however residuals exhibit a structure or present any special aspect that does not seem "random", it sheds a "bad light" on the regression.

The problems that can be diagnosed during the analysis of residuals are, for instance:

- ✓ outliers as, often, very big residuals;
- ✓ non-linear relation between residuals and variables;
- ✓ non-constant variation of the residuals, called heteroscedasticity.

For the basic analysis of residuals, I used the usual scatterplots, plotting both independent variables and residuals, time and residuals and the distribution of residuals.

I analysed all together the group of residuals of previous analysis, because of their cumulative properties of sum and mean values.

In Figure 54 is represented the distribution of residuals to verify the normality of the sample. The group of residuals has mean value and sum equal to zero and it was made the Kolmogorov-Smirnov test to evaluate the comparison with the normal distribution: the maximum value is 0,022 < 0,044 of critical end point of this test, then the hypothesis is confirmed.

The P.D.F. of Figure 54 is also equipped with the Skewness and Kurtosis values, to describe the shape of the distribution. In this case, the distribution are lightly right skewed and peaked.

The scatter plots in Figure 55 show the residuals on the vertical axis and the independent variables, temperature and precipitation, on the horizontal axis. The points in these residual plots are randomly dispersed around the horizontal axis, and then it is possible to confirm that the regression model is appropriate for the data.

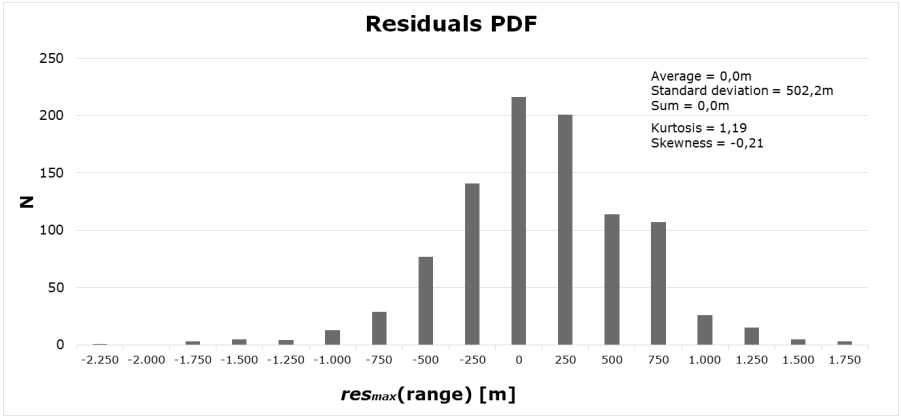

Figure 54: Histogram of residuals of mass balance multi-linear regression (eq. 3.2) with statistical analysis.

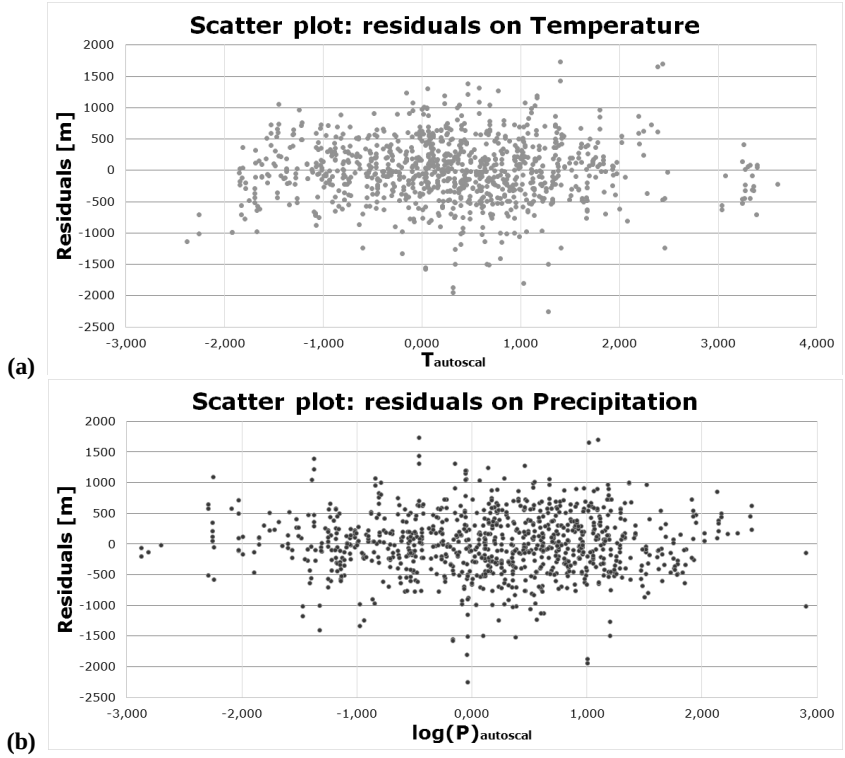

Figure 55: Scatter plots of residual (y-axis) with the independent variables, (a) summer temperature and (b) winter precipitation.

At the end of this analysis, in Figure 56 is represented the variation of the residuals, with all series from the different regressions. This plot evidences that the random sequence has a finite variance and confirm the homoscedasticity of residuals, in other words the homogeneity of variance.

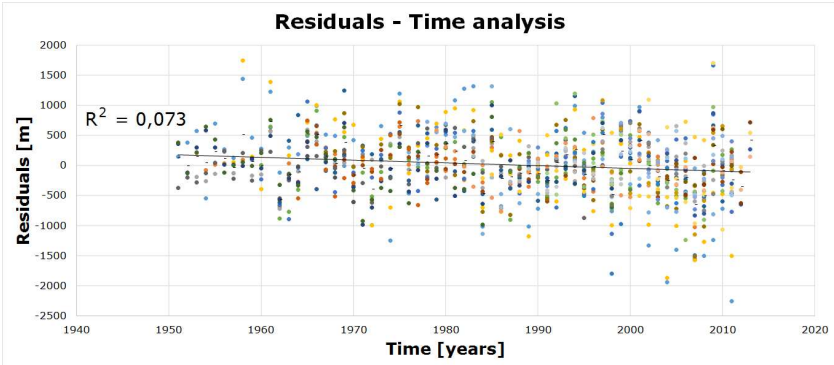

Figure 56: Scatter plot of residuals variation on time, adding all the series of residuals for all analysed glaciers.

The plot in Figure 56 also underlines that there is not evident correlation into residuals, except few singular series that show a lightly negative-linear structure with very small value of R^2, minor to 0,2. These relative trends can point at other components to complete the regression of eq. 3.2 for future works about it.

Cluster analysis of mass balance parameters

To better understand the climatic effect of the linear regression, I made a cluster analysis using the previous coefficients (Tab. 8) and other parameters, such as geographical positions or geomorphological conditions, related to the climate trends.

The term cluster analysis, first used by Tryon at 1939 (Tryon, 1939), encompasses a number of different methods for grouping objects of similar kind into respective categories. It is useful to organize observed data into meaningful structures, that is, to develop taxonomies. In other words, cluster analysis is an exploratory data analysis, which aims at sorting different objects into groups. Given the above, cluster analysis can be used to discover structures in data without providing an explanation/interpretation: it simply discovers structures in data without explaining why they exist.

The first step is the creation of the scores plots to analyse the behavior of the studied elements referring to their components. I chose the two components, which are the two axis of the plot, and it is possible to evaluate the occurrence of possible groups (clusters), the presence of particular objects (outliers) and the existence of certain distribution.

The first scores plot are composed by the temperature parameter 'a' and the precipitation parameter 'b' of eq. 3.2. Observing Figure 57, we can identify two possible different groups, which are encircled by orange and green lines.

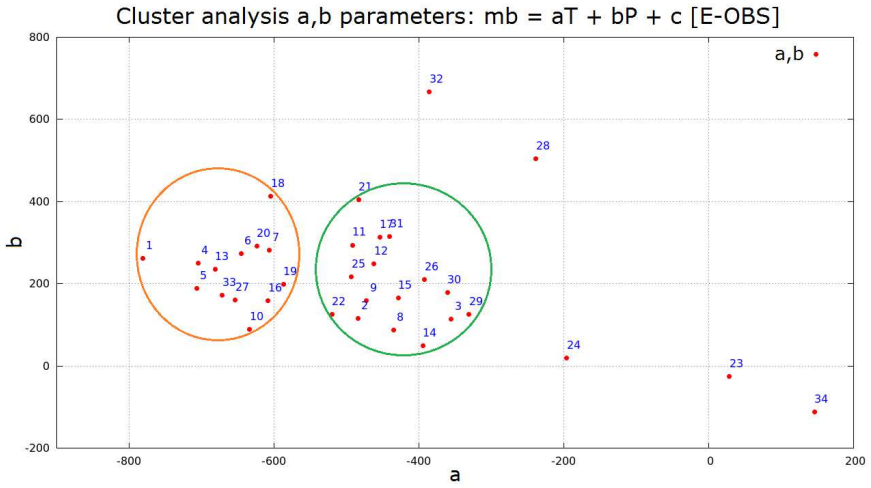

Figure 57: Scores plot with x-axis the temperature parameter 'a' and y-axis the precipitation parameter 'b'. Orange and green circles define two possible clusters.

Then I analysed the central point and the related characteristics of these clusters to validate the classification:

- ✓ The "orange" cluster has the barycentre at B_o = (a ; b) = (-654,48 ; 229,11) and the "green" cluster at B_g = (a ; b) = (-437,40 ; 195,59).
- ✓ The distance between the two barycentre is $d(B_o,B_g)$ = 219,65.
- ✓ The average distance between points of orange cluster and their barycentre is $d_A(B_o)$ = 83,44 and the maximum distance is $d_M(B_o)$ = 119,14.
- ✓ The average distance between points of green cluster and their barycentre is $d_A(B_g)$ = 99,72 and the maximum distance is $d_M(B_o)$ = 214,25.

Observing these values, I can confirm the existence of the two cluster, demonstrating them because of the distance between the two barycentres is greater than the average distance of glacier points with their barycentre. However, these cluster are not well defined because of their outskirts are more distance than the two barycentres.

Furthermore, there are five glacier outliers, much more distant from the centres of the orange and green clusters: the nearest outlier to the green barycentre is the 24th glacier, with distance $d_{24}(B_g)$ = 298,25 that is three times the average distance of green points. Analysing the outlier, it possible to recognise this elements as the glaciers with the lowest R^2 value.

To understand the characteristics of clustered glaciers, according to their latitude and longitude they are represented in Figure 58. The orange cluster (red dots) represents glaciers of the Southwestern flank of Alps, instead the green cluster (blue dots) groups the further Northern glaciers, most at East.

The precipitation of each cluster have similar range than the other, so the most important difference between these clusters is due to the temperature. The Northern glaciers (green cluster) have the minor coefficient, because of their position preserves the air temperature and maintains the values lesser than the others, which are most exposed to warming (red-orange cluster).

These considerations confirm that the eq. 3.2 draws the climate image of G.A.R. and the glaciers follows the different behaviors of temperature and precipitation, proving that the climate evaluations of Chapeter 3 (Fig. 25) and the North-South transect (Maffezzoni master thesis, 2015) are ready to use during the classification of future MGM results.

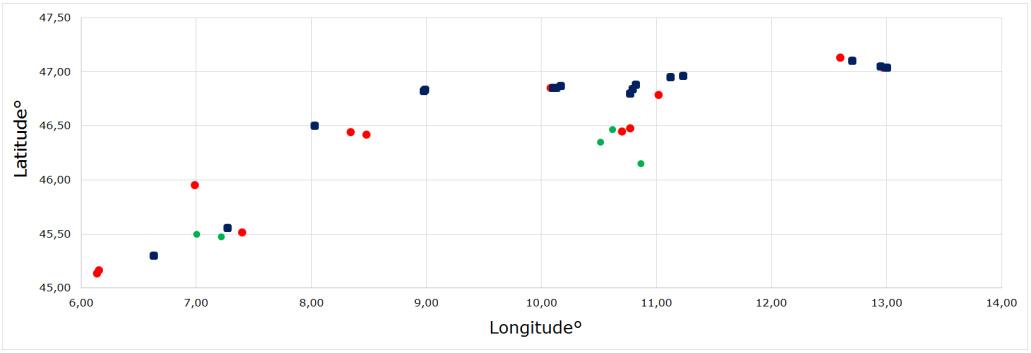

Figure 58: Spatial distribution of clusters, visualizing the latitude - longitude position of green (blue dots) and orange (red dots) clusters and the outliers. This plot evidences the same conclusion of Figure 25.

Later, I applied the cluster analysis on the other combinations between parameters 'a', 'b' and 'c' of eq. 3.2.

In Figure 59 is represented the score plot of 'a' and 'c' and in Figure 60 of 'b', and 'c' parameters. In both cases it is unrealistic the definition of different cluster: I identified only one group with the same outliers of the previous combination, confirming that the glacier follows only differences driven by temperature and precipitation, without other contributions (the intercepts).

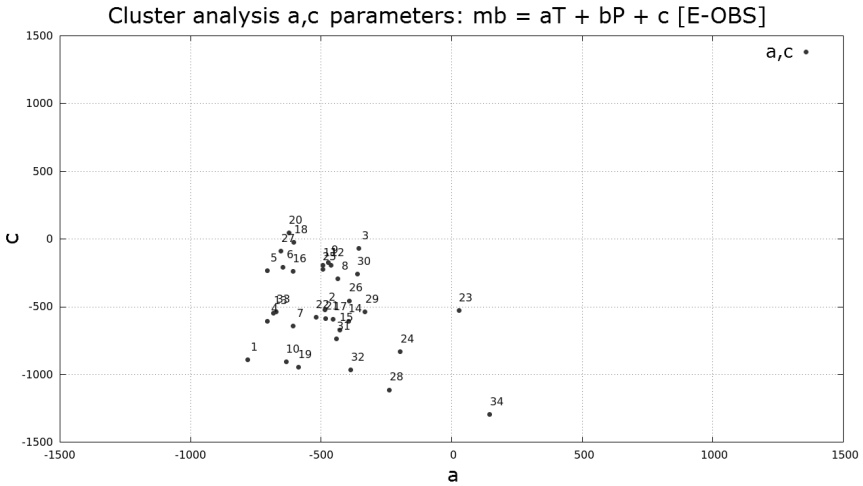

Figure 59: Scores plot with x-axis the temperature parameter 'a' and y-axis the intercepts parameter 'c'.

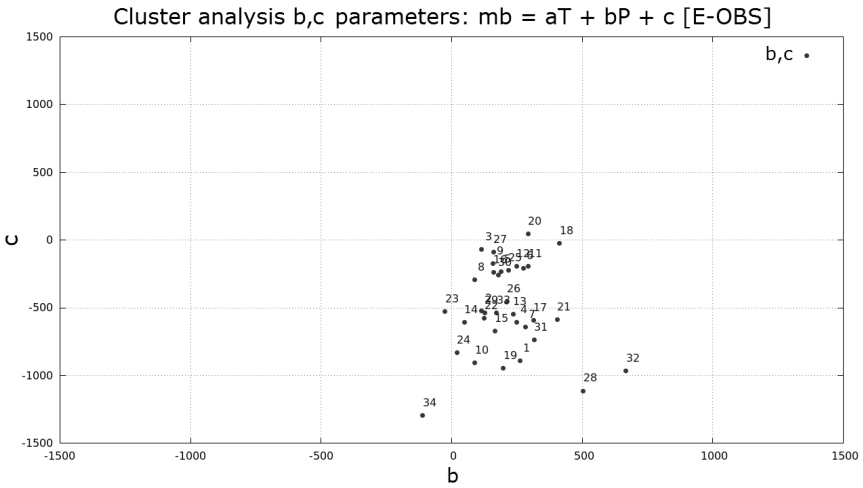

Figure 60: Scores plot with x-axis the precipitation parameter 'b' and y-axis the intercepts parameter 'c'.

Minimal Glacier Model future assessments

To illustrate the future glaciers behavior, I drove the MGM by the GCM ensemble CMIP5 from the NASA Earth Exchange Global Daily Downscaled Projections (NEX-GDDP) dataset, as explained in Chapter 3, focussing on the emission scenarios RCP 4.5 and RCP 8.5.

The spatial resolution of the dataset is 0.25 degrees (~25 km x 25 km) and then I can compare the previous analysis made on E-OBS during past period with the Prospective runs of NEX-GDDP dataset. This resolution highlights a significant focus on the local climate of studied glaciers.

I used the listed values in Tab. 8 to apply eq. 3.2 on future: each glacier was identified by its set of three multiplicative coefficients and I applied these sets to estimate future series of mass balance, driven by temperatures and precipitations of NEX-GDDP dataset. Therefore, each glaciers had 20 input sequences of MGM and consequently 20 different assessments of future glacier length.

Analysing the climate dataset, I noticed a lot of missing values of temperature and precipitation, after 2092. Therefore, I applied MGM driven by NEX-GDDP on GAR glacier up to 2092, to avoid this lack of values and to homogenize the followed statistical analysis with a complete dataset. Then I referred the last year of future consideration to 2092 and not to 2100.

Uncertainty in climate model projections is often characterized by the measure of spread across an ensemble of simulations (Tebaldi and Knutti, 2007; Knutti at al., 2013). The results depend on the range covered by the distribution of the responses and, assuming that all the models are independent, we used the spread of the different solutions to indicate the forecast range.

All the length assessments are cut off at 200 m as minimum value, because the uncertainty bars are of the order of 200 m, thus any estimate beyond this minimum threshold is not significant. Moreover, when a glacier become too small can covered by debris and its volume is mixed up with rubble, distorting its dynamics.

ID	Glaciers	Δh m	Slope °	Length m	$\alpha_m \pm \varepsilon\alpha_m$ $m^{1/2}$
SAR1	Sarennes	271	24,6	615	3,11 ± 0,35
HIN2	Hintereisferner	1258	13,4	7230	3,72 ± 0,67
KES3	Kesselwandferner	717	13,0	4038	3,42 ± 0,64
SAS4	Saint Sorlin	767	18,1	2752	3,82 ± 0,52
STU5	Stubacher Sonnblick	493	21,0	1667	3,54 ± 0,43
SIL6	Silvretta	585	13,4	2912	3,25 ± 0,59
GRI7	Gries	937	14,0	5392	3,68 ± 0,63
VER8	Vernagtferner	443	12,0	2689	2,89 ± 0,59
ALE9	Grosser Aletsch	2506	9,9	22125	2,39 ± 0,57
CAR10	Careser	388	9,6	1200	3,68 ± 0,90
PLA11	Plattalva	232	18,9	792	2,55 ± 0,38
LIM12	Limmern	1117	22,1	3448	4,36 ± 0,49
ARG13	Argentiere	2124	15,6	9220	3,23 ± 0,50
PAS14	Pasterze	1355	12,3	7927	3,64 ± 0,71
WUR15	Wurten	172	14,1	804	2,05 ± 0,41
FON16	Fontana Bianca	279	23,6	829	3,00 ± 0,36
JAM17	Jamtal	698	19,3	2415	3,81 ± 0,49
BAS18	Basodino	490	20,1	1486	3,47 ± 0,44
CIA19	Ciardoney	136	13,7	767	1,83 ± 0,41
GEB21	Gebroulaz	378	13,4	2267	2,8 ± 0,52
PEN22	Pendente	281	16,2	1160	2,62 ± 0,53
SFO24	Sforzellina	209	24,7	499	2,71 ± 0,33
KLE25	Kleinfleisskees	334	17,9	1208	2,9 ± 0,43
TMR26	Timorion	344	23,3	854	3,27 ± 0,37
GOL27	Goldberg	399	17,3	1621	3,06 ± 0,45
AGL28	Agola	288	25,1	632	3,12 ± 0,36
MAL29	Malavalle	665	12,9	4054	3,35 ± 0,63
OCH30	Ochsentalergl	633	16,7	2350	3,53 ± 0,53
VRM31	Vermuntgl	399	16,7	1637	3,03 ± 0,46
RUI32	Ruitor	866	12,9	4458	3,56 ± 0,67
LAN33	Langtaler	844	13,6	4285	3,59 ± 0,64
LUN34	Lunga Vedretta	718	16,9	2919	3,67 ± 0,54

Table 9: List of geomorphological parameters used to apply MGM on GAR glaciers. These parameters are altitude range (Δh), mean slope of the flow line and length of the analysed flow line. They are obtained by GIS-DEM analysis (Maffezzoni master thesis, 2015). In last column are listed α_m values with errors, as described in Chapter 2.

First, I grouped for each glacier the 20 runs of MGM to evaluate annual length variations of every model, in order to calculate the average value of fluctuation year by year. The MGM inputs are the mass balance driven by temperature and precipitation and the initial and surrounding conditions are obtained by GIS-DEM analysis of digital elevation model of all studied glaciers (Tab. 9) (Maffezzoni master thesis, 2015).

I excluded Fillek (n°20) because of its very small size and Grand Etret (n°23) because its R^2 of bivariate regression is close to zero.
After that, I reconstructed the average series of length retreat by using MGM, starting from the glacier size at 2011. This procedure was repeated for both the future scenarios, RCP 4.5 and 8.5, as explained before.

Any telling glaciers

All the analysed plots are archived at Appendix B, and here I want to show some significant glaciers, for their different future. I chose: Grosser Aletschgletscher because of its Himalayan size, Hinterisferner because it is a large-medium glacier and Kleinfleisskees, a small glacier.
The first significant glacier is the Grosser Aletschgletscher, the largest glacier in the Alps. It has a length of about 22 km at 2011 and it is in the Eastern Bernese Alps in the Swiss canton of Valais. The whole area of these mountains, including other glaciers, is part of the Jungfrau-Aletsch Protected Area, which was declared a UNESCO World Heritage site in 2001 (Fig 61).

Figure 61: Jungfrau-Aletsch area from space (NASA - International Space Station Imagery, 2006).

This glacier has a dynamics similar to the Himalayan glacier, because of its size, length and shape from the upper part (accumulation area) to the lowest tongue on the valley.
Since the last glaciation, the glacier generally retreated. However, slight climatic changes happened and, in 1860, the glacier was 3 km longer and the ice level 200 m higher. As for many other glaciers, records show a major longer-term retreat trend. The Aletschgletscher receded by 100 m between 2005 and 2006 (data from the Swiss Glacier Monitoring network, http://glaciology.ethz.ch).
Appling MGM driven by future climate conditions, it is possible to confirm these assumptions and to make the assessment worse.

In Figure 62 are represent the distributions of the length variation, analysed by 20 different models year by year, with their statistical values for both RCP scenarios. It is evident that the distributions have a Gaussian shape and the average values underline that the future retreat of Aletschgletscher increase, confirming the current trend: about -170 m and -210 m of average up to 2092, for RCP 4.5 and 8.5 respectively.

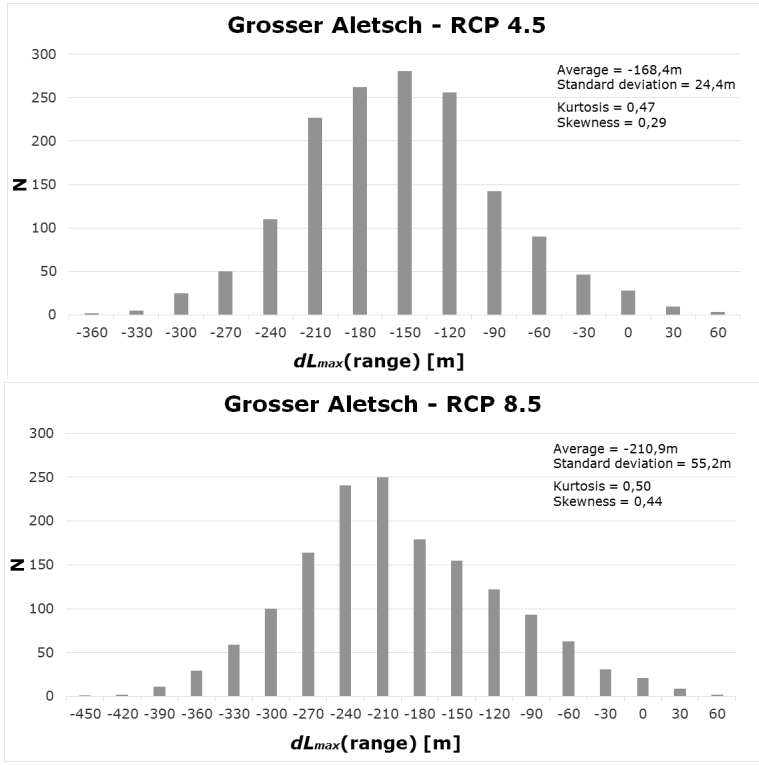

Figure 62: Aletschgletscher, histogram of length variations with statistical values of the referred probability distribution function for (a) RCP 4.5 and (b) RCP 8.5 analysis.

The results of these variations are represent in Figure 63: there are the future evolution of Aletschgletscher, obtained using the MGM driven by NEX-GDDP dataset. The coloured lines are the results of the different models of the ensemble and the trace-thick line is the average trend of all the runs year by year.
The starting point of the major flow line is 22.125 m and at 2092 this assessments reveal that the length of Aletschgletscher will become about 8400 m or 5000 m according to RCP 4.5 or RCP 8.5 respectively. Therefore, the most conservative scenario marks a retreat of about the 62% of the entire length and the 77% with the most extreme.

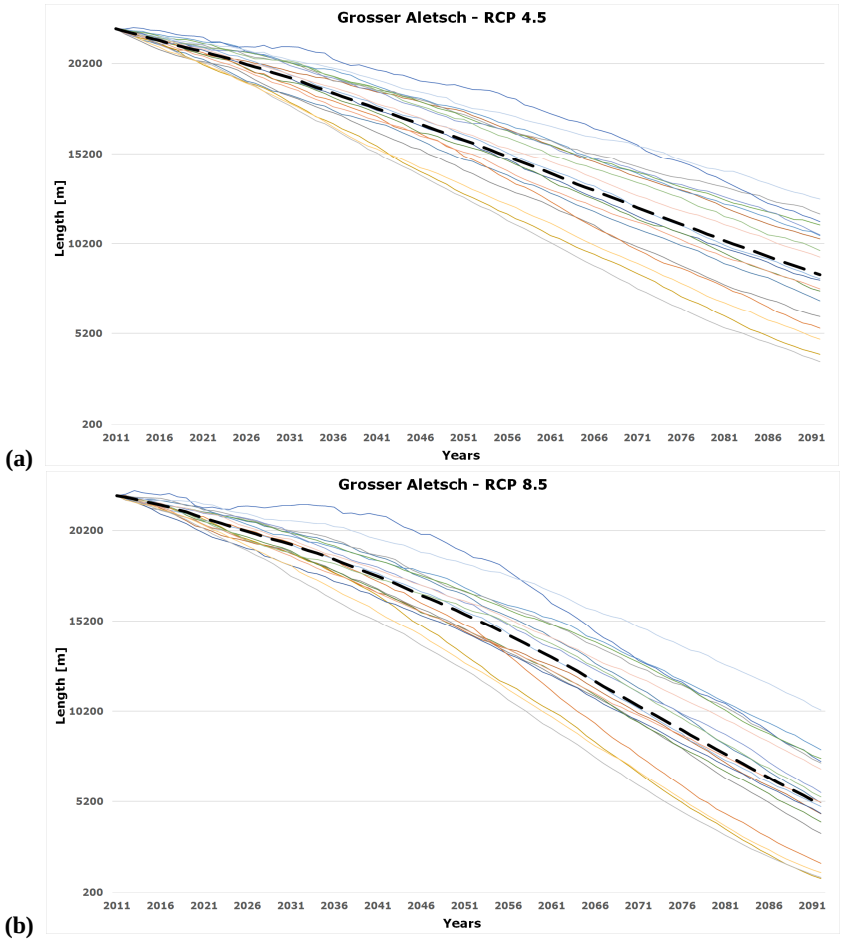

Figure 63: Future evolution of Grosser Aletsch glacier using MGM driven by NEX-GDDP climatic dataset and according to (a) RCP 4.5 and (b) RCP 8.5, from 2011 (22.125m) to 2092. The coloured lines represent the different models of the dataset and the trace-thick line is the average trend.

Then I chose Hinterisferner glacier, a valley glacier located in the inner Ötztal Alps, Austria (Fig. 64). It is the key research site for glaciological studies carried out at the Institute of Atmopsheric and Cryospheric Sciences of the University of Innsbruck (ACINN) since many decades. In historical documents, the glacier is mentioned in 1601 for the first time, which is in the context of the formation of an ice-dammed lake in front of the glacier. Similar references date from 1678, 1774, 1770, and 1816. More systematic observations, mainly referring to length changes, began in 1847 and the first regional maps were produced in 1870 and 1888. The first detailed map of Hintereisferner dates from 1894, followed by a long series of maps from terrestrial surveys and since 2001 upgraded by one or two airborne LIDAR surveys per year for geodetic determination of ice volume changes.

The ACINN hosts one of the longest mass balance series in the world, which is also an important issue in the context of recent climate variability. Hintereisferner was always considered in the context of neighbouring glaciers (Kesselwandferner and

Vernagtferner) yielding important knowledge on regional glacier behaviour (as seen in followed paragraphs).

Figure 64: Hintereisferner in the inner Ötztal Alps, Austria. On the right the other glaciers of this chain. (Jakob Abermann, Universität Innsbruck, September 2008).

Hintereisferner is a glacier with a good dynamics and an interesting valley tongue where I can apply the MGM.

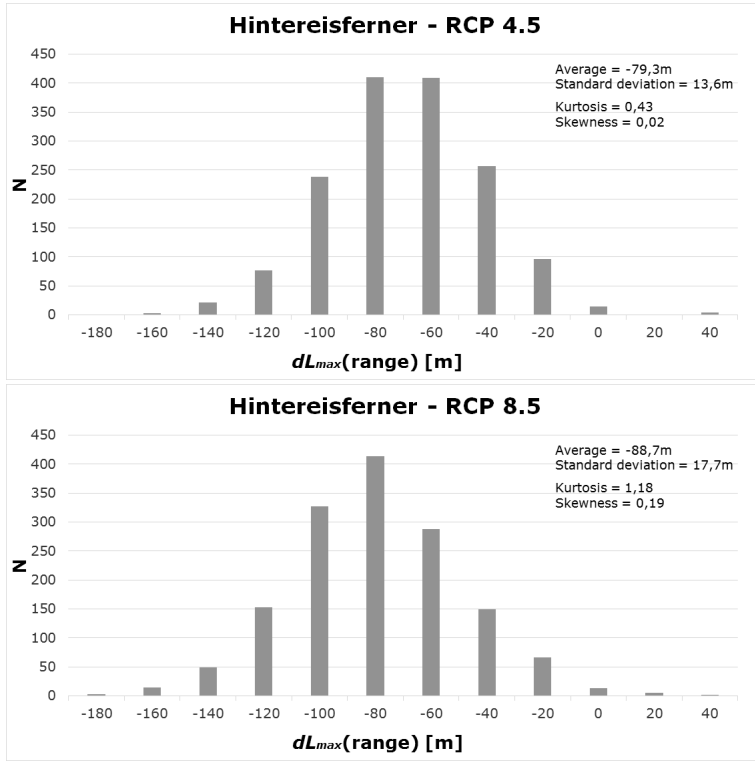

Figure 65: Hintereisferner glacier, histogram of length variations with statistical values of the referred probability distribution function for (a) RCP 4.5 and (b) RCP 8.5 analysis.

In Figure 65, the distributions of the length variation have a Gaussian shape with Skewness values near to zero; the average values of length retreat up to 2092 are about -79 m and -89 m, for RCP 4.5 and 8.5 respectively.
The results in Figure 66 start from 7.230m at 2011. The MGMs assess that Hintereisferner will disappear about 2085-2090 according to RCP 8.5 and will reach 800m of length at 2092, losing the 89% of the entire flow line, with RCP 4.5. Then, at the end of this century, Hintereisferner is intended to disappear o or become a very small glacier.

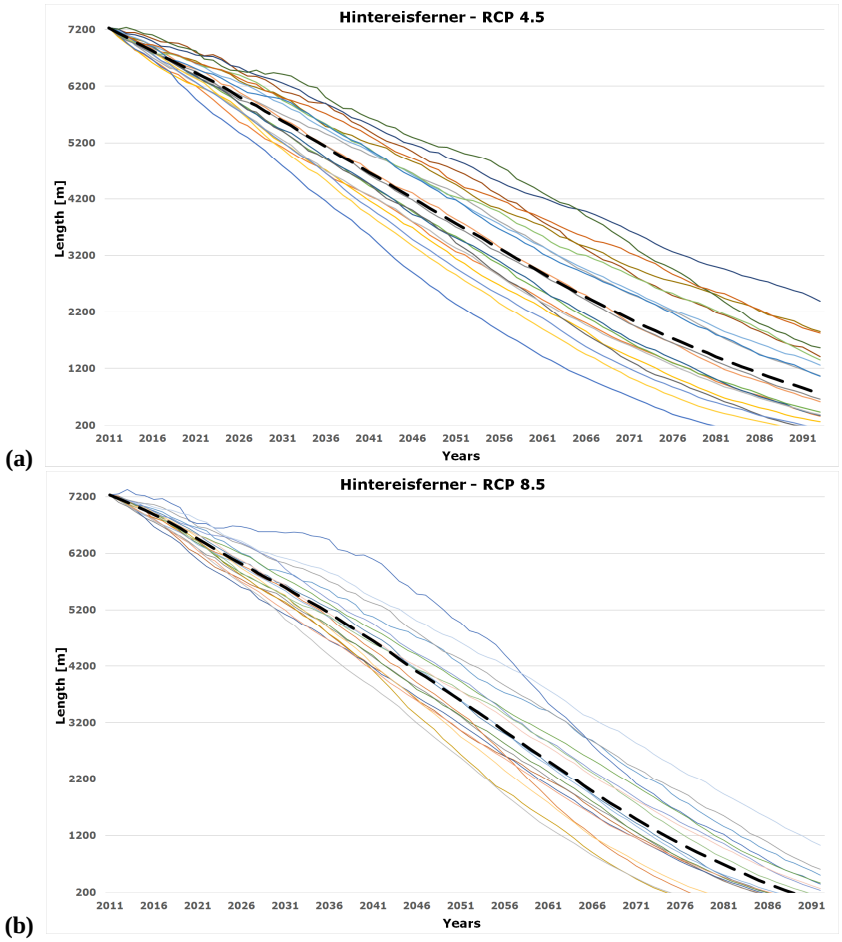

Figure 66: Future evolution of Hintereisferner glacier using MGM driven by NEX-GDDP climatic dataset and according to (a) RCP 4.5 and (b) RCP 8.5, from 2011 (7.230m) to 2092. The coloured lines represent the different models of the dataset and the trace-thick line is the average trend.

At the end of this short-list, I want to show Kleinfleisskees, a small glacier in the Hohe Tauern region, Goldberg group, in the Eastern Austrian Alps. The glacier had an area of 0.87 km^2 in 2004. The glacier is located adjacent to the Sonnblick Observatory (3106m) (Fig. 67), which has both a long-term climate record and a webcam. The mass balance of this glacier has been assessed since 1999 (Hynek et al., 2011). From 1999-

2012 the glacier has lost 7 m of water equivalent, which is over 8m of glacier thickness (WGMS) and its retreat is similar to that of Oschentaler glacier.

Figure 67: Kleinfleisskees from Sonnblick Observatorium (KleinFliess Glacier. Ge, 8/9/2014).

Kleinfleisskees is a small glacier and it is interesting to study the consequence of MGM on glacier without a long tongue or a complete accumulation-ablation dynamics.

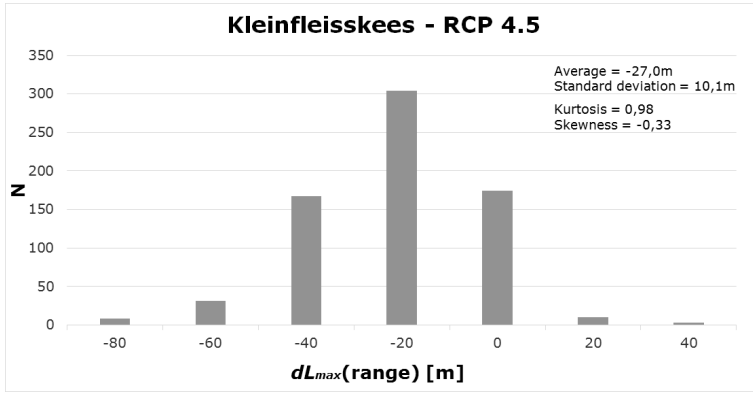

(a)

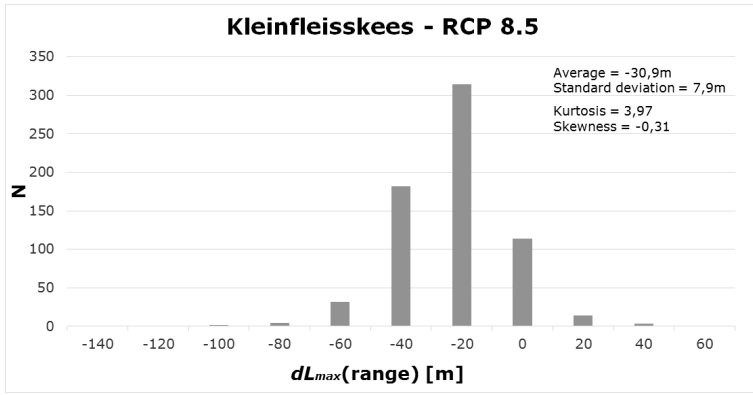

(b)

Figure 68: Kleinfleisskees glacier, histogram of length variations with statistical values of the referred probability distribution function for (a) RCP 4.5 and (b) RCP 8.5 analysis.

Applying MGM on the alive flow line of Kleinfleisskees, the average length retreat for the next decades are about -27 m for RCP 4.5 and -31 m for RCP 8.5, not much different (Fig. 68). The probability distribution function of these variation are very picked around the average values (see Kurtosis: 0,98 and 3,97 for RCP 4.5 and RCP 8.5 respectively).
Figure 69 shows the future of Kleinfleisskees: it is clear that this glacier will disappear before 2050, in particular RCP 4.5 suppose the last year at about 2047 and RCP 8.5 at about 2049.

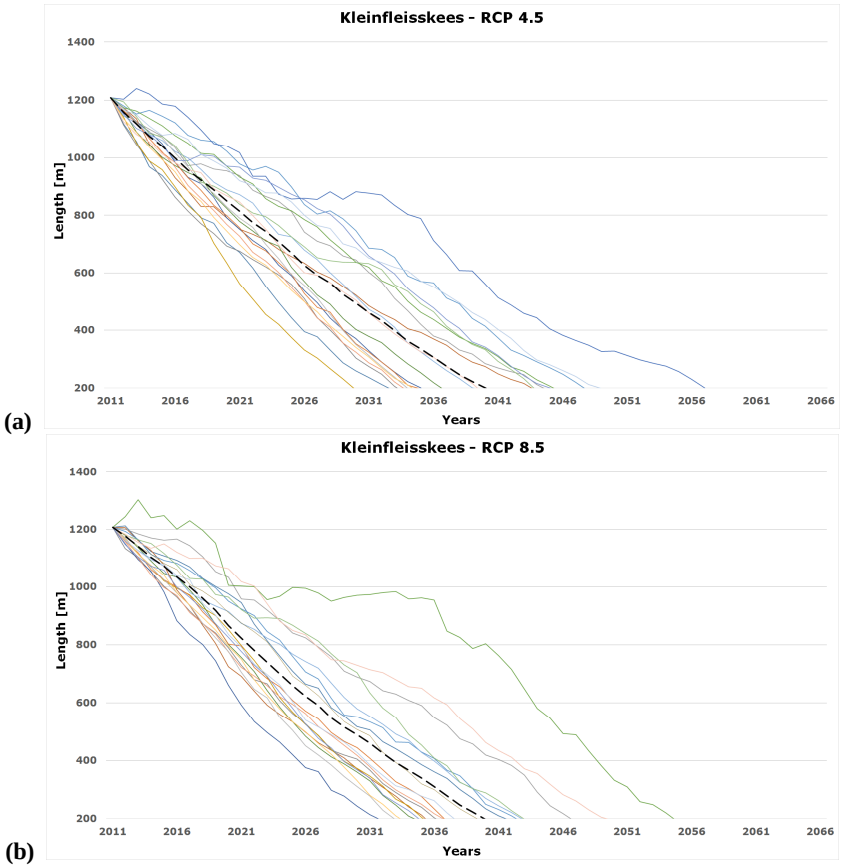

Figure 69: Future evolution of Kleinfleisskees glacier using MGM driven by NEX-GDDP climatic dataset and according to (a) RCP 4.5 and (b) RCP 8.5, from 2011 (1.208m) to 2092. The coloured lines represent the different models of the dataset and the trace-thick line is the average trend.

The comparison between the analyses about these glaciers first evidences that longer glaciers retreat with higher amount of annual variation. Referring to the discussion in Chapter 2, from the eq. 2.11 is marked that the length variation depends on the flow line length as $\frac{dL}{dt} \propto L^{1/2}$, that also contemplates the MGM formulation of mean thickness (eq. 2.2).

RCP analysis

In this paragraph, I want to compare the average future assessment of all studied glaciers dividing the ensemble for the two different RCP scenarios. The summarized distributions of annual length variation are represented in Figure 70 with the average and the median of the sample of values.

These distributions are not normal but remind a Poissonian distribution with an extended tail on the left side. This spread shape is due to the different contributions of initial conditions, where the most important is the initial length as seen before, and the behavior of the climate drivers.

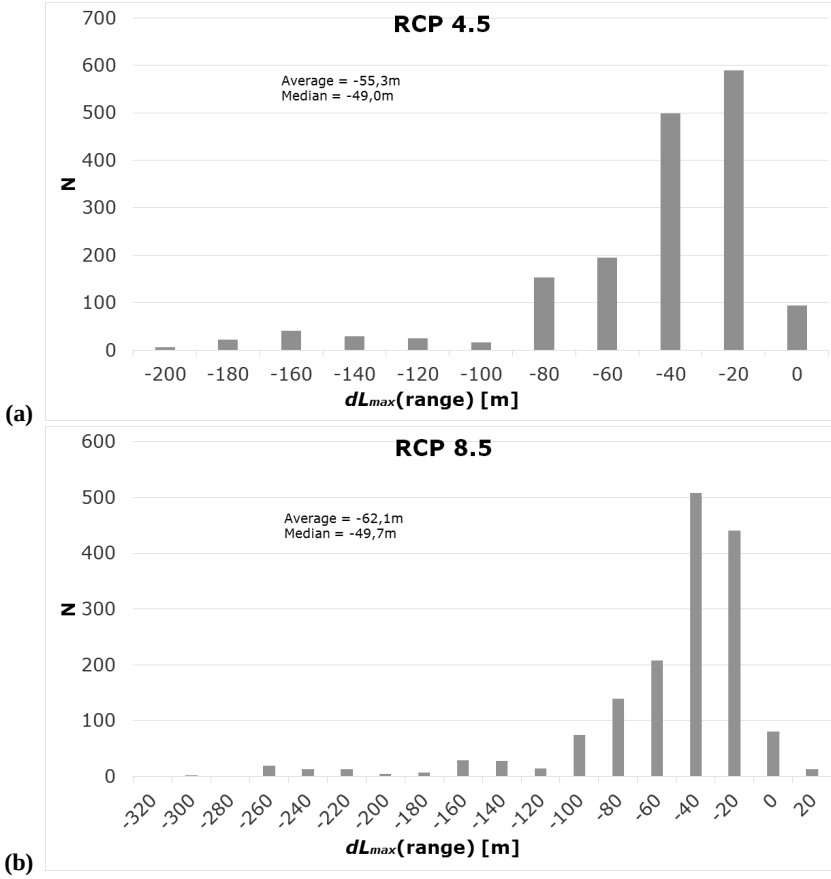

Figure 70: Summarize histograms of annual length variations driven by MGM, according to (a) RCP 4.5 and (b) RCP 8.5 scenarios of NEX-GDDP dataset, for all studied glaciers.

Therefore, the left tail represents the amount of the retreat of glaciers as Grosser Aletsch, Argentiere, Pasterze or Hintereisferner because of their longer flow line than the others, and the peak of the distribution characterizes the retreat of glaciers with medium-small flow line, which are the most numerous elements.

The two different distribution of Figure 70 underline a different statistical average of the analysed sample but a similar median. Comparing the median with the average it

is possible to understand how is the distribution and if it is share uniformly. Therefore, the averages evidence obviously that RCP 4.5 is more conservative than RCP 8.5 and the medians position the consistency of data on the right side of the distribution.
This first grouping with all glaciers divided only according to RCP scenarios is not consistent, because of the presence of glaciers with very dissimilar size, conditions and parameters that cause a significant spread of fluctuations.

Classification of MGM results

Afterwards, the last step of my Ph.D thesis is the classification of these results according to the climate of GAR, mass balance behaviors (Chapter 3) and the initial length of flow line at 2011. The aim is to link comparable glacier terminus fluctuation and to define future average trends with good correlations.
The first real problem is the same of the previous paragraph: the presence of glaciers with very dissimilar size creates a large spread of variations and any statistical analysis risk to become inconsistent and superficial. Then I want to start classifying glacier according to flow line length, to direct other possible considerations and conclusions. All these classifications are made for RCP 4.5 and RCP 8.5 separately.

Classification by length

I divided the 32 analysed glacier into 4 groups (Tab. 10), characterized by flow line length range, to assembly elements with similar mathematical behavior, as seen before, according to the dependence of variation from the flow line length: $\frac{dL}{dt} \propto L^{1/2}$ (eq. 5.1). Also considering that the length of the year *i* is an input of the model for the *i+1* years, this parameter are the most fundamental to classify series of retreats and dominates all followed considerations.
In Table 10 are listed the groups of this classification, with the number of glaciers per group and the ID of used elements. There is an outlier, the Grosser Aletsch glacier, because its dimension (more than 22Km of length) is at least two times bigger than the longer glacier of the last group.

Maximum length at 2011	N° of glaciers	ID glaciers	Mean variance and standard deviation	Mean % of retreat
1.000 m	8	SAR1, PLA11, WUR15, FON16, CIA19, SFO24, TMR26, AGL28	RCP 4.5: (-31,4 ± 12,6) m RCP 8.5: (-30,4 ± 11,8) m	RCP 4.5: 3,6% RCP 8.5: 3,5%
2.000 m	7	STU5, CAR10, BAS18, PEN22, KLE25, GOL27, VRM31	RCP 4.5: (-36,5 ± 11,6) m RCP 8.5: (-38,1 ± 10,7) m	RCP 4.5: 2,4% RCP 8.5: 2,5%
5.000 m	12	KES3, SAS4, SIL6, VER8, LIM12, JAM17, GEB21, MAL29, OCH30, RUI32, LAN33	RCP 4.5: (-43,9 ± 16,7) m RCP 8.5: (-48,3 ± 17,7) m	RCP 4.5: 1,3% RCP 8.5: 1,3%
10.000 m	4	HIN2, GRI7, ARG13, PAS14	RCP 4.5: (-88,0 ± 29,0) m RCP 8.5: (-99,5 ± 30,2) m	RCP 4.5: 1,3% RCP 8.5: 1,3%
Others	1	ALE9	RCP 4.5: (-168,4 ± 24,4) m RCP 8.5: (-210,9 ± 55,2) m	RCP 4.5: 1,2% RCP 8.5: 1,2%

Table 10: Classification of 32 glaciers into 4 groups according to the flow line maximum length, with the list of used glaciers. The two last columns (on the right) characterize this classification with mean value of annual retreat and mean percentage of annual retreat, referring to cumulative period of fluctuation 2012 – 2092 for RCP 4.5 and 8.5. The last one, Grosser Aletsch glacier, is the outliers. Vedretta Lunga (n°34) and Grand Etret (n°23) are not considered.

The last right columns of Table 10 represent:

- ✓ the mean annual variation and the related standard deviation for each group, calculating during period 2012 – 2092 for both used RCP scenarios;
- ✓ the mean percentage of annual variation, referring to the cumulative mean retreat calculated for each class at 2092 or when the class will disappear.

The hypothesis is also confirmed: as the initial length increases, so the absolute variation. However, observing last right column, small glaciers will lose more length than big glaciers, relatively to their initial dimension. The difference between RCP 4.5 and 8.5 is evident only for glaciers with considerable size, because small glaciers will become too small to show different behaviors or will disappear before the significant distinction of the RCP scenarios.

The followed figures represent the amount of glaciers retreat for each class. They show the cumulative retreat of every glacier as long as it exist and the average trend of the group when this approach is consistent.

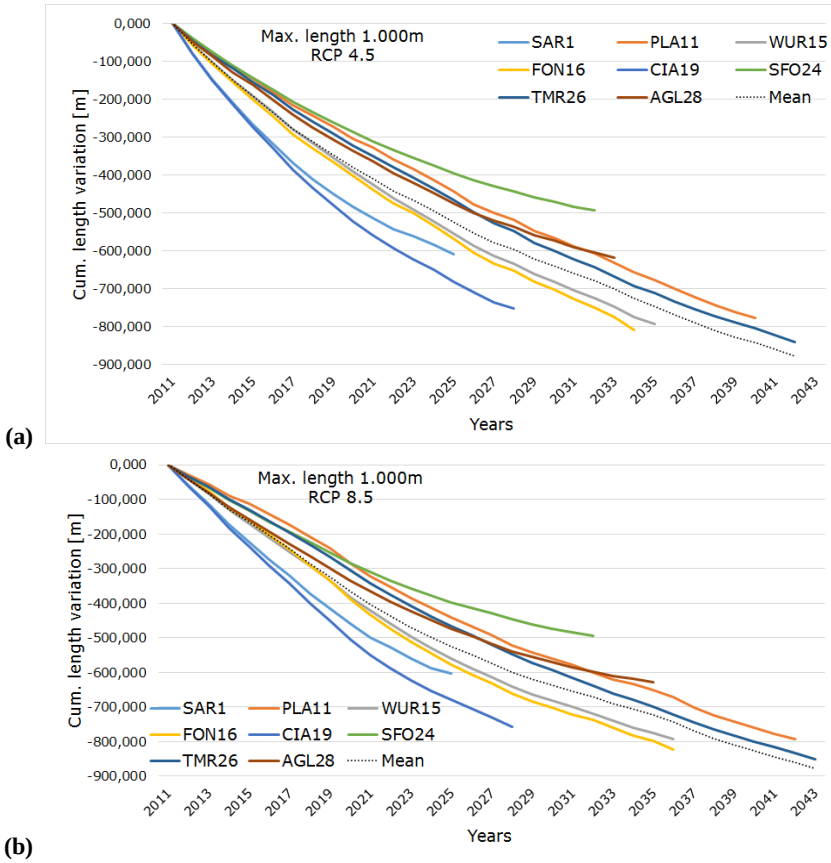

Figure 71: Results of MGM assessments on glacier with initial length lesser than 1.000m for (a) RCP 4.5 and (b) RCP 8.5. The dot lines is the average cumulative variation of this class.

Figure 71 represents glaciers with initial length lesser than 1.000m. Both scenarios identify the mean of variation about -30m per years and all these small glaciers will disappear before 2045, losing about 3,5% of their total length. The long-lived are Timorion and Plattalva glacier, because the first has the longest flow line of this group and Plattalva the best climate condition.

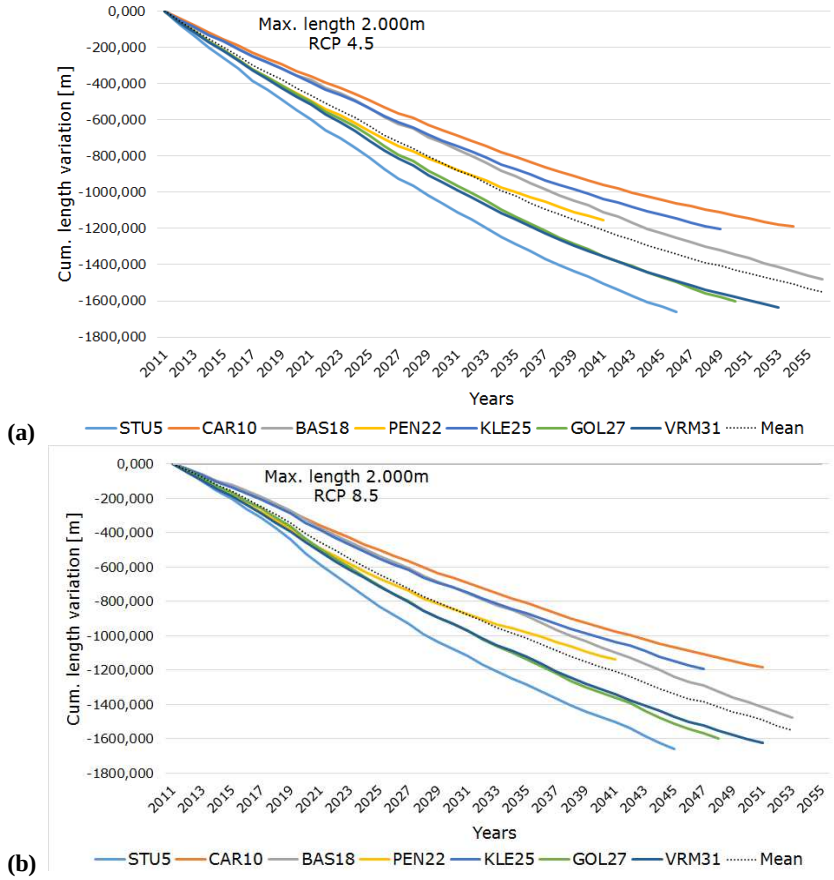

Figure 72: Results of MGM assessments on glacier with initial length lesser than 2.000m for (a) RCP 4.5 and (b) RCP 8.5. The dot lines is the average cumulative variation of this class.

Figure 72 represents glaciers with initial length between 1.000m and 2000m. These glaciers have a medium-small dimension and they are dived from the previous class to better understand their behavior.

As in Table 10, they will lose about 35-40m of their terminus, that is about the 2,5% of their total length. The last one, Basodino glacier, will disappear before 2055-2060.

Making this assessment with E-OBS dataset as historical series and using downscaled data of CMIP5 project, the future condition of Careser glacier is approximately confirmed, rising the plausibility of climate conditions because of their spatial resolution of about 25Km around the glacier.

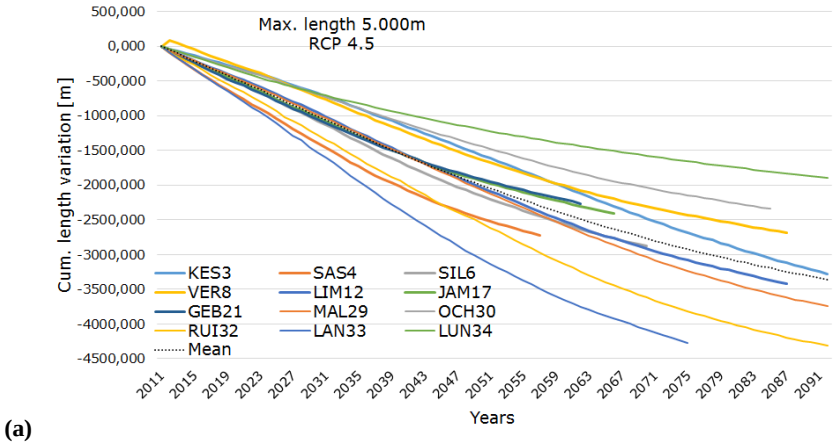

(a)

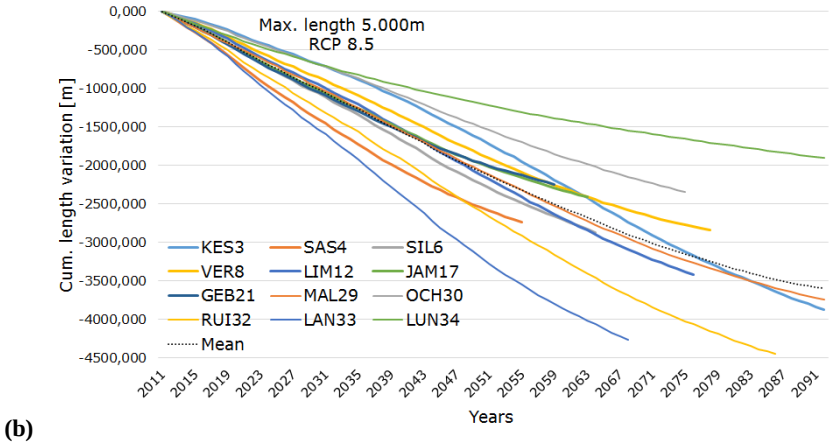

(b)

Figure 73: Results of MGM assessments on glacier with initial length lesser than 5.000m for (a) RCP 4.5 and (b) RCP 8.5. The dot lines is the average cumulative variation of this class.

In Figure 73 are represented glaciers with initial length between 2.000 and 5.000. The average variations are about 45 or 50m per year, about 1,3% of their total variation during 2012 – 2092: some glaciers will disappear and some will survive. The simulation about Vedretta Lunga show some problem due to the shortest mass balance series of the entire group, which probably does not fit with an appreciable trend.
Some glaciers, Kesselwandferner and Malavalle, will survive and become very small glacier with flow line length at most 500m. Two similar glaciers, Sarennes and Silvretta, have different behavior because of their different climate conditions: Silvretta will disappear about 30 years later than Sarennes, because the last glacier is in the Southwestern part of GAR and will receive the worst temperature condition. Silvretta will receive more conservative forcing due to its central location (see Chapter 3).

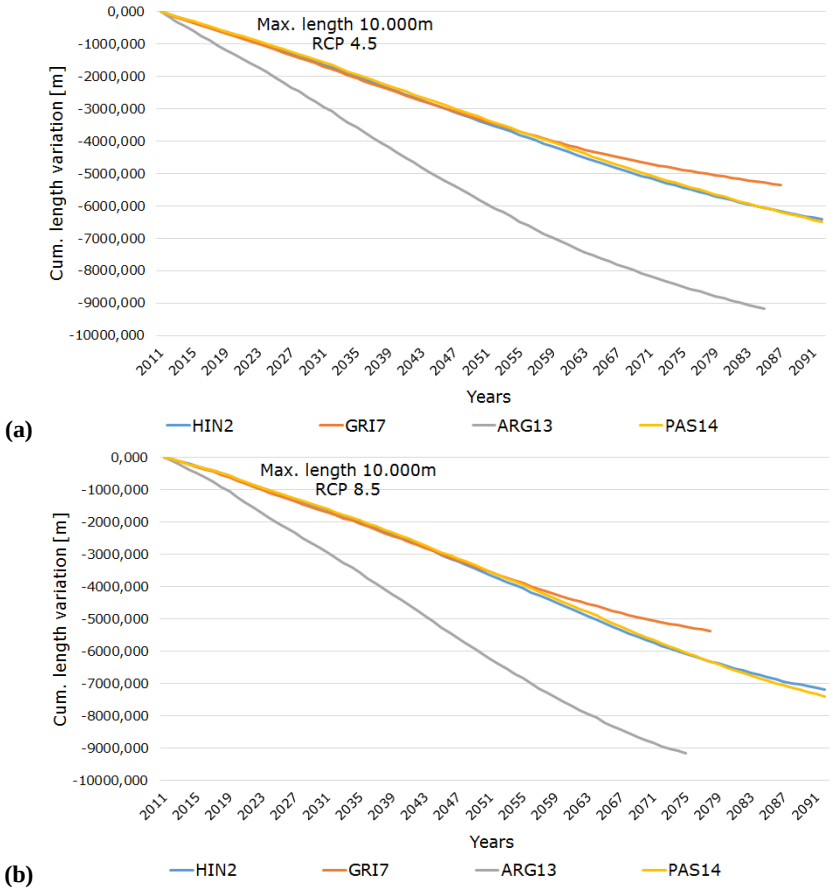

Figure 74: Results of MGM assessments on glacier with initial length lesser than 10.000m for (a) RCP 4.5 and (b) RCP 8.5.

The last representation in Figure 74 shows the four glaciers with dimension between 5.000m and 10.000. The span of this group does not allowed the formulation of an average trend, but they will lose with good accordance about 1,3% of their total variation at 2092.

Only Hintereisferner and Pasterze will survive, becoming medium small glaciers at most 1.000m of flow line at 2092 (Hintereisferner will disappear for RCP 8.5). Argentiere glacier, in spite of its longest initial length of about 9.000, will disappear before the others, because of its location on the Western part of GAR and its worst assessed climate conditions.

Grosser Aletsch is the outlier of GAR glacier, and then I did not grouped this glacier because of its particular and different dynamics and behavior, as seen before. It will lose about the 1,2% of its total variation during this century.

Classification by mass balance longitudinal sectors

Now I used considerations of Chapter 3 about mass balance series of GAR, from which we divided glaciers into 4 classes (Tab. 11), to understand some eventual sub-structure according to West – East direction.

These groups include glacier with different level of length, then the mean variances of Table 11 represent values that contain not only the mass balance behavior, but also the contribution of initial dimension of glacier. Then this classification is only a useful direction to follow climate grouping.

GAR sector	N° of glaciers	ID glaciers	Mean variance and standard deviation
Western	8	SAR1, SAS4, GRI7, ARG13, CIA19, GEB21, TMR26, RUI32	RCP 4.5: (-66,7 ± 36,0) m RCP 8.5: (-72,6 ± 39,5 m
Central	8	SIL6, PLA11, LIM12, JAM17, BAS18, OCH30, VRM31	RCP 4.5: (-39,3 ± 12,4) m RCP 8.5: (-43,1 ± 12,8) m
Central-Eastern	10	HIN2, KES3, VER8, CAR10, FON16, PEN22, SFO24, AGL28, MAL29, LAN33	RCP 4.5: (-47,3 ± 21,6) m RCP 8.5: (-52,6 ± 23,7) m
Eastern	5	STU5, PAS14, WUR15, KLE25, GOL27	RCP 4.5: (-54,2 ± 22,9) m RCP 8.5: (-59,3 ± 28,1) m

Table 11: Classification of 31 glaciers into 4 groups according to mass balance sectors of Chapter 3, that are identified by the mean value of annual retreat and the mean percentage of annual retreat, referring to cumulative period of fluctuation 2012 – 2092 for RCP 4.5 and 8.5. Grosser Aletsch (n°9) and Vedretta Lunga (n°34) are not considered, as Grand Etret (n°23).

The first sector will lose about -70m per years during 2012 – 2092 period, and all these 8 glaciers will disappear. These values of retreat are the worst on average, because of the dimension of considered glaciers and their climate locations. The central glaciers, without Grosser Aletsch, are the most conservative of entire GAR, but because of their small size, they will disappear. The long-lived glacier is the Limmerfirn (3448 m at 2011) and Ochsentaler (2350 m at 2011). The mean annual variation of Central-East sector is about -45 m because of its most conservative climate conditions (as seen before). Some glaciers can survive, such as Hintereisferner, Kesselwandferner and Langtaler. In the last Eastern sector only Pasterze will survive at 2092, because of 7927 m of flow line at 2011 are sufficient to preserve a glacier with about 1000 m of length. The glaciers of this area will lose about -55 m or -60 m for RCP4.5 and RCP 8.5 respectively.

Improved climate classification

After considerations about the initial length and classification according to longitude with mass balance behavior, I added the climate knowledge and hypothesis of Chapter 3. We divided our sample into two classes, by a simple manually digitized transect that is angle as the curvature of the Alpine chain (Fig. 22): North glaciers above transect and South Glaciers under (Maffezzoni master thesis, 2015). We focused our attention on climate contributions and, using E-OBS climate data, we improved this classification with precipitation and temperature trends.

We also studied the different behaviors inside the two sectors and, summarizing the analysis of Chapter 3:

- ✓ North and South flank of Alps are divided by different conditions, because Northern glaciers have larger winter precipitation and lower summer temperature than the Southern glaciers;
- ✓ the Western part of Alps receives biggest amount of winter precipitation and the North-Western glaciers have the highest summer temperature;
- ✓ the Central sector has the littlest amount of winter precipitation and the South part of this area has the lowest summer temperature of the entire Southern flank;
- ✓ the Central and Eastern glaciers usually have the lowest summer temperature of Northern flank.

The comparison only between Northern and Southern classes is complicated, because the dimension of glaciers are very different. As in Figure 75, the Southern glaciers are on average small, about 1300 m of length at 2011, and they do not exceed the 2900 m. Instead, the Northern glaciers are small, medium and very large: 10 glaciers are bigger than 3000 m and Grosser Aletsch is about 22 Km. Therefore, this difference of length would accentuate the difference of annual variations.

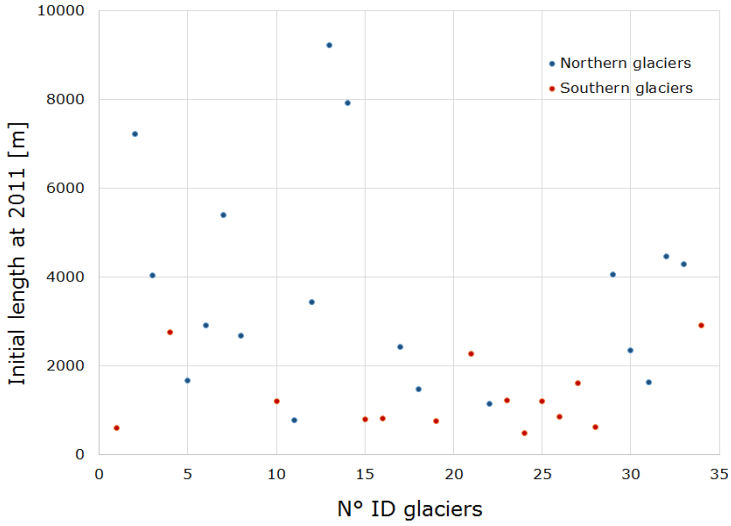

Figure 75: Scatter plot of initial length at 2011, divided for Northern (blue dots) and Southern glaciers (red dots).

With this assumption, I identified these classes with the mean annual variation:

- ✓ Northern glaciers about (-55,7 ± 28,2) m and Southern ones about (-39,0 ± 15,9) m for RCP 4.5;
- ✓ Northern glaciers about (-62,5 ± 30,5) m and Southern ones about (-39,4 ± 15,8) m for RCP 8.5.

These mean values represent, referring to the cumulative retreat from 2012 to 2092, the annual variation of about 1,3% for Northern glaciers and 2,2-2,3% for Southern ones. All these last glaciers will disappear before 2060-2062 (RCP 4.5-8.5) and the long-lived is the Gebroulaz glacier.

Then in Table 12, I divided the Northern glaciers into three classes of length to better understand the climate forcing comparing glaciers with the same level of dimension. Table 12 and Figure 76 explains that Southern glaciers and the smallest Northern glaciers will lose the same mean amount of length, but it is necessary an in-depth analysis.

GAR sector	Maximum length at 2011	N° of gl.	ID glaciers	Mean variance and st. deviation	Mean % of retreat
South	3000 m	12	SAR1, SAS4, CAR10, WUR15, FON16, CIA19, GEB21, SFO24, KLE25, TMR26, GOL27, AGL28	RCP 4.5: (-37,7 ± 15,6) m RCP 8.5: (-38,3 ± 15,4) m	RCP 4.5: 2,1% RCP 8.5: 2,2%
North	3000 m	9	STU5, SIL6, VER8, PLA11, JAM17, BAS18, PEN22, OCH30, VRM31	RCP 4.5: (-38,3 ± 13,5) m RCP 8.5: (-41,6 ± 11,6) m	RCP 4.5: 1,5% RCP 8.5: 1,6%
	5000 m	5	KES3, LIM12, MAL29, RUI32, LAN33	RCP 4.5: (-49,7 ± 15,2) m RCP 8.5: (-56,3 ± 14,1) m	RCP 4.5: 1,3% RCP 8.5: 1,3%
	10000 m	4	HIN2, GRI7, ARG13, PAS14	RCP 4.5: (-88,0 ± 29,0) m RCP 8.5: (-99,5 ± 30,2) m	RCP 4.5: 1,3% RCP 8.5: 1,3%

Table 12: Classification of 31 glaciers between Northern e Southern ones, according to the climate transect described in Chapter 3. The Northern glaciers are divided into 3 classes of length and all these groups are identified by the mean value of annual retreat and the mean percentage of annual retreat, referring to cumulative period of fluctuation 2012 – 2092 for RCP 4.5 and 8.5. Grosser Aletsch (n°9) and Vedretta Lunga (n°34) are not considered, as Grand Etret (n°23).

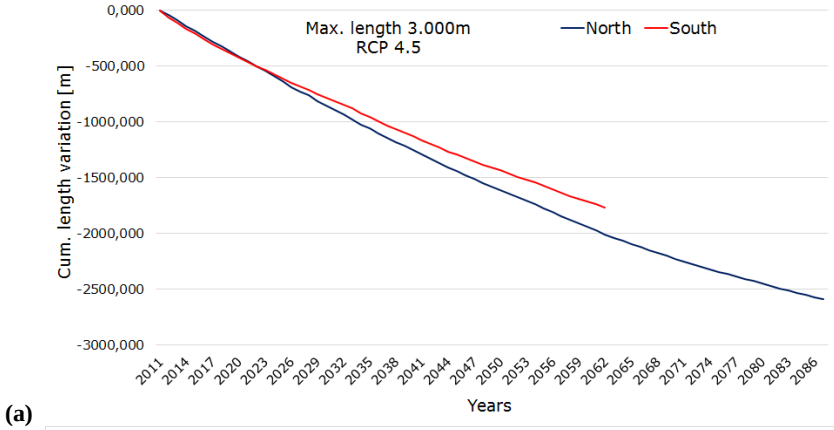

(a)

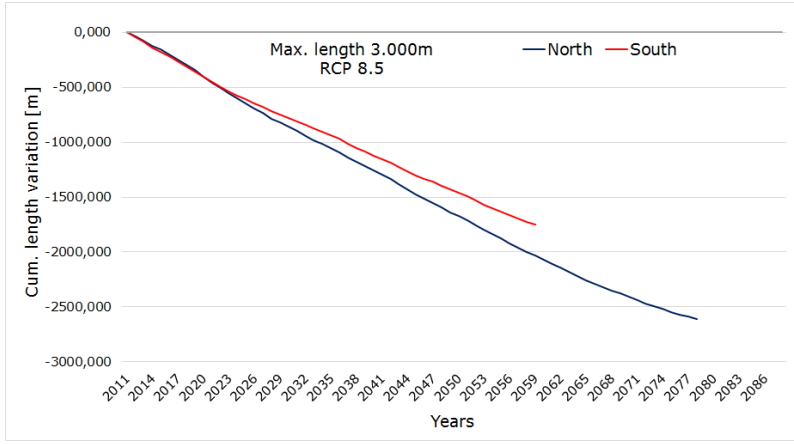

(b)

Figure 76: Average trends of MGM assessments for glaciers with initial length lesser than 3.000m, according to (a) RCP 4.5 and (b) RCP 8.5. Diagrams represent the cumulative mean variations from 2011 to the year when all elements will disappear, for Southern (red line) and Northern glaciers (blue line).

Within the Southern glaciers, the longest is the Saint Sorlin: near to Sarennes, they are the most meridional glaciers of entire GAR, not so far from the Tyrrhenian Sea and during the past they showed the worst conservative behavior. At 2011 Saint Sorlin is about 2752m of flow line length and according to future climate forcing (high precipitation but high temperature), it will disappear before 2055-2060. The most conservative glacier is the Gebroulaz, that it will disappear around the 2060 and starts with about 2267 m of length, to underline the worst climate condition of Saint Sorlin.

Instead, within smallest Northern glaciers the assessments evidence a more conservative condition, because of the lower temperature and on average the higher precipitation than the Southern ones. Then, Vernagtferner and Ochsentaler glaciers (2689 m and 2350 m) will disappear around 2090 for RCP 4.5 and 2080 for RCP 8.5, Silvretta and Jamtal glaciers (2912 m and 2415 m) around 2070 for RCP 4.5 and 2065 for RCP 8.5.

According to these analysis and observing average trends of South and North in Figure 76, it is clear that Northern glaciers had and will have the most conservative

climate scenarios as during the past, also observing the mean percentage of annual retreat (Tab. 12), calculated on the cumulative mean retreat from 2012 to the year when each class will disappear.

	Northern		Southern	
West	***RCP 4.5*** (-64,4 ± 37,4) m 1,3%	***RCP 8.5*** (-71,4 ± 40,9) m 1,4%	***RCP 4.5*** (-45,2 ± 17,9) m 2,1%	***RCP 8.5*** (-46,4 ± 17,0) m 2,2%
Central	***RCP 4.5*** (-46,3 ± 19,9) m 1,3%	***RCP 8.5*** (-52,9 ± 21,0) m 1,2%	***RCP 4.5*** (-28,5 ± 9,6) m 2,6%	***RCP 8.5*** (-28,4 ± 9,3) m 2,7%
East	***RCP 4.5*** (-59,6 ± 19,7) m 1,3%	***RCP 8.5*** (-66,1 ± 23,0) m 1,2%	***RCP 4.5*** (-35,7 ± 10,2) m 2,6%	***RCP 8.5*** (-36,6 ± 10,4) m 2,7%

Table 13: List of mean values of the annual retreat and mean percentages of the annual retreat, referring to cumulative period of fluctuation 2012 – 2092 for RCP 4.5 and 8.5. Grosser Aletsch (n°9) and Vedretta Lunga (n°34) are not considered, as Grand Etret (n°23).

The last step is the partition of Northern and Southern glaciers to create subgroups that follow longitudinal behavior, as explained in Chapter 3 and in previous paragraphs. The mean results of future assessments are listed in Table 13.
The Southern glaciers show an approximately uniform retreat and the little difference between West and other groups is due to the presence of Saint Sorlin and Gebroulaz, the longest glaciers of entire class. This means that the future climate forcing on the Southern flank of Alps do not generate significant differences on studied glaciers.
Then, the Northern glaciers are well distributed on the Alps and analysing them, is evident that the Central group is the most conservative, confirming previous hypothesis. For example, Argentiere glacier (West side of Alps) will disappear although it has 9 km of initial length, instead Hintereisferner and Kesselvandferner glaciers (Central Alps) or Pasterze glacier (Eastern flank) despite have initial length lower than Argentiere glacier will disappear later or even become small glaciers at 2092.

Conclusion

In this thesis, I had to improve the Minimal Glacier Model with GIS analysis to assess and classify the evolution of the length of Alpine glaciers, using climate dataset to drive the net mass balance.
First, I gave an overview of the structure of a glacier and of the processes involved in ablation and accumulation, which compose the mass balance processes. This first summary also shows evidences of climate change and the importance of Alpine glaciers in studying the effect of climate on the mountain environment.
Chapter 2 is a more in-depth explanation of the physical basis of MGMs algorithm, which simulates the annual variation of flow line length of a glacier with a given mass balance input, the most important variable in generating these kinds of results.
Then, supervising the bachelor thesis of Matteo Sali, I had to study the behavior of mass balance series of GAR glaciers. At the beginning of Chapter 3, I considered the mass balance datasets of 50 glaciers within GAR, reached by WGMS database and other atlas or internet archives. Therefore, I spatialized these glaciers to allow for a classification by longitudinal sector, dividing them into 4 homogeneous sector.
This analysis has shown that the Western glaciers have the worst conditions and that different types of behavior were identified durino the period from 1950 to 2010, for example, the positive trend before 1985. In other words, the period from 1950 to 2010 was characterized, in any case, by a significant loss in mass of the GAR glaciers, with several differences due to size and position.
Then, I conducted a study to assess the importance of summer temperature and winter precipitation as a climate driver of the mass balance, in collaboration with a student of the University of Turin and researchers of the ISAC-CNR of Turin.
During the master thesis of Jacopo Balocco, we analysed three gridded datasets of precipitation and temperature, coming from actual records and widely used in climatology to apply climate forcing on mass balance of GAR glaciers: CRU, E-OBS and HISTALP. According to the Akaike Information Criterion and the residuals analysis of Balocco on these dataset, we chose the linear regression with only T and P components as the best simple model to be considered in explaining mass balance variability (eq. 3.2). As far as scientific literature is concerned, nobody had ever used CRU and E-OBS before our project to reconstruct interannual mass balance series of Alpine glaciers.
Because I used the NASA NEX-GDDP dataset to drive the MGM during the future, I had to use only E-OBS dataset, the first high-resolution gridded data set of daily climate over Europe by (ECA&D), as past climate forcing. The reason was that I had to connect past mass balance analyses and future assessments between comparable datasets; in other words, I had to use the same spatial resolution of 0.25° x 0.25° for each pixel.

Then, supervising the master thesis of Luca Maffezzoni, we used E-OBS to analyse the behaviour of climate dataset on GAR. Observing summer temperature and winter precipitation trends, we confirmed that the geographical position is one of the most important factors of the health of Alpine glaciers. To better understand these contributions, we created a transect that divides Northern and Southern glaciers and we focused our attention on the dependences between climate and topography.
From the precipitation point of view, we confirmed that the entire Alpine arc is subject to the influence of Atlantic or Mediterranean storm; the North-Western Alps are the most influenced by both these weather situations. The Eastern sector (South and North area) is also often affected by precipitation that comes from low pressure near or over the Adriatic Sea, which emerges when the Azores anticyclone lies in the Northwest of Europe. In conclusion, only the Central area is less influenced, in particular the Southern sector because it is also protected by mountain chains from the orographic precipitation.
Studying temperature trends, the positive gradient of 1.5° during last three decades on entire GAR was evident. Calculating the average seasonal temperature during 1951 – 2013, we divided the Northern and Southern area with an approximate and imaginary line at 11 °C: this difference is due to the proximity of Southern glaciers to the subtropical anticyclones, which are hot air masses. The temperatures also decrease starting from the west side, due to the location of high pressure over the Alps.
At a later stage, I calibrated MGM-GIS procedure investigating the dynamics of two important glaciers on the southern side of the Alps, namely the Careser glacier in Ortles-Cevedale group, Eastern Italian Alps, and the Rutor glacier in Aosta Valley, Western Italian Alps. This was the preparatory work of the first months of this thesis for formulating the correct algorithm by using FORTRAN and Python programming languages. The MGM was then created for use via web and is available on the DISAT Geomatic Laboratory web site.
In Chapter 5, this MGM approach became a Geographic Information System Python module used in order to obtain a spatial representation of glacier retreat. With Dr. Daniele Strigaro, we created and released the platform of this module, called r.glacio.model, in a GRASS GIS environment. The main goal is to evaluate glacier behavior using a simple spatialized model, in order to reproduce this methodology on a larger amount of glaciers.
Finally, I showed the simulated results of the application of MGM on GAR glaciers, assessing response to climate scenarios up to 2100 with NASA NEX-GDDP dataset for two different RCP scenarios: the most conservative still plausible 4.5 and the most dramatic 8.5. The aim is the classification of glaciers according to the future climate conditions and their size.
Therefore, I statistically analysed and transformed the climate dataset to prepare the elements of further analysis. To create a solid model, beyond the application of the regression model (eq. 3.2) on the entire sample of glaciers, I also studied the coefficients of determination and the residuals of the model, confirming the goodness of a regression.

Using the geomorphological parameters of studied glaciers, obtained by the GIS analysis of Luca Maffezzoni and Dr. Matteo Mattavelli (Mattavelli Ph.D thesis, 2016), I applied the 20 runs of the climate NEX-GDDP dataset and for each glacier I represented the MGM average assessment and its uncertainty.
The most important parameter, α_m, is evaluated with the Haberli-Hoelze-Linsbauer method described in Chapter 2, starting from the altitude range of the glacier and calculating its basal share stress; this fundamental parameter describes the correlation between horizontal variation and thickness fluctuation during accumulation-ablation phases.
The last step was the classification of the simulations according to size and climate. It was clear that the length of the flow line (the vector line on which MGM is applied by this approach) is the most important parameter, which drives the amount of annual fluctuation of glacier terminus: as the initial length increases, so the absolute variation. Nonetheless, small glaciers with regards to their dimension will lose more length than big glaciers.
From the climate point of view, I divided GAR glaciers not only with the North-South transect, but also with their longitudinal position. Moreover, I divided the Northern glaciers into three classes of length to better understand the climate forcing comparing glaciers with the same level of size. The comparison between Northern and Southern glaciers with the same length confirmed the more conservative condition of the first sector, as during the past.
To better understand the future climate influence on GAR glaciers, I also created three subgroups that follow longitudinal behavior, as explained in Chapter 3. The future climate forcing on the Southern flank of Alps does not generate any significant difference, with no diversity also between RCP 4.5 and 8.5, because glaciers will become too small to show different behavior or will disappear before the significant distinction of RCP contribution. Therefore, the Northern glaciers showed that the Central-Eastern groups are the most conservative, confirming the climate consideration of low summer temperatures and high orographic winter precipitations.
Finally, I can conclude that up to 2100 all GAR glaciers will lose from 70-80% to 100% of their initial length and the most dramatic RCP 8.5 scenario will kill more glaciers than RCP 4.5. Thus, the biggest will become medium or small glaciers and the actual medium and small glaciers will disappear following their climate fate.
I also have to recall that MGMs are applicable if the glacier is not a debris-covered glacier, because the covering interrupts the normal dynamics and usual accumulation-ablation processes. Therefore, these assessments do not contemplate possible covering of glaciers during the next decades and are valid if this condition is respected.
During these analyses, I have always excluded the Grosser Aletsch glacier, because it is the biggest glacier of the GAR and is more than twice the size of the second biggest glacier. Grosser Aletsch futures dynamics similar to the Himalayan glacier, because of its size, length and shape from the upper part (accumulation area) to the lowest tongue on the valley. Moreover, the application of MGM-GIS approach with climate dataset is a good way to practice extending this procedure on this type of glaciers.

I think that the combination of the Minimal Glacier Model with the GIS analysis, the improved regression model to reconstruct the mass balance and the use of downscaled GCM for future climate condition can be an exciting idea if it is applied on Himalayan glaciers.
The objective of this thesis was to provide simple methods for reproducing and assessing glacier behavior, using reachable parameters and datasets in order to reproduce this methodology on a larger amount of glaciers.
I hope and have the impression, that this goal was achieved. However, in the future this procedure will be improved in particular for the reconstruction of mass balance and will be calibrated and developed on other regions, modifying the MGM algorithm for all kinds of glaciers.

Acknowledgements

Firstly, I would like to express my sincere gratitude to my advisor Prof. Valter Maggi for the support of my Ph.D study and for his motivation and patience, and Prof. Antonello Provenzale, tutor of NexData project, for his knowledge and supervision.
I have to thanks also Prof. Marco Vighi, coordinator of Ph.D school, and Prof. Carlo Baroni for his useful comments during this work.

Besides my advisor, I would like to thank the rest of my thesis helper: Dott. Elisa Palazzi and Dott. Jost Von Hardenberg, for their comments, contributions and encouragement, but also for the hard question, which recommended me to widen my research from various perspectives.

My sincere thanks also go to Dr. Matteo Mattavelli, Dr. Daniele Strigaro, Dr. Roberto Garzonio and Dr. Ivan Frigerio, who provided me an opportunity to join their team as intern. Without their precious support it would not be possible to conduct this research. In addition, I have to thank Dr. Luca Maffezzoni, Dr. Jacopo Balocco and Dr. Matteo Sali, master and bachelor students, with which I collaborated and supervised during these years.

Also, I thank my friends Dr. Massimiliano Clemenza of Physical Department – INFN Milano – Bicocca, for enlightening me the first glance of research, for his support during difficulties and for experiments and events inside the physics and faraway from PC.

Last but not the least, I would like to thank all my friends and my family: my parents for supporting me also economically and my girlfriend, my morning star, which sustain me spiritually and materially throughout writing this thesis and my life.

*This work was supported by the **Project of Interest NextData** of the Italian Ministry of Education, University and Research.*

To Tania

List of figures

List of tables

References

Articles and books

Abdalati W., Krabill W., Frederick E., Manizade S., Martin C., Sonntag J., Swift R., Thomas R., Wright W., Yungel J., (2001): Outlet glacier and margin elevation changes: Near-coastal thinning of the Greenland ice sheet, 2001. *Journal of Geophysical Research*, 106(D24): 33,729–33,742.

Arendt A., Echelmeyer K., Harrison W. D., Lingle G., Valentine V., (2002): Rapid wastage of Alaska Glaciers and their contribution to rising sea level. *Science,* 297: 382–386.

Barry R. G. (2013): Mountain weather and climate, *Routledge.*

Bartzokas A. (1989): Annual variation of pressure over the Mediterranean area. *Theor. Appl. Climatol.* 40, 135- 146

Bellouin N. et al (2013): Aerosol forcing in the Climate Model Intercomparison Project (CMIP5) simulations by HadGEM2-ES and the role of ammonium nitrate. *J. of Geoph. Res.* Volume 116, Issue D20.

Beniston, M. (2000): Environmental change in mountains and uplands.

Beniston M. (2005): Mountain climates and climatic change: an overview of processes focusing on the european alps, *Pure and Applied Geophysics,* 162(8-9), 1587–1606.

Beniston M. (2006). Mountain weather and climate: a general overview and a focus on climatic change in the Alps. *Hydrobiologia*, *562*(1), 3-16.

Benn D. I., Evans D. J. A. (1998): Glaciers and Glaciation, *A Hodder Arnold Publication*

Benson, C.S. (1961): Stratigraphic studies in the snow and firn of the Greenland Ice Sheet, *Folia Geographica Danica*, vol. 9, pp. 13–37.

Bi D. et al (2013): The ACCESS Coupled Model: Description, Control Climate and Evaluation. *Aust. Met. Oceanog. J.* CMIP5 Special Issue.

Bonanno R., Ronchi C., Cagnazzi B, Provenzale A. (2013): Glacier response to current climate change and future scenarios in the northwestern Italian Alps. *Reg. Environ. Change*. v.13, n.4

Bonanno, R., C. Ronchi, B. Cagnazzi, and A. Provenzale (2014), Glacier response to current climate change and future scenarios in the northwestern italian alps, *Regional Environmental Change*, 14(2), 633–643.

Braithwaite R. J., Raper S. C., Candela R. (2013): Recent changes (1991–2010) in glacier mass balance and air temperature in the European alps. *Annals of Glaciology*, 54(63), 139–146.

Brunetti M., Maugeri M., Nanni T., Auer I., Böhm R., Schöner W. (2006): Precipitation variability and changes in the greater alpine region over the 1800–2003 period. *Journal of Geophysical Research: Atmospheres* (1984–2012), 111(D11).

Burnham K. P., Anderson D. R. (2003): Model selection and Multimodel Inference: a practical Information-Theoretic approach, *Springer Science & Business Media.*

Calmanti, S., L. Motta, M. Turco, and A. Provenzale (2007), Impact of climate variability on alpine glaciers in northwestern Italy, *International Journal of Climatology*, 27(15), 2041–2053.

Cantu V. (1977). The climate of Italy. *World survey of climatology*, *6*, 127-183.

Carturan L., Seppi R. (2007): Recent mass balance results and morphological evolution of Careser Glacier (Central Alps). *Geogr. Fìs. Din. Quat.*, 30(1), 33–42.

Carturan L., Seppi R. (2009): Comparison of current behavior of three glaciers in western Trentino (Italian Alps). In *Epitome: Geoitalia 2009, Settimo Forum Italiano di Scienze della Terra, 9–11 September 2009, Rimini, Italy,* Vol. 3. Federazione Italiana di Scienze della Terra, 298.

Carturan L., Dalla Fontana G., Cazorzi F. (2009a): The mass balance of La Mare Glacier (Ortles-Cevedale, Italian Alps) from 2003 to 2008. In *Epitome: Geoitalia 2009, Settimo Forum Italiano di Scienze della Terra, 9–11 September 2009, Rimini, Italy,* Vol. 3. Federazione Italiana di Scienze della Terra, 298.

Carturan L., Cazorzi F., Dalla Fontana G. (2012): Distributed mass-balan ce modelling on two neighbouring glaciers in Ortles-Cevedale, Italy, from 2004 to 2009, *J. of Glac.*, vol 58, No 209.

Carturan L., Baroni C., Becker M., Bellin A., Cainelli O., Carton A., Casarotto C., Dalla Fontana G., Godio A., Martinelli T., Salvatore M.C., Seppi R. (2013): Decay of a long-term monitored glacier: Careser Glacier (Ortles-Cevedale, European Alps). *The Cryosphere*, 7, 1819-1838.

Casty C., Wanner H., Luterbacher J., Esper J., Böhm R. (2005): Temperature and precipitation variability in the european alps since 1500, *International Journal of Climatology,* 25(14), 1855–1880.

Cogley, J. G. (2009): Geodetic and direct mass balance measurements: Comparison and joint analysis, *Ann. Glaciol.*, 50, 96–100.

Cubasch U., Wuebbles D., Chen D., Facchini M.C., Frame D., Mahowald N., Winther J.-G. (2013): Introduction. *In: Climate Change 2013: The Physical Science Basis. Contribution of Working Group I to the Fifth Assessment Report of the Intergovernmental Panel on Climate Change,* Cambridge University Press, Cambridge, United Kingdom and New York, NY, USA

Durand Y., Laternser M., Giraud G., Etchevers P., Lesaffre B., Mérindol L. (2009): Reanalysis of 44 yr of climate in the french alps (1958-2002): Methodology, model validation, climatology, and trends for air temperature and precipitation. *Journal of Applied Meteorology and Climatology*, 48(3), 429–449.

Dyurherov M.B., Meier M.F. (2005): Glaciers and the Changing Earth system, a 2004 snapshot. *Institute of Arctic and Alpine Research, University of Colorado,* occasional paper 58, INSTAAR/OP-58, ISSN 0069-6145.

Echelmeyer K., Harrison W., Larsen C., Sapiano J., Mitchell J., DeMallie J., Rabus B., (1996): Airborne elevation profiling of glaciers: A case study in Alaska. *Journal of Glaciology,* 42(142): 538–547.

Evans I. S. (1990): Climatic effects on glacier distribution across the southern Coast Mountains, BC, Canada. *Annals of glaciology,* 14, 58-64.

Evans I. S. (2006): Glacier distribution in the Alps: statistical modelling of altitude and aspect. *Geografiska Annaler: Series A, Physical Geography*, 88(2), 115-133.

Fountain A. G., Krimmel R. M., Trabant D. C. (1997): A strategy for monitoring glaciers (No. 1132). USGPO; *Free on applications to the US Geological Survey, Information Services.*

Frei C., Schär C. (1998): A precipitation climatology of the Alps from high-resolution rain-gauge observations. *International Journal of Climatology*, *18*(8), 873-900.

Gardelle, J., Berthier, E., Arnaud, Y. (2012): Slight mass gain of Karakoram glaciers in the early twenty-first century. *Nature Geoscience*, DOI: 10.1038/NGEO1450.

Gardner, A. S., Moholdt, G., Wouters, B., Wolken, G. J., Burgess, D. O., Sharp, M. J., Cogley, J. G., Braun, C., and Labine, C. (2011): Sharply increased mass loss from glaciers and ice caps in the Canadian Arctic Archipelago, *Nature*, 473, 357–360, doi:10.1038/nature10089.

Giorgetta, M. A. et al. (2013): Climate and carbon cycle changes from 1850 to 2100 in MPI-ESM simulations for the Coupled Model Intercomparison Project phase 5. *J. of Adv. In Mod. Earth Sys.* VOL. 5, 572–597.

Gray D. M., Male D. H. (1981): Handbook of Snow: Principles, Processes, Management and Use. *Toronto, Pergamon Press*, 776pp.

Haeberli W., (1995): Glacier fluctuations and climate change detection. *Geogr. Fis. Dinam. Quat*, 18, 191-199

Haeberli W., Hoelzle M. (1995): Application of inventory data for estimating characteristics of and regional climate-change effects on mountain glaciers: a pilot study with the European Alps. *Annals of Glaciol*. 21, 206–212.

Hamming R.W. (1986): Numerical Methods for Scientists and Engineers, *Unabridged Dover*, republication of the 2nd edition published by McGraw-Hill 1973

Haylock M. R. et al (2008): A European daily high-resolution gridded data set of surface temperature and precipitation for 1950-2006. *J. Geophys. Res*., 113, D20119.

Hazeleger W. et al (2013): EC-Earth V2.2: description and validation of a new seamless earth system prediction model. *Clim. Dyn.* 39:2611–2629.

Hynek B., Unger R., Schöner W., Binder D. and Weyss G. (2011): Comparison of volumetric and glaciological mass balances of Goldbergkees, Kleinfleißkees (1998-2009) and Wurtenkees (1998-2006), Austria. Abstract of Poster presentation of "*15th Alpine Glaciology Meeting 2011, Munich, Germany*".

Hofierka J., Mitásová H., and Neteler M. (2009): Geomorphometry. Concepts, Software, Applications, *volume 33 of Developments in Soil Science*. Elsevier, ISBN 9780123743459.

Hurrell J. W. et al (2013): The Community Earth System Model: A Framework for Collaborative Research. *Am. Met. Soc.* Volume 94, Issue 9.

Huss M., Hock R., Bauder A., Funk M. (2010): 100-year mass changes in the swiss alps linked to the atlantic multidecadal oscillation, *Geophysical Research Letters*, 37(10).

Huss M. (2012): Extrapolating glacier mass balance to the mountain-range scale: the European Alps 1900-2100. *The Cryosphere*, 6, 713-727.

Huybrechts P., Steinhage D., Wilhelms F., Bamber J. (2000): Balance velocities and measured properties of the Antarctic ice sheet from a new compilation of gridded data for modelling. *Annals of Glaciology,* volume 30, pages 52–60.

Jeffrey S., Rotstayn L., Collier M., Dravitzki S., Hamalainen C., Moeseneder C., Wong K. and Syktus J. (2012): Australia's CMIP5 submission using the CSIRO-Mk3.6 model. *Austr. Meteo. Ocean. Journ.* V.63 1-13.

Jouvet, G., Huss M., Blatter H., Picasso M., Rappaz J. (2009): Numerical simulation of Rhonegletscher from 1874 to 2100. *J. Computational Physics,* 228, 6426–6439.

Kappenberger G. (2009): Ghiacciaio del Basodino, bilancio di massa 2008-2009.

Knutti R., Masson D., Gettelman A. (2013): Climate model genealogy: Generation CMIP5 and how we got there. *Geophy. Res. Lett.,* Vol 40, Issue 6, pages 1194–1199.

Krimmel R. M. (1999): Analysis of difference between direct and geodetic mass balance measurements at South Cascade Glacier, Washington. *Geografiska Annaler: Series A, Physical Geography,* 81(4), 653-658.

Kuhn M., Dreiseitl E., Hofinger S., Markl G., Span N. and Kaser G. (1999): Measurements and Models of the Mass Balance of Hintereisferner. *Geografiska Annaler: Series A, Physical Geography*, 81: 659–670. doi: 10.1111/1468-0459.00094

Le Bris R., Paul F. (2013): An automatic method to create flow lines for determination of glacier length: A pilot study with alaskan glaciers. *Computers and Geosciences,* 52: 234–245.

Linsbauer A., Paul F., Haberli W. (2012): Modeling glacier thickness distribution and bed topography over entire mountain ranger with GlabTop: Application of fast and robust approach. *Journal of Geo. Res.,* Vol. 117, F03007.

Lolis C. J., Bartzokas A., Katsoulis B. D. (2002): Spatial and temporal 850 hPa air temperature and sea-surface temperature covariances in the Mediterranean region and their connection to atmospheric circulation. *Int. J. Climatol*. 22: 663–676.

Male D.H. (1980): The seasonal snow cover. In Colbeck, S., editor, *Dynamics of snow and ice masses, New York: Academic Press*, 305–91.

Martin G. M. et al (2012): The HadGEM2 family of Met Office Unified Model Climate configurations. *Geosci. Model Dev. Discuss*. 4, 765-841, 2011.

Marzeion B., Nesje A. (2012): Spatial patterns of north atlantic oscillation influence on mass balance variability of european glaciers, *The Cryosphere*, 6(3), 661–673.

Matthews, H. D., Weaver A.J. (2010): Committed climate warming. *Nature Geosci.*, 3, 142–143.

Maurer E. P., Hidalgo H. G. (2008): Utility of daily vs. monthly large-scale climate data: an intercomparison of two statistical downscaling methods. *Hydrology and Earth System Sciences,* 12(2), 551-563.

Meehl G. A. et al (2012): Climate System Response to External Forcings and Climate Change Projections in CCSM4. *J. of Climate* 25, 3661–3683.

Meinshausen M., Smith S. J., Calvin K., Daniel J. S., Kainuma M. L. T., Lamarque J. F., … Van Vuuren D. P. P. (2011): The RCP greenhouse gas concentrations and their extensions from 1765 to 2300. *Climatic change*, 109(1-2), 213-241.

Mitasova H., Hofierka J., Zlocha M., Iverson L.R. (1996): Modelling topographic potential for erosion and deposition using GIS. *International Journal of Geographical Information Systems*, 10(5):629–641.

Müller, F. (1962): Zonation in the accumulation area of the glaciers of Axel Heiberg Island, *Journal of Glaciology*, vol. 4, 1962, pp. 302–313.

Nesje A, Dahl S. O. (2000): Glaciers and Environmental Change. *Arnold Publishers: London.*

Oerlemans, J. (1994): Quantifying global warming from the retreat of glaciers. *Science-AAAS-Weekly Paper Edition-including Guide to Scientific Information*, 264(5156), 243-244.

Oerlemans J. (2001): Glaciers and climate change. *Balkema Publishers,* Lisse

Oerlemans J. (2010): The Microclimate of Valley Glacier. *Second print. Igitur, Utrecht Publishing & Archiving Services,* Universiteitsbibliotheek Utrecht. ISBN 978-90-393-5305-5.

Oerlemans J. (2011): Minimal glacier models. *Second print. Igitur, Utrecht Publishing & Archiving Services,* Universiteitsbibliotheek Utrecht. ISBN 978-90-6701-022-1.

Oerlemans J., Van der Veen CJ (1984): Ice sheets and climate. *Reidel, Dordrecht*, 217 pp.

Østrem, G., Haakensen, N., Eriksson, T. (1981). The glaciation level in southern Alaska. *Geografiska Annaler. Series A. Physical Geography*, 251-260.

Østrem G., Brugman M., (1991): Glacier mass-balance measurements, a manual for field and office work. *N.H.R.I. Science Report*, 4, 224 pp.

Orombelli G. (2005): Il ghiacciaio del ruitor (valle d'aosta) nella piccola età glaciale. *Geografia Fisica e Dinamica Quaternaria*, n. suppl. 7, pp 239–251.

Paterson W. (2010), The Physics of Glaciers, *Pergamon,* Tarrytown, N.Y.

Paul F., Kaab A, Maisch M., Kellenberger T., Haeberli W. (2004): Rapid disintegration of Alpine glaciers observed with satellite data. *Geophysical Research Letters,* 31, L21402

Pepin N., and 20 others (2015). Elevation-Dependent Warming in Mountain Regions of the World. *Nature Climate Change*, in press.

Rangwala I., Miller J.R. (2012): Climate change in mountains: a review of elevation-dependent warming and its possible causes. *Climatic Change* 114, 527-547

Reeh, N. (1988): A flow-line model for calculating the surface profile and the velocity, strain-rate, and stress fields in an ice sheet. *J. of Glac*. Vol 34, Issue 116, 46-54

Reijmer, C. and Hock, R. (2008): Internal accumulation on Storglaciaren, Sweden, in a multi-layer snow model coupled to a distributed energy-and mass-balance model, *J. Glaciol.,* 54, 61–72.

Rotstayn L. D. et al (2012): Aerosol- and greenhouse gas-induced changes in summer rainfall and circulation in the Australasian region: a study using single-forcing climate simulations. *Atmos. Chem. Phys.* 12, 6377–6404.

Schmidli J., Schmutz C., Frei C., Wanner H., Schär C. (2002): Mesoscale precipitation variability in the region of the european alps during the 20th century. *International Journal of Climatology*, 22(9), 1049–1074.

Strigaro D., Moretti M., Mattavelli M., De Amicis M., Maggi V., Provenzale A. (2015) Development of GIS methods to assess glaciers response to climatic fluctuations: a Minimal Model approach, *Geomorphometry for Geosciences* (pp.205-208).

Taylor K. E., Stouffer R. J. and Meehl G.A. (2012): An Overview of CMIP5 and the Experiment Design. *Am. Meteo. Soc.* DOI: 10.1175.

Tebaldi C., Knutti R. (2007): The use of the multi-model ensemble in probabilistic climate projections. *Phil. Trans. R. Soc. A.* Vol. 365, Issue 1857.

Thrasher B., Maurer E. P., McKellar C., Duffy P. B. (2012): Technical Note: Bias correcting climate model simulated daily temperature extremes with quantile mapping. *Hydrology and Earth System Sciences,* 16(9), 3309-3314.

Tryon R. C. (1939): Cluster analysis: correlation profile and orthometric (factor) analysis for the isolation of unities in mind and personality. *Edwards brother, Incorporated, lithoprinters and publishers*.

Uppala S. M. et al (2005): The ERA-40 re-analysis. *Q. J. R. Meteorol. Soc.* 131, pp. 2961–3012.

Van Vuuren D.P and others (2011): The representative concentration pathways: an overview. *Climatic Change*, 10.1007/s10584-011-0148-z.

Villa F., De Amicis M., Maggi V. (2007): GIS analysis of Rutor glacier (Aosta Valley, Italy) volume and terminus variations. *Geogr. Fis. Dinam. Quat.,* 30, 87–95.

Villa F., Tamburini A., De Amicis M., Sironi S., Maggi V., Rossi G. (2008): Volume decrease of Rutor glacier (Western Italian Alps) since Little Ice Age: a quantitative approach combining GPR, GPS and cartography. *Geogr. Fis. Dinam. Quat.,* 31, 63-70.

Voldoire A. et al (2013): The CNRM-CM5.1 global climate model: description and basic evaluation. *Clim. Dyn.* 40:2091–2121.

Waddington E. (1998): Principles of Glacier Mechanics. *Eos, Transactions American Geophysical Union*, 79(10):123–123, 1998. ISSN 0096-3941.

Watanabe M. et al (2010): Improved Climate Simulation by MIROC5: Mean States, Variability, and Climate Sensitivity. *J. of Clim.* Vol. 25, Issue 23, 6312–6335.

WGMS: Fluctuations of Glaciers, (2000–2005), Vol. IX, edited by: Haeberli, W., Zemp, M., Kaab, A., Paul, F. and Hoelzle, M. ICSU(FAGS)/IUGG(IACS)/UNEP/UNESCO/WMO, 2008.

WGMS: Glacier Mass Balance Bulletin No. 11 (2008–2009), edited by: Zemp, M., Nussbaumer, S. U., Gartner-Roer, I., Hoelzle, M., Paul, F., and Haeberli, W., ICSU(WDS)/IUGG(IACS)/UNEP/UNESCO/WMO, 2011.

Wigley T. M. L. (2005): The climate change commitment. *Science,* 307, 1766–1769.

Wood A. W., Maurer E. P., Kumar A., Lettenmaier D. P. (2002): Long-range experimental hydrologic forecasting for the eastern United States. *Journal of Geophysical Research: Atmospheres (1984–2012),* 107(D20), ACL-6.

Wood A. W., Leung L. R., Sridhar V., Lettenmaier D. P. (2004): Hydrologic implications of dynamical and statistical approaches to downscaling climate model outputs. *Climatic change,* 62(1-3), 189-216.

Wu T. et al (2013): Global carbon budgets simulated by the Beijing Climate Center Climate System Model for the last century. *J. of Geoph. Res.* Volume 118, Issue 10, pages 4326–4347.

Yukimoto S. et al (2012): A New Global Climate Model of the Meteorological Research Institute: MRI-CGCM3 -Model Description and Basic Performance-. *J. of the Met. Soc. of Jap.* Vol. 90A, pp. 23-64

Zampieri M., Scoccimarro E., Gualdi S. (2013): Atlantic influence on spring snowfall over the alps in the past 150 years, *Environmental Research Letters*, 8(3), 034,026.

Zanon G. (1982): Recent glaciological research in the Ortles- Cevedale region (Italian Alps). *Geogr. Fìs. Din. Quat.*, 5(1), 75–81, 1982.

Zemp M., Haeberli W., Hoelzle M., Paul F. (2006): Alpine glaciers to disappear within decades? *Geophysical Research Letters*, 33(13).

Thesis

Balocco J. (master thesis 2015): Modelling climate influence on Alpine glacier Mass Balance, *master thesis, University of Torino.*

Maffezzoni M. (master thesis 2015): Geomorphological-climatic analysis and classification aimed at modelling the glaciers response to climate change, *master thesis, University of Milano-Bicocca.*

Mattavelli M. (Ph.D. thesis 2016): Development a Glaciological Data Spatial Infrastructure to assess glaciers response to climatic fluctuation, *Ph.D. thesis, University of Milano - Bicocca*.

Peano D. (master thesis 2011): Dynamical models for Alpine glacier response to climate variability, *master thesis, University of Torino.*

Sali M. (bachelor thesis 2015): Bilancio di massa dei ghiacciai alpini: valutazione analogie di andamento e caratterizzazione geografico-morfologica per dataset previsionali, *bachelor thesis, University of Milano-Bicocca.*

Zemp M. (Ph.D. thesis 2006): Glaciers and Climate Change – Spatio-temporal Analysis of Glacier Fluctuations in the European Alps after 1850 dissertation, *Ph.D. thesis, University Zurich*.

Appendix A

To obtain these programming files (Python and Fortran77 versions), please contact me at: *massimiliano.moretti86@gmail.com*

MGM algorithms

Python file: mgm_exe.py

```
#!/usr/bin/env python


##### Minimal Glacier Model: multiple glaciers


##### Import
import math
import functionmod
import csv
import glob
import os
import sys

print "\n##### Minimal Glacier Model #####"


##### Climate forcing files
path = '../g24'+os.sep
fileName = functionmod.datafolder(path)


##### Glacier parameter files
pathp = 'parameters/par24'+os.sep
paraName = functionmod.datafolder(pathp)


##### Model elaborations
i = 0
for d in paraName:
    execfile(pathp + d)
    q = 0
    j = 0
    senal = math.sin(math.radians(s))
    ipo = hrange/senal
    rapp = ipo/li
    e1 = ehrange/senal
    e2 = math.radians(es)*hrange*math.fabs(math.sin(math.radians(s)))
/math.pow(senal,2)
    esumm = math.pow(e1,2) + math.pow(e2,2)
```

```
    eipo = math.pow(esumm,0.5)
    thick, stress, ethick = functionmod.linsbauer(hrange,s,ehrange,es)
    alfam, ealfam =
functionmod.alfathick(ipo,thick,nu,s,eipo,ethick,es)
    for c in fileName:
        print "Glacier: " + d , "/ Elaboration: " + c
        l = li
        el = eli
        with open(path + c, 'rb') as fin:
            in_file = csv.reader(fin, delimiter=' ')
            for row in in_file:
                if (len(row)==0):
                    continue
                else:
                    if (l>=50):
                        dany = filter(lambda a: a != '', row)
                        if (int(dany[0])>=2012):
                            bpmm =
functionmod.fitbiv(float(dany[1]),float(dany[2]),a,b,tn)
                            bp = bpmm/1000
                            bp_list=[]
                            bp_list.append(bp)
                            ebp = abs(bp_list[0]*errc/100.0)
                            dl,lout,edl,el =
functionmod.rungekutta(h,float(bp_list[0]),l,alfam,nu,s,ebp,el,ealfam,e
s)
                            datarow=[]
                            if (q==0):
                                datarow.append(int(dany[0])-1)
                                datarow.append(li)
                                datarow.append(eli)
                                outdata.append(datarow)
                                datarow=[]
                            datarow.append(int(dany[0]))
                            datarow.append(lout)
                            datarow.append(el)
                            outdata.append(datarow)
                            l = lout
                            q = q + 1
            fin.close()


##### Opening and writing files
            print "L ( 2011 ) =", li
            gradm = (li-l)/(int(dany[0])-2011)
            print "L-gradient =", gradm
            print "l (",dany[0],") =" ,l,"+-",el
            print "_____________________________________"
            outp = 'results/g24'+os.sep
            with open(outp + "l_" + c, 'wb') as fout:
                writer = csv.writer(fout)
                writer.writerows(outdata)
            fout.close()
            outdata=[]
        q = 0
        j = j + 1
    i = i + 1
```

```
print "\n##### Parameter"
print "Alfam =",alfam,"+-",ealfam
print "Ratio Ipi/Li =",rapp
print "##### Output counts"
print "Number of glaciers: ", i
print "Number of climate models: ", j
print "Number of output files: ", i*j, "\n"
```

Python functions file: functionmod.py

```
########## Import libraries ##########
import math
import glob
import os


########## Folder data input ##########
def datafolder(path):
    fileName = []
    for infile in sorted(glob.glob( os.path.join(path, '*') )):
        print "Current file is: " + infile
        infileSplt = infile.split(os.sep)
        infileSpltLen = len(infileSplt)
        fileName.append(infileSplt[infileSpltLen-1])

    return fileName


########## Linsbauer method to estimate mean thickness ##########
def linsbauer(hrange,s,ehrange,es):
    hrange = hrange/1000.0
    stress = 0.005+1.598*hrange-0.435*(math.pow(hrange,2))
#    if (hrange>=1.6):
#        stress = 150
    thick = stress*100000/(0.8*900*9.81*math.sin(math.radians(s)))

    alfa = math.radians(s)
    ealfa = math.radians(es)
    sena = math.sin(alfa)
    estress = (ehrange/1000)*(1.598-2*0.435*hrange)
    dthick1 = estress*100000/(0.8*900*9.81*sena)
    dthick2 =
ealfa*stress*100000*math.fabs(math.fabs(math.cos(alfa)))/(0.8*900*9.81*
math.pow(sena,2))
    etsum = math.pow(dthick1, 2)+math.pow(dthick2,2)
    ethick = math.pow(etsum,0.5)

    return thick,stress,ethick
```

```
########## Function to calculate Alfam ##########
def alfathick(lr,thick,nu,s,el,ethick,es):

    sp = math.tan(math.radians(s))
    esp = math.tan(math.radians(es))

    v1 = 1+nu*sp
    alfam = thick*v1/(math.pow(lr,0.5))

    ea1 = ethick*v1/(math.pow(lr,0.5))
    ea2 = esp*thick*nu/(math.pow(lr,0.5))
    ea3 = -el*thick*v1/(2*math.pow(lr,1.5))
    easum = math.pow(ea1,2)+math.pow(ea2,2)+math.pow(ea3,2)
    ealfam = math.pow(easum,0.5)

    return alfam,ealfam


########## Function to relate climate forcing on mass balance
##########
def fitbiv(ts,pw,a,b,tn):
    bp = a*ts+b*pw+tn
    return bp


########## Minimal Glacier Model algorithm ##########
def minmod(bp,l,alfam,nu,s,ebp,el,ealfam,es):

    sp = math.tan(math.radians(s))
    esp = math.tan(math.radians(es))

    v1 = 1+nu*sp
    Hm = (math.pow(l,0.5)*3*alfam)/(2*v1)
    dl = (bp*l)/Hm

    Hm1 = ealfam*(math.pow(l,0.5))/v1
    Hm2 = -esp*nu*alfam*(math.pow(l,0.5))/(math.pow(v1,2))
    Hm3 = el*alfam/(2*v1*(math.pow(l,0.5)))
    Hsum = math.pow(Hm1,2)+math.pow(Hm2,2)+math.pow(Hm3,2)
    eHm = math.pow(Hsum,0.5)

    ed1 = (ebp*l)/Hm
    ed2 = el*bp/Hm
    ed3 = -eHm*bp*l/(math.pow(Hm,2))
    edsum = math.pow(ed1,2)+math.pow(ed2,2)+math.pow(ed3,2)
    edl = math.pow(edsum,0.5)

    return dl,edl
```

```
########## Runge-Kutta method to solve MGM ##########
def rungekutta(h,bp,l,alfam,nu,s,ebp,el,ealfam,es):

    mm,emm = minmod(bp,l,alfam,nu,s,ebp,el,ealfam,es)
    h2 = h/2
    h6 = h/6
    k1 = h*mm
    k12 = k1/2
    ek1 = emm/6

    mm1,emm1 = minmod(bp,l+k12,alfam,nu,s,ebp,ek1,ealfam,es)
    k2 = h*mm1
    k22 = k2/2
    ek2 = 2*emm1/3

    mm2,emm2 = minmod(bp,l+k22,alfam,nu,s,ebp,ek2,ealfam,es)
    k3 = h*mm2
    ek3 = 2*emm2/3

    mm3,emm3 = minmod(bp,l+k3,alfam,nu,s,ebp,ek3,ealfam,es)
    k4 = h*mm3
    ek4 = emm3/6

    dlrk = (k1+2*k2+2*k3+k4)/6
    lrk = l+dlrk

    ksum =
math.pow(ek1,2)+math.pow(ek2,2)+math.pow(ek3,2)+math.pow(ek4,2)
    edlrk = math.pow(ksum,0.5)
    lsum = math.pow(el,2)+math.pow(edlrk,2)
    elrk = math.pow(lsum,0.5)

    return dlrk, lrk, edlrk, elrk
```

Appendix B

MGM on GAR glaciers

All the length assessments are cut off at 200 m, because the uncertainty bars are of the order of 200 m, thus any estimate beyond this minimum threshold is not significant. Moreover, when a glacier become too small may become covered with debris and its volume is mixed up with rubble, distorting its dynamics.

For each glacier, 20 different runs of the NASA NEX-GDDP dataset simulate the glacier behaviors. The glacier IDs (referred to Table 8) composes the legends under the figures, with the end dates for RCP 4.5 and RCP 8.5 and the related uncertainties (1σ deviation of the ensemble).

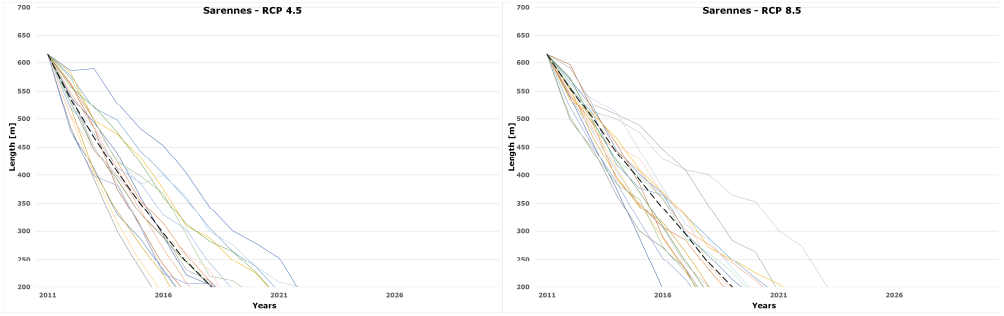

ID glacier 1: Sarennes. End date: RCP 4.5 = (2018 ± 2)y / RCP 8.5 = (2019 ± 2)y

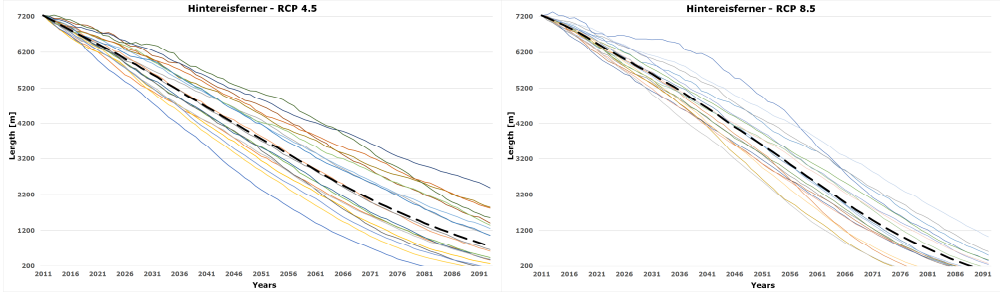

ID glacier 2: Hintereisferner. End date: after 2092 / RCP 8.5 = (2089 ± 5)y

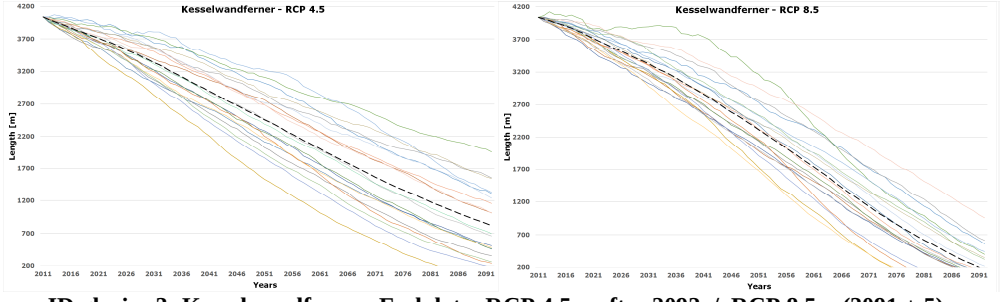

ID glacier 3: Kesselwandferner. End date: RCP 4.5 = after 2092 / RCP 8.5 = (2091 ± 5)y

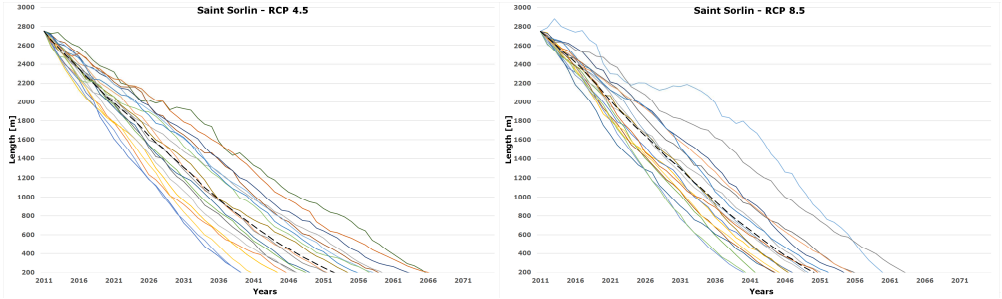

ID glacier 4: Saint Sorlin. End date: RCP 4.5 = (2052 ± 9)y / RCP 8.5 = (2050 ± 8)y

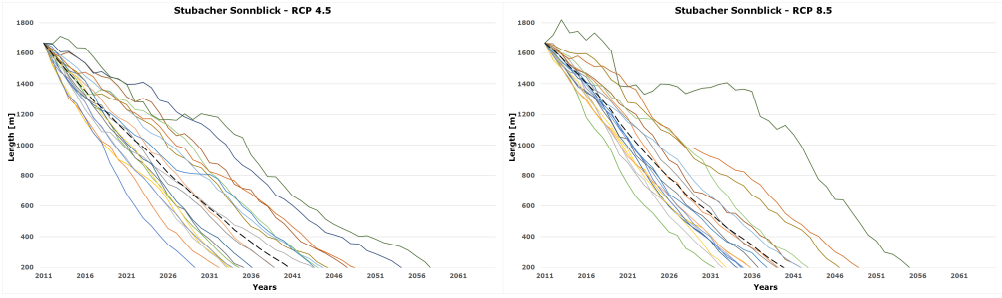

ID glacier 5: Stubacher. End date: RCP 4.5 = (2041 ± 8)y / RCP 8.5 = (2040 ± 8)y

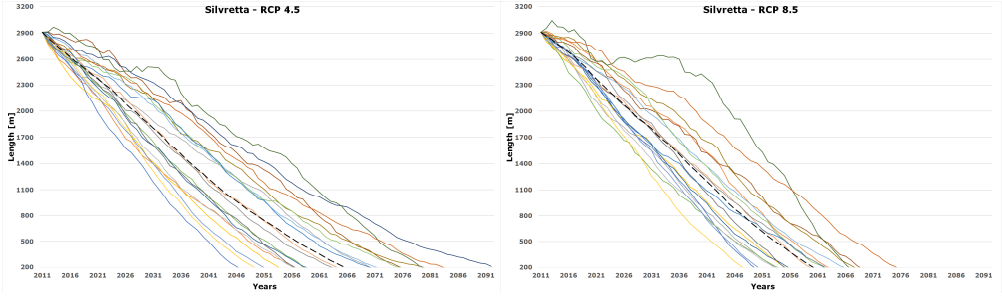

ID glacier 6: Silvretta. End date: RCP 4.5 = (2066 ± 11)y / RCP 8.5 = (2060 ± 9)y

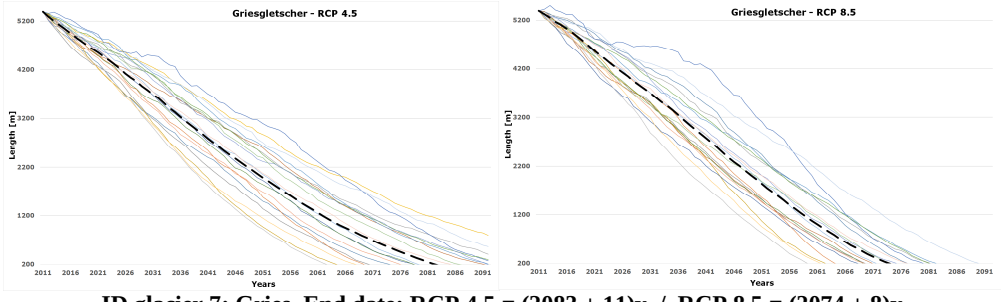

ID glacier 7: Gries. End date: RCP 4.5 = (2083 ± 11)y / RCP 8.5 = (2074 ± 8)y

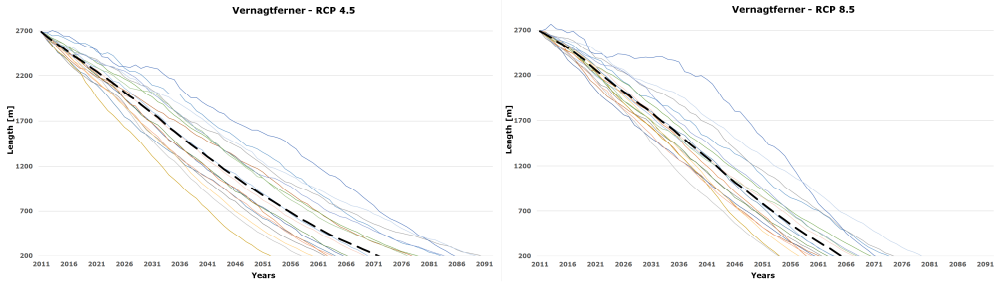

ID glacier 8: Vernagtferner. End date: RCP 4.5 = (2072 ± 9)y / RCP 8.5 = (2066 ± 5)y

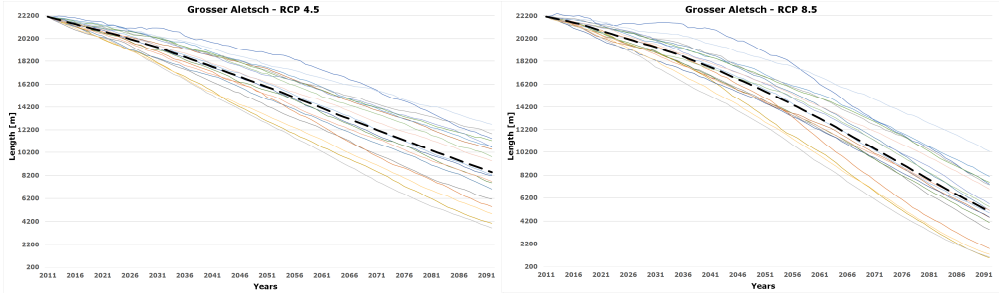

ID glacier 9: Aletsch. End date: RCP 4.5 = after 2092 / RCP 8.5 = after 2092

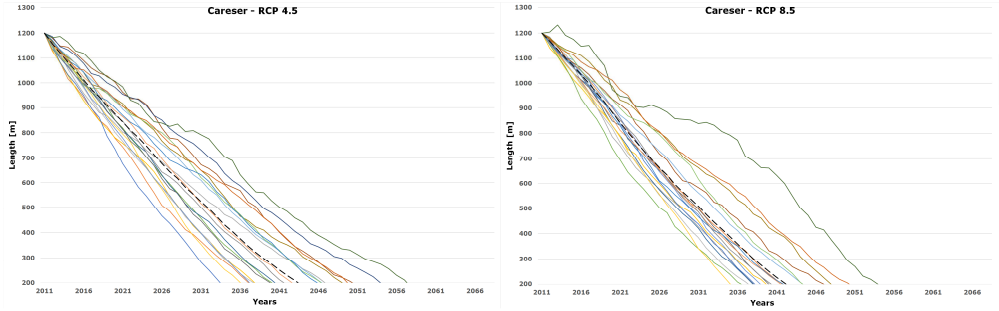

ID glacier 10: Careser. End date: RCP 4.5 = (2044 ± 8)y / RCP 8.5 = (2042 ± 6)y

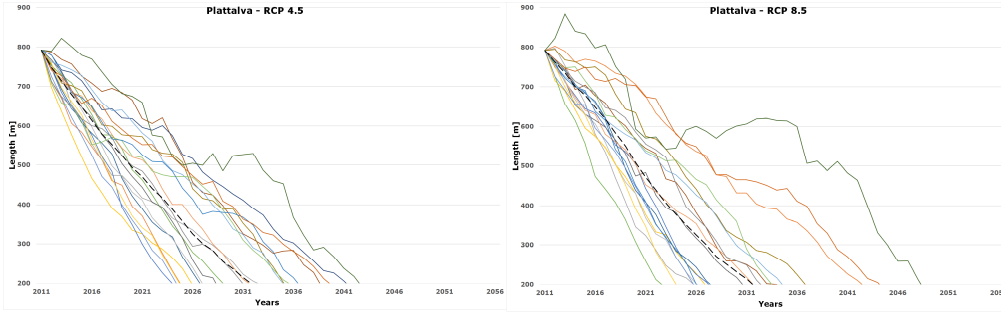

ID glacier 11: Plattalva. End date: RCP 4.5 = (2031 ± 5)y / RCP 8.5 = (2031 ± 6)y

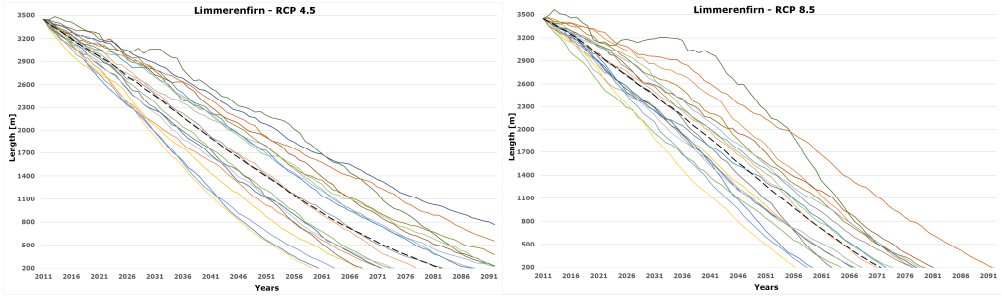

ID glacier 12: Limmeren. End date: RCP 4.5 = (2083 ± 10)y / RCP 8.5 = (2071 ± 9)y

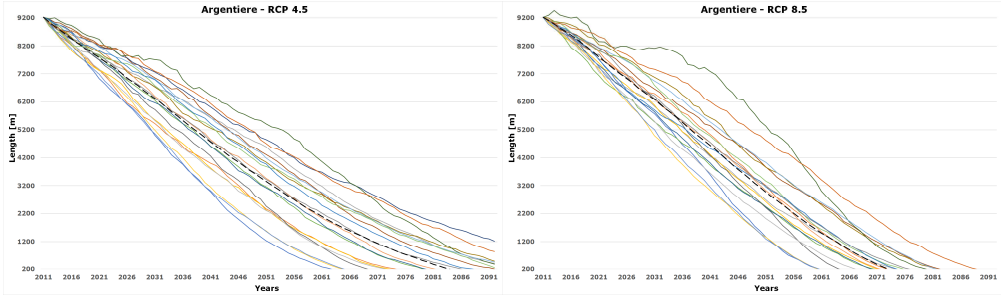

ID glacier 13: Argentiere. End date: RCP 4.5 = (2084 ± 10)y / RCP 8.5 = (2073 ± 8)y

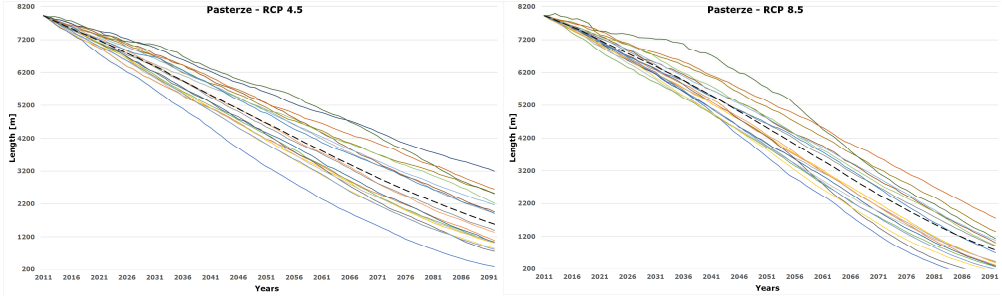

ID glacier 14: Pasterze. End date: RCP 4.5 = after 2092 / RCP 8.5 = after 2092

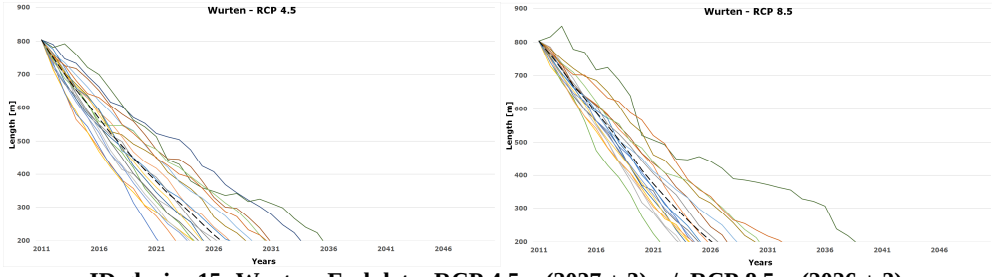

ID glacier 15: Wurten. End date: RCP 4.5 = (2027 ± 3)y / RCP 8.5 = (2026 ± 3)y

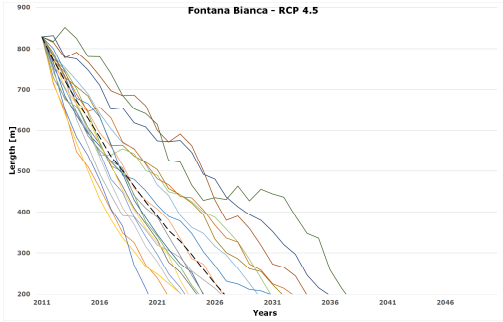

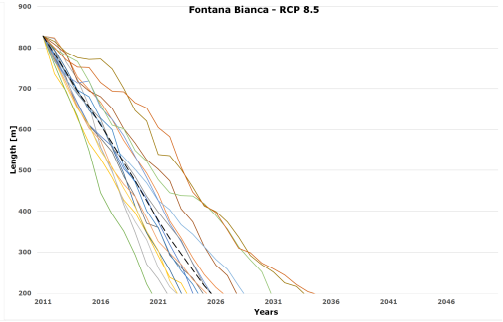

ID glacier 16: Fontana Bianca. End date: RCP 4.5 = (2027 ± 5)y / RCP 8.5 = (2026 ± 4)y

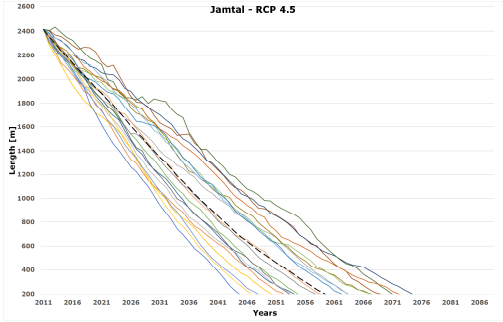

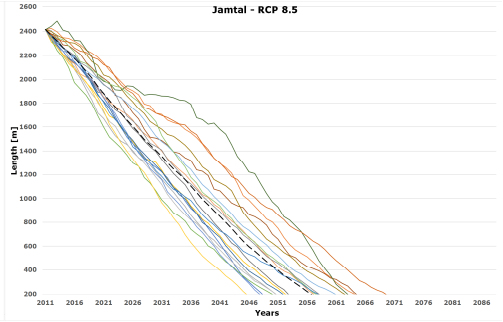

ID glacier 17: Jamtal. End date: RCP 4.5 = (2060 + 9)y / RCP 8.5 = (2056 + 7)y

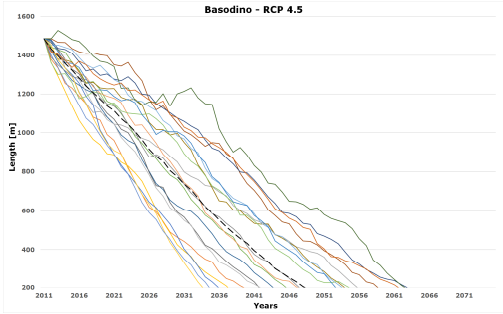

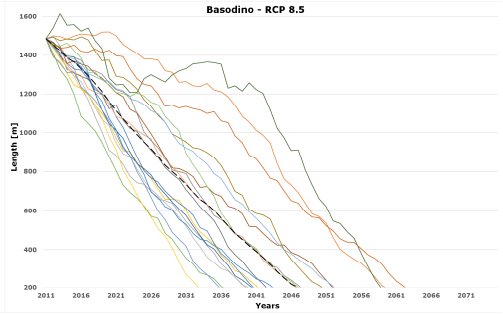

ID glacier 18: Basodino. End date: RCP 4.5 = (2048 ± 9)y / RCP 8.5 = (2046 ± 7)y

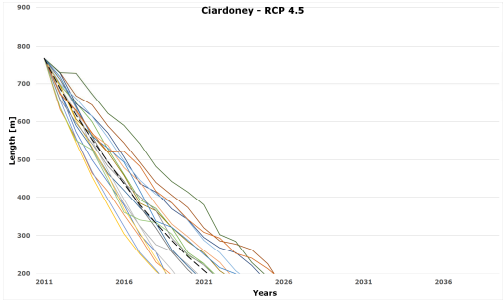

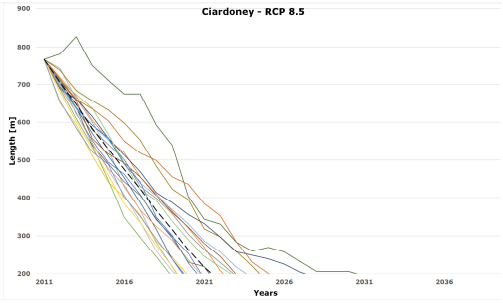

ID glacier 19: Ciardoney. End date: RCP 4.5 = (2021 ± 2)y / RCP 8.5 = (2022 ± 2)y

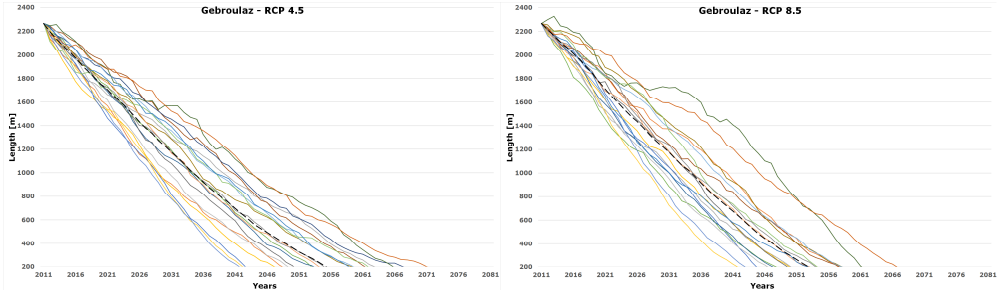

ID glacier 20: Gebroulaz. End date: RCP 4.5 = (2055 ± 8)y / RCP 8.5 = (2053 ± 7)y

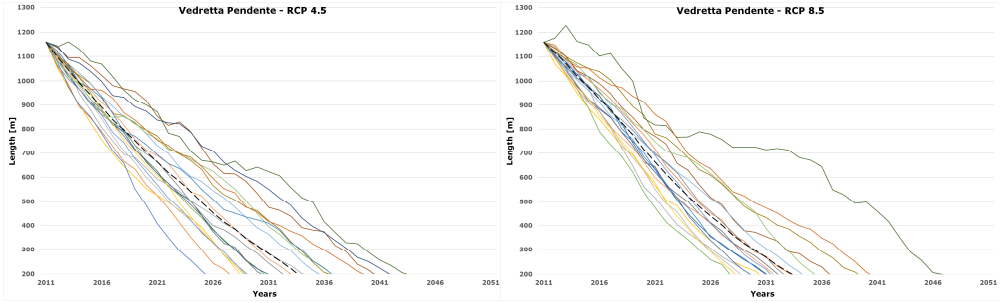

ID glacier 21: Pendente. End date: RCP 4.5 = (2034 ± 5)y / RCP 8.5 = (2034 ± 5)y

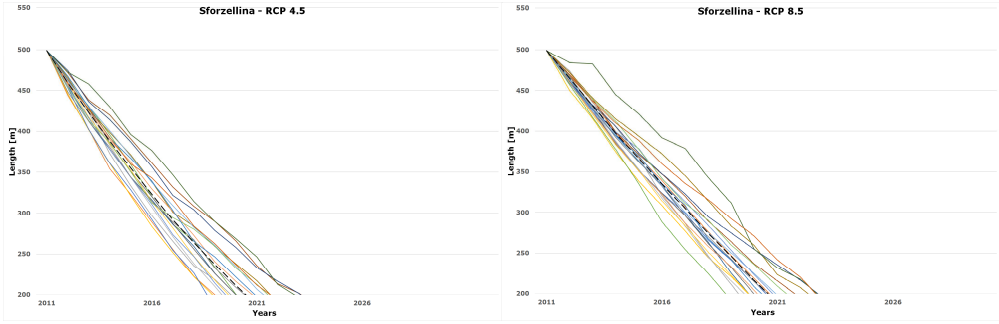

ID glacier 22: Sforzellina. End date: RCP 4.5 = (2020 ± 2)y / RCP 8.5 = (2021 ± 2)y

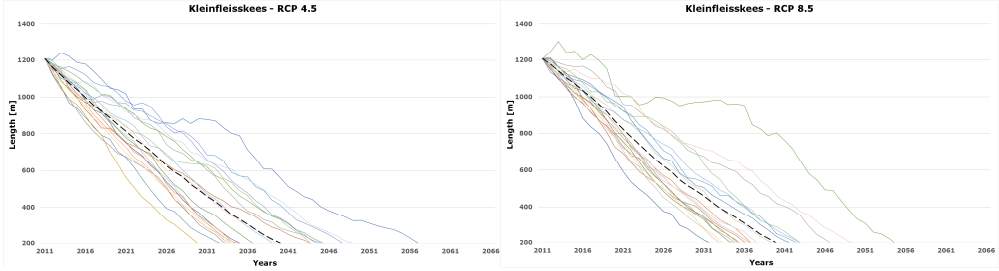

ID glacier 23: Kleinfleisskees. End date: RCP 4.5 = (2040 ± 7)y / RCP 8.5 = (2040 ± 7)y

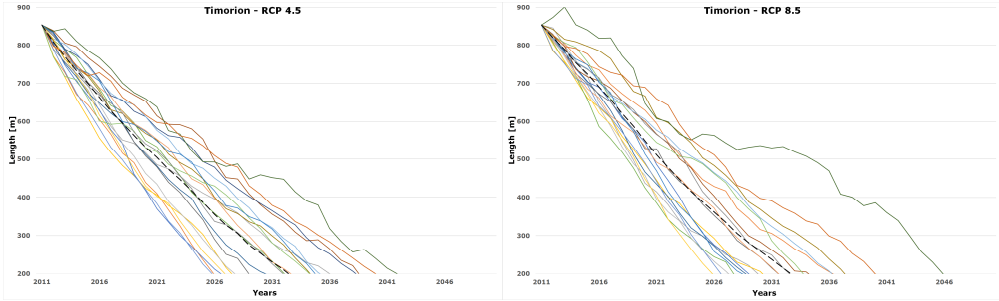

ID glacier 24: Timorion. End date: RCP 4.5 = (2032 ± 6)y / RCP 8.5 = (2033 ± 6)y

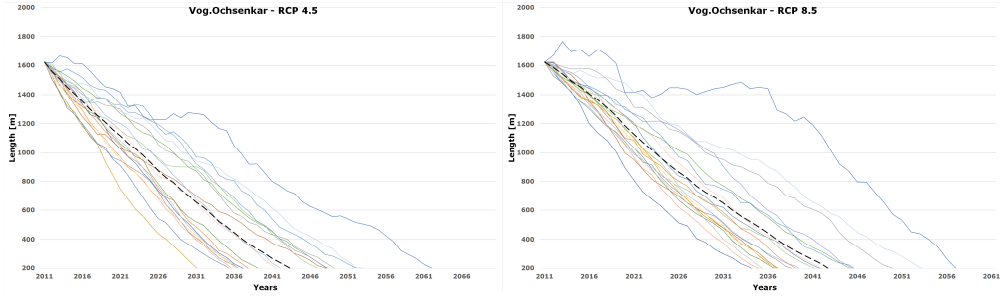

ID glacier 25: Vog.Ochsenkar. End date: RCP 4.5 = (2044 ± 8)y / RCP 8.5 = (2043 ± 9)y

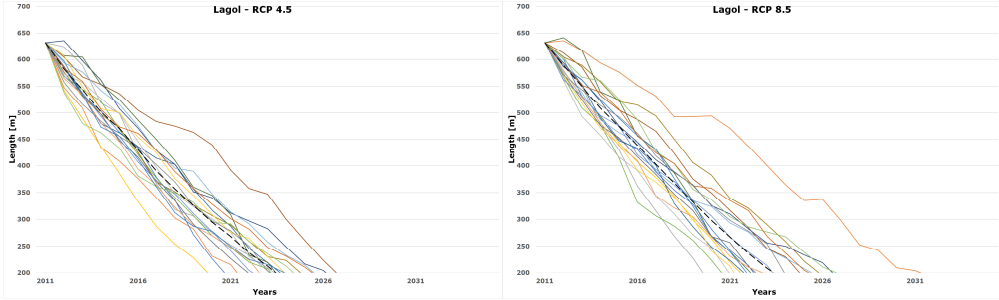

ID glacier 26: Lagol. End date: RCP 4.5 = (2024 ± 3)y / RCP 8.5 = (2023 ± 3)y

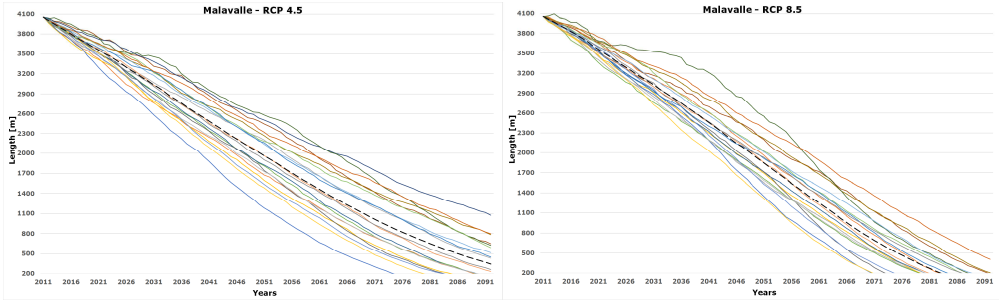

ID glacier 27: Malavalle. End date: after 2092 / RCP 8.5 = (2083 ± 8)y

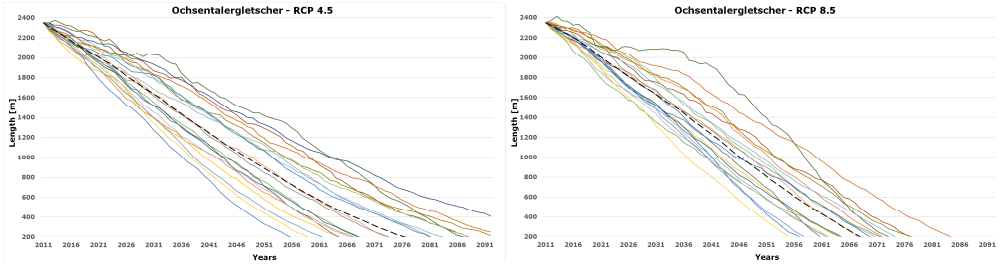

ID glacier 28: Ochsentaler. End date: RCP 4.5 = (2076 ± 12)y / RCP 8.5 = (2068 ± 9)y

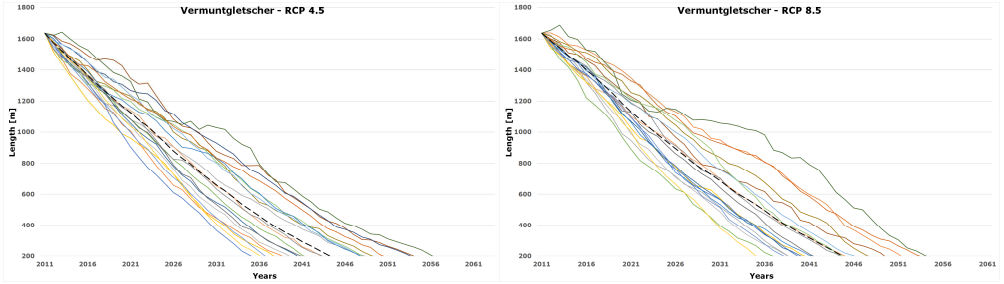

ID glacier 29: Vermunt. End date: RCP 4.5 = (2044 ± 8)y / RCP 8.5 = (2045 ± 8)y

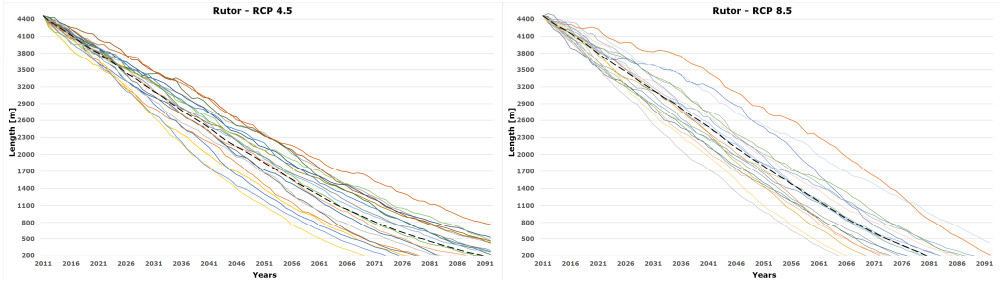

ID glacier 30: Rutor. End date: RCP 4.5 = (2090 ± 13)y / RCP 8.5 = (2081 ± 10)y

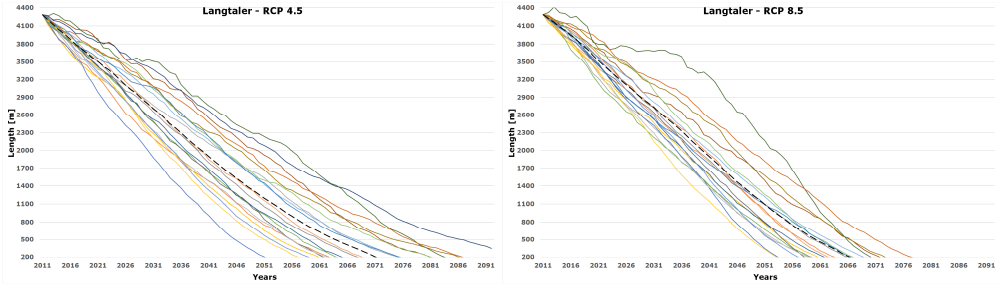

ID glacier 31: Langtaler. End date: RCP 4.5 = (2071 ± 10)y / RCP 8.5 = (2066 ± 9)y